University of Massachusetts Amherst
ScholarWorks@UMass Amherst

Doctoral Dissertations | Dissertations and Theses

Fall November 2014

On the Assembly of Functionalized CdSe Nanorods

Sirinya Chantarak
University of Massachusetts - Amherst

Follow this and additional works at: https://scholarworks.umass.edu/dissertations_2

 Part of the Physical Chemistry Commons, and the Polymer Chemistry Commons

Recommended Citation

Chantarak, Sirinya, "On the Assembly of Functionalized CdSe Nanorods" (2014). *Doctoral Dissertations*. 164.
https://doi.org/10.7275/dzq2-hd29 https://scholarworks.umass.edu/dissertations_2/164

This Open Access Dissertation is brought to you for free and open access by the Dissertations and Theses at ScholarWorks@UMass Amherst. It has been accepted for inclusion in Doctoral Dissertations by an authorized administrator of ScholarWorks@UMass Amherst. For more information, please contact scholarworks@library.umass.edu.

ON THE ASSEMBLY OF FUNCTIONALIZED CdSe NANORODS

A Dissertation Presented

by

SIRINYA CHANTARAK

Submitted to the Graduate School of the
University of Massachusetts Amherst in partial fulfillment
of the requirements for the degree of

DOCTOR OF PHILOSOPHY

September 2014

Polymer Science and Engineering

© Copyright by Sirinya Chantarak 2014

All Rights Reserved

ON THE ASSEMBLY OF FUNCTIONALIZED CdSe NANORODS

A Dissertation Presented

by

SIRINYA CHANTARAK

Approved as to style and content by:

_____
Todd S. Emrick, Co-Chair

_____
Thomas P. Russell, Co-Chair

_____
Paul M. Lahti, Member

_____
David A. Hoagland, Department Head
Polymer Science and Engineering

DEDICATION

To my parents and my grandmother

ACKNOWLEDGMENTS

I would like to thank my advisors, Prof.Thomas Russell and Prof.Todd Emrick, for their guidance and support during the years I worked with them. They are great mentors in scientific and academic wise. I always enjoyed a special lecture Prof.Russell gave to the students during the group meeting. I also would like to thank Prof.Paul Lahti for being my research committee. He is always nice and kind giving me questions and suggestions that were very valuable to my research. I thank the Ministry of Science and Technology, Thailand for the fellowship during my 5 year Ph.D. study.

I am grateful to my collaborators, Feng Liu, Yu Gu, Sunzida Ferdous, Paul Kim and Hsin-wei Wang, for their help and useful suggestions. I enjoyed learning about X-ray scattering from Feng and Sunzida, photovoltaic device fabrication from Yu and Hsin-wei, and also observing a great skill in SEM of Paul.

I appreciate the help and valuable discussions from the group members, Russell group and Emrick group, especially to Dephine Chan-seng and Beth Cooper who taught me doing synthesis at the beginning of my research, Sangwoo Kim and Weiyin Gu who always helped and gave me suggestions on AFM, Caroline Miesch, Irem Kosif, Jimmy Lawrence, Xiaobo Chen and Rachel Letteri who always had stimulating discussions with me in lab. It was enjoyable to work in the same group with them. I would like to thanks PSE staffs, Volodimyr Duzhko, Alexander Ribbe, Louis Raboin, Sekar Thirunavukkarasu, Jacob Hirsch, Weiguo Hu, Linda Strzegowski, Laurie Banas, and Lisa Groth for helping me in research and graduate studies.

Finally, I really appreciate my family for their support, love and encouragement during my Ph.D. study.

ABSTRACT

ON THE ASSEMBLY OF FUNCTIONALIZED CdSe NANORODS

SEPTEMBER 2014

SIRINYA CHANTARAK, B.S., PRINCE OF SONGKLA UNIVERSITY

M.S., CHULALONGKORN UNIVERSITY

Ph.D., UNIVERSITY OF MASSACHUSETTS AMHERST

Directed by: Professor Todd S. Emrick and Professor Thomas P. Russell

High aspect ratio (AR) CdSe nanorods (NRs) of well-defined sizes were synthesized to optimize the geometries of photovoltaic devices made from these nanorods. Long-range ordering of hexagonal arrays of high AR NRs is achieved by a combination of controlled solvent evaporation and the use of an applied electric field. Regioregular P3HT chains and oligothiophene were functionalized with ligating end-groups to provide contact to the NRs. Vertically oriented assemblies of CdSe NRs functionalized with terthiophene and polythiophene are also obtained. Hexagonal arrays of these nanocomposites were characterized by transmission electron microscopy (TEM). Three types of polythiophenes: poly(3-hexylthiol thiophene), poly(3-hexylamine thiophene), and poly(3-hexylphosphonate thiophene) with thiol, amine, and phosphonate functional groups, were synthesized to anchor to the NRs. This led to a thin layer of p-type conducting polymer covering tips of the n-type inorganic NRs forming end-to-end assembly. Ternary nanocomposites of CdSe-polythiophene-graphene were obtained *via* π-π stacking. These oriented CdSe NRs-polythiophenes nanocomposites have potential applications in organic-inorganic hybrid bulk heterojunction photovoltaic devices.

TABLE OF CONTENTS

LIST OF FIGURES

Figure Page

CHAPTER 1

ORGANIC-INORGANIC SOLAR CELLS

1.1 Introduction

1.1.1 Energy Consumption and Renewable Energies

Renewable and non-CO_2 releasing energy sources now make significant contributions to the world's energy consumption. Numerous natural energy sources are abundant and costless, such as wind, geothermal, hydroelectric, and solar, making them beneficial for producing energy.[1] **Figure 1.1** depicts energy consumption from various energy sources in 2011, and the growth of clean energy consumption during the past 60 years. This plot shows that the majority of energy consumed is from petroleum, natural gas, and coal, while the minority comes from nuclear power and renewable energies including solar, geothermal, wind, biofuels, hydroelectric power, waste and wood. Among these clean and renewable energy sources, capturing solar energy by photovoltaics (PV) is a promising area of research.

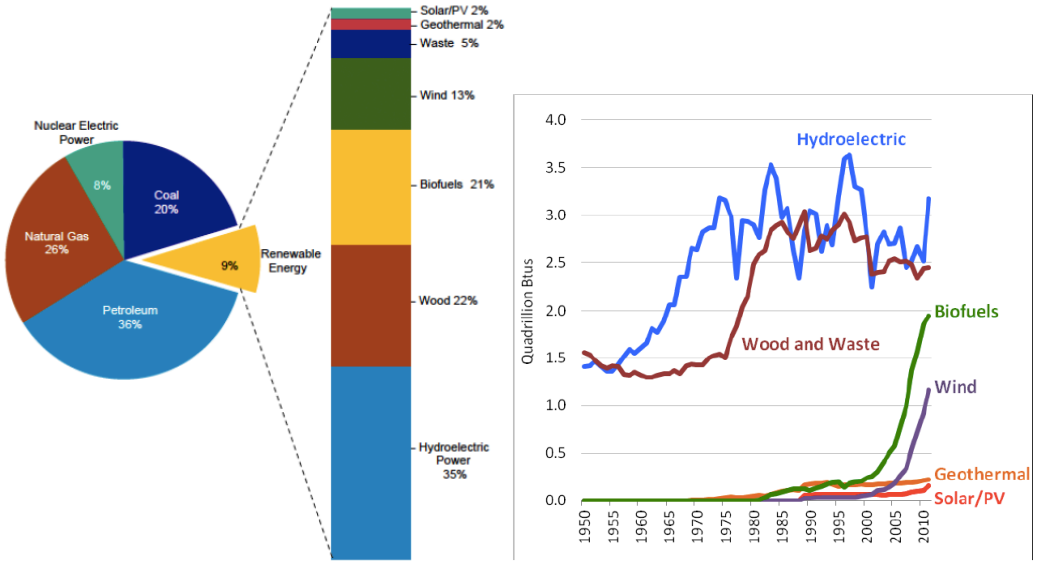

Figure 1.1 Renewable energy as a fraction of total primary energy consumption in 2011 (left), and growth of renewable energy consumption, 1950–2011 (right).[1]

1.2 Organic Photovoltaic Solar Cells

Solar cells convert visible light into electricity. PV cells based on crystalline silicon have high manufacturing and installation costs. Many research groups have been focusing on photovoltaic cells with the aim of producing high efficiency devices at lower cost, so as to reduce the cost per watt of solar energy. Recent work on PVs centers on semiconducting photoactive polymers and flexible substrates using solution-processing techniques, which are potentially amenable to constructing large area devices at a lower cost as compared to silicon solar cells.[2]

Three different types of organic PV devices, depending on the morphology of the active layer, include bilayer, bulk, and ordered heterojunction devices, **Figure 1.2(a)**. Typical PV devices are multilayered structures, as illustrated in **Figure 1.2(b)**. The first layer is a transparent substrate that allows light to pass through. This substrate layer can

be glass or a more flexible material, such as polyethylene terephthalate (PET). The second layer is the anode, which serves as the hole collecting layer, and is usually made of a semitransparent oxide layer (*e.g.* indium tin oxide, ITO). A thin layer of the conductive polymer mixture (poly(3,4-ethylene-dioxythiophene)-poly(styrenesulfonate), PEDOT–PSS) is coated on top of the anode and serves as a hole transporting layer and exciton blocker. Additionally, it coats the ITO surface and prevents oxidation of the photoactive layer. The next layer is a photoactive layer, which contains the donor and acceptor materials. This layer is located between two electrodes that have different work functions. The top layer of the device is the cathode, which serves as an electron collecting layer.

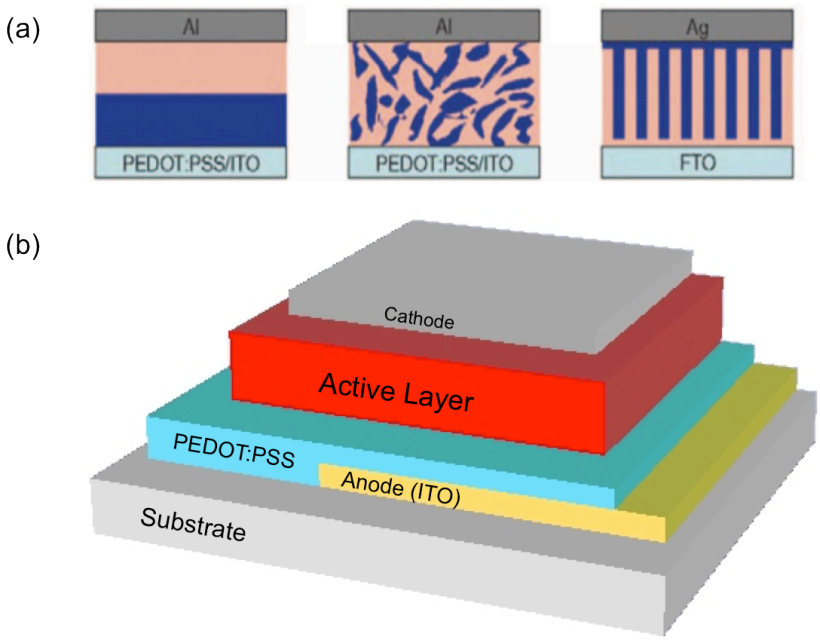

Figure 1.2 Diagram illustrating (a) three types of heterojunction morphologies (bilayer, bulk heterojunction, and ordered heterojunction),[3,4] and (b) a structure of photovoltaic device.

Bulk heterojunction (BHJ) PV cells can be divided into four important types. The first type is a composite of two conjugated polymers with offset energy levels. The second type is a blend of a conjugated polymer (*e.g.* poly(3-hexylthiophene), P3HT) with a soluble fullerene derivative (*e.g.* [6,6]-phenyl C-$_{61}$-butyric acid methyl ester fullerene, PCBM), which currently shows the best power conversion efficiency (PCE) ~ 5%.[5] The third type is a composite of semiconducting polymers and metal particles (*e.g.* titania, TiO_2), called a Schottky junction PV cell, currently receiving attention due to the possibility of patterning TiO_2 into a continuous network for electron transport.[6] The last type is semiconductor-sensitized quantum dot solar cells.[7]

The mechanism of energy generation from PV cell, **Figure 1.3**, begins when light penetrates to the photoactive layer, and an exciton, an electron-hole pair bound by Coulombic forces, is generated in the donor phase, the material having the higher occupied molecular orbital (HOMO) level. The exciton diffuses to the interface between the donor and acceptor phase and dissociates by electron transfer, driven by the energy offset between these materials. The fully free charge carriers are transported to the respective electrodes, generating photocurrent.

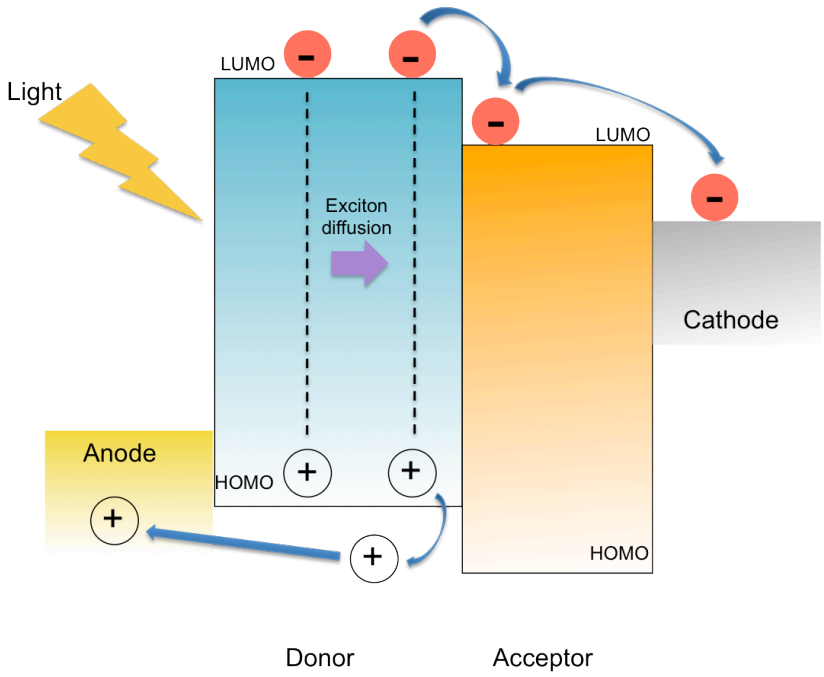

Figure 1.3 Schematic depletion of the mechanism of energy generation from the photovoltaic cell.

1.3 Nanostructure in Solar Cells

Ideally, phase separation of the two components, electron donor and electron acceptor materials in the active layer, should be on the nanometer scale in order to prevent loss of absorbed photons and to achieve a high yield of exciton dissociation before charge recombination occurs.[3] Since the exciton diffusion length is very small (between 5-20 nm), it is crucial that the dispersion of the two materials in the active layer is optimized. Several methods are used to develop continuous morphologies within the active layer,[4] such as thermal annealing, solvent annealing, additives, fibrilization, and various methods for constructing nanoarchitectures.

1.3.1 Thermal Annealing Approach

Thermal annealing is the simplest method towards achieving a continuous morphology in the active layer, and improving the crystallinity of the polymer within the active layer. Thermal annealing can be performed before or after cathode deposition (*i.e.* pre-annealing or post-annealing). Both techniques lead to enhanced crystallization of the photoactive polymers.[5] Cross section of a P3HT/PCBM based PV device is shown in **Figure 1.4**. Before thermal annealing, voids between the PEDOT:PSS layer and the active layer were observed, and P3HT and PCBM appear to be mixed uniformly. After thermal annealing at 150 ˚C for 30 minutes, TEM imaging clearly showed improved adhesion, and evidence for diffusion between the PEDOT:PSS layer/active layer, and active layer/Al electrode. Additionally, phase separation of P3HT and PCBM generated a bi-continuous morphology with the average domain size ~ 10 nm to 15 nm, suitable for the exciton diffusion length.

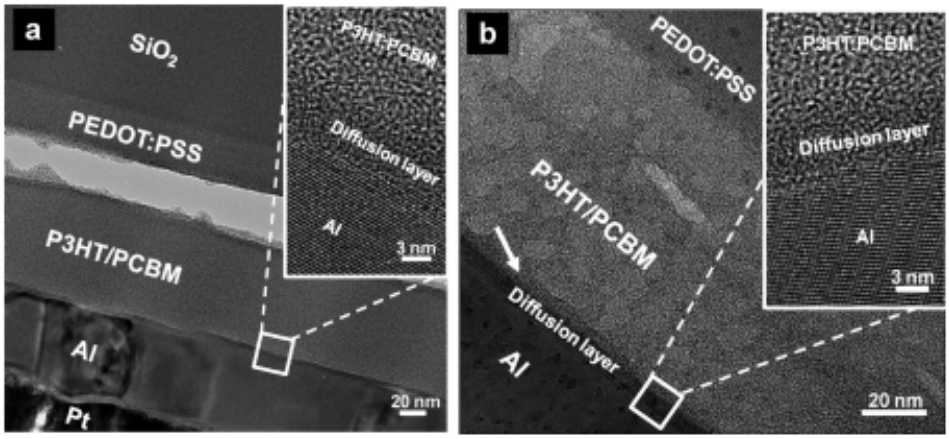

Figure 1.4 High resolution TEM images of cross sections of P3HT/PCBM based multilayered samples, (a) as spun, and (b) post-annealed at 150 ˚C.[8]

1.3.2 Solvent Annealing Approach

Solvent annealing is another method used to improve nanoscale phase separation in the active layer. During the annealing process, the solvent evaporates and the solvent vapor penetrates into the film increasing mobility of the materials, leading to crystallization of the polymers.[9]

1.3.3 Additive Approach

Mixing a small amount of soluble additives, such as alkanedithiols, into a casting solvent is another method used to improve the continuous morphology of the active layer. The additive molecules induce crystallization of the polymers, and thereby enhance the performance of the devices.[10]

1.3.4 Nanofibril Semiconducting Polymers

Fibrillar formation of the semiconducting polymers is another method used to develop controlled morphology of the active layer. P3HT is a polymer that can form crystalline fibrillar structures by solvent annealing or by casting from a marginal solvent such as *p*-xylene, 1,2-dichlorobenzene, or dichloromethane. Fibrils are typically about 10 nm to 20 nm in width and 5 μm to 10 μm in length, depending on aging time. This crystalline nanofibrillar structure shows improved charge mobility, a broader absorption region, and enhancement of the device efficiency.[11] TEM images of the P3HT nanowires film and the P3HT nanowires blended with PCBM were shown in **Figure 1.5**. It is

obviously seen that the preformed fibrils of the P3HT enhanced an interconnection network and the contact area between the P3HT nanowires and the PCBM.

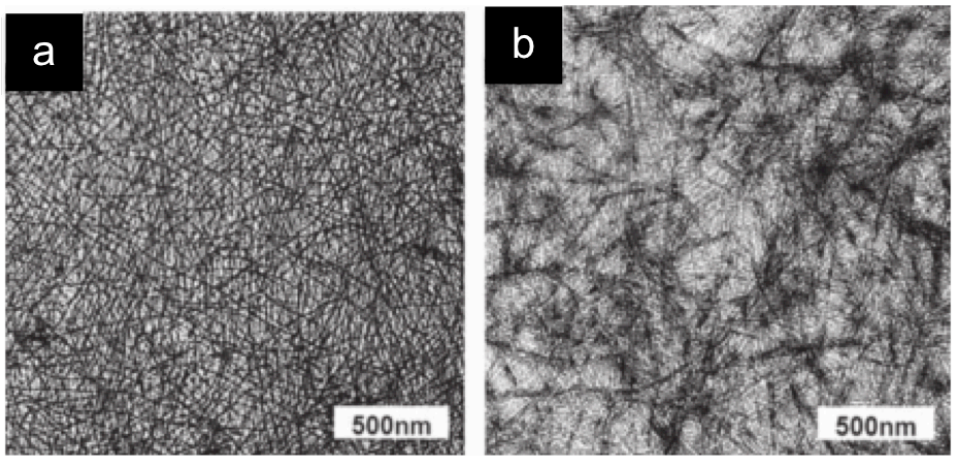

Figure 1.5 TEM images of the films of (a) P3HT nanowires, and (b) P3HT nanowires blended with PCBM.[11]

1.3.5 Nanoarchitecture

Other methods, such as patterning the active layer using nanoimprint lithography techniques, and anodization, are used to create continuous morphologies with precisely controlled sizes of the donor and acceptor materials. These techniques not only control the size of features in the blend but also the orientation of the materials. For example, **Figure 1.6(a)** showed nanoarchitecture of P3HT posts (80 nm in depth) formed by imprinting with a silicon master, and **Figure 1.6(b)** showed titanium nanotubes (20 μm in length) forming vertical array by anodization.

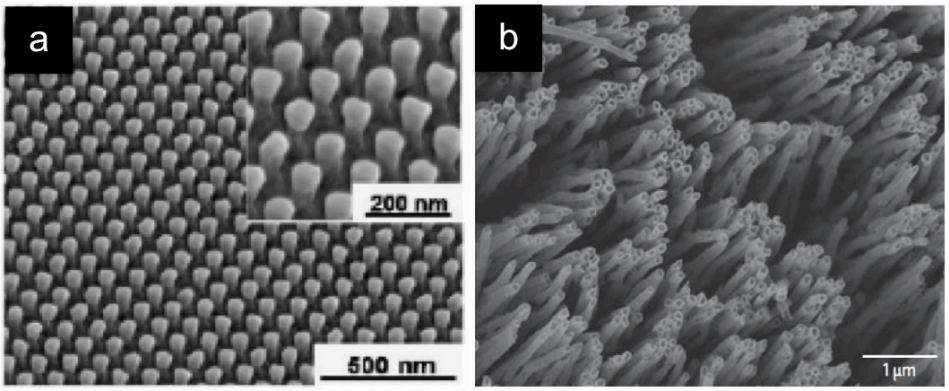

Figure 1.6 SEM images of (a) P3HT posts formed by imprinting with a Si master, and (b) a titanium nanotube array (pore size, 95 nm; wall thickness, 10 nm) formed by anodization.[12,13]

1.4 Semiconducting Polymers

To achieve the best device efficiencies, the active layer in PV devices is required to have a broad region of sunlight absorption and an optimized morphology of the donor and acceptor materials. Modification of the chemical structure and conjugation length of the conjugated polymers can be used to tune the optical properties. Moreover, addition of alkyl side chains solubilizes the polymers in several organic solvents, allowing the polymers to be processed with solution techniques. Appropriate solvents for solution casting are required to retain strong phase separation and to promote polymer chain packing.[2] Typical chemical structures that have been widely used in PV devices are shown in **Scheme 1.1**.

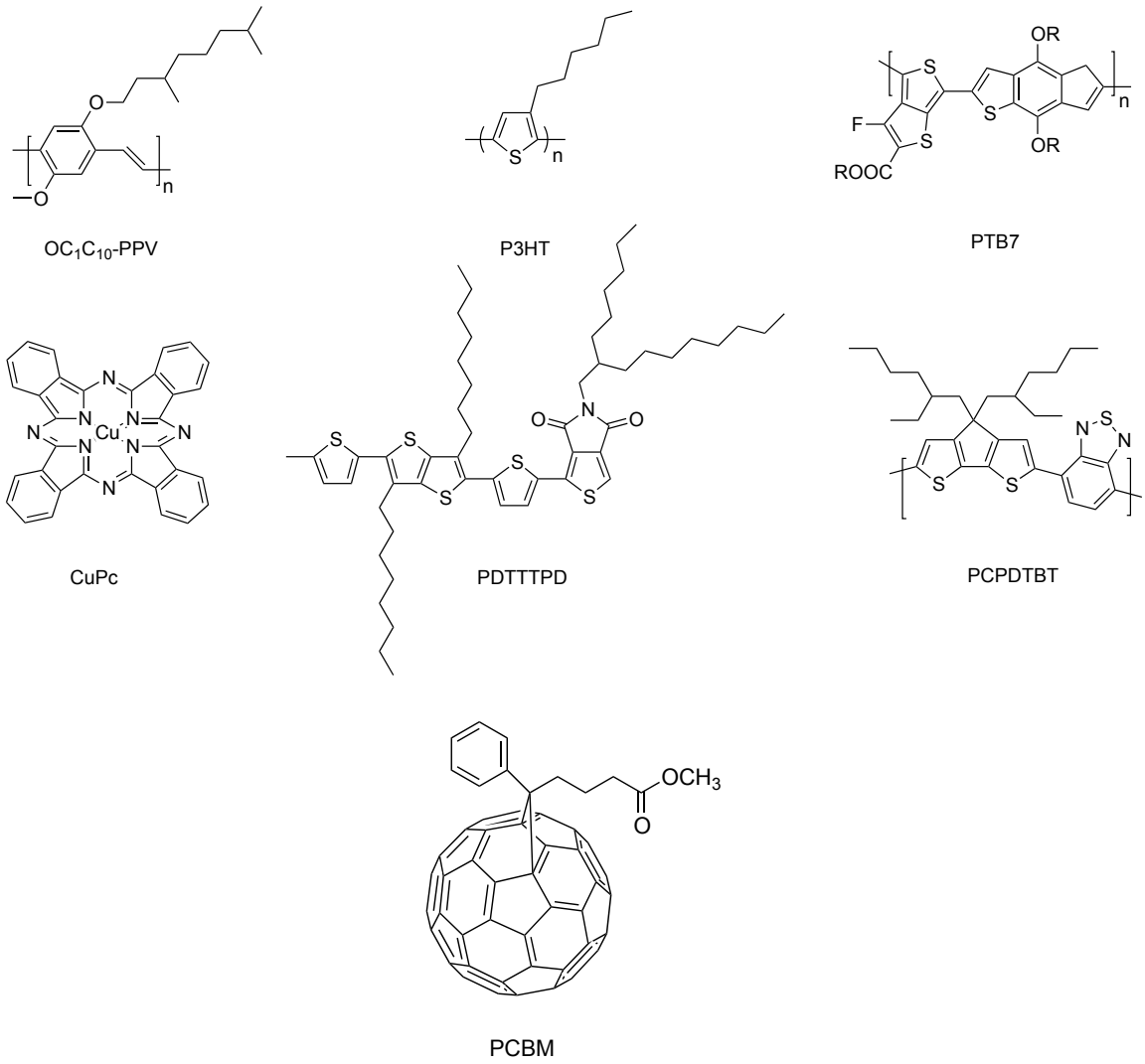

Scheme 1.1 Chemical structures for materials typically used as organic semiconductors.[2]

To select suitable donor materials, it is essential to consider both electronic properties (HOMO and LUMO levels) and hole mobility of the polymer. Among those polymers, P3HT has many advantages, such as environmental stability and a high hole mobility. The P3HT-PCBM blends have been systematically studied to optimize

parameters such as the solvent system, mixing ratio, and annealing to improve the morphology.[3]

1.5 Organic-Inorganic Hybrid Solar Cells

This thesis focuses on organic-inorganic solar cells employing semiconductor-sensitized quantum dots (*i.e.* CdSe QDs) to replace PCBM as the electron acceptor material. The inorganic NCs are beneficial components of PV cells for several reasons, including their high environmentally stability, low cost processibility, and the contribution of light absorption in the PV devices.[14] CdSe nanocrystals (NCs) are attractive for numerous materials applications, including biosensing,[15,16] light emitting diodes,[17,18] and photovoltaics.[19–21] The optical properties, such as the band gap and absorption profile, of the QDs can be altered by tuning their size and, to some degree, their shape during synthesis.[22,23] The shape of the NCs also influences the excited-state dynamics of the NCs. Nozik and coworkers reported that changing the diameter of CdSe nanorods (NRs) from 2.5 to 8.0 nm resulted in intraband energy relaxation 8 times faster than the smaller rods.[24] Three types of QD solar cell configurations utilizing inorganic particles as electron acceptors are metal-semiconductor junction, polymer-semiconductor, and semiconductor-semiconductor system, as shown in **Figure 1.7**.[25]

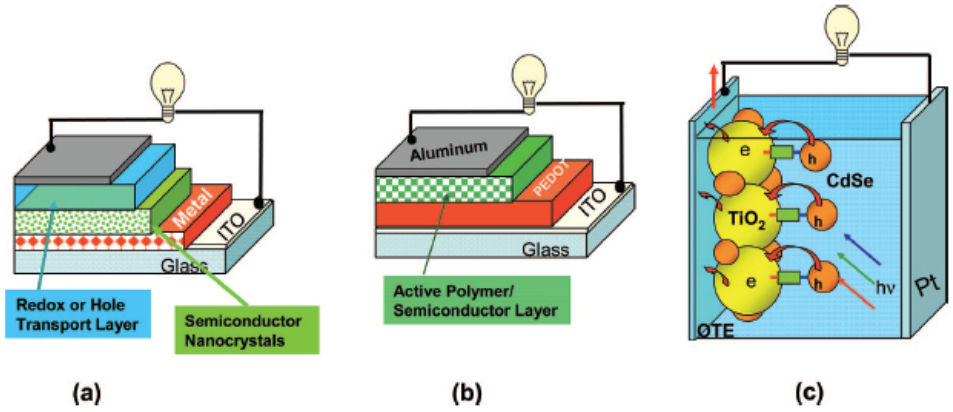

Figure 1.7 Schematic diagram of quantum dot based solar cells: (a) metal-semiconductor junction, (b) polymer-semiconductor, and (c) semiconductor-semiconductor systems.[7]

1.5.1 Photoelectrodes Composed of Quantum Dot Arrays

In this configuration, the monodisperse NCs are oriented into 3-dimentional arrays with small interparticle spacings, creating a superlattice with miniband energy level structure. This structure provides a multiple exciton generation (MEG) characteristic, where several electrons can be generated per one absorbed photon. The electrons are then transported along the 3D arrays due to strong electronic coupling between NCs.

1.5.2 Quantum Dots Dispersed in Organic Semiconductor Polymer Matrices

In this type, the QDs form intimate contacts with semiconducting polymers. The exciton formation occurs in the QDs upon the light absorption, generating holes that are transferred to the polymer phase. The electrons remaining in the QD phase diffuse through the NC percolation network and are collected at the cathode.

1.5.3 Quantum Dot-Sensitized Nanocrystalline TiO_2 Solar Cells

In this configuration, the QDs are used as dye molecules that are chemisorbed on the surface of nanocrystalline porous-TiO_2 layers. Upon light absorption, photoexcitons are generated in the QDs, and the electrons are transported from the excited state to the conduction band of TiO_2, and charge separation occurs. The QDs that have been reported in this type of solar cells are InP, CdSe, CdS, and PbS.

1.5.4 Polymer-Nanocrystal Blend

This thesis focuses on type II of the QD based solar cells. The energy level of CdSe NCs is appropriate to couple with most conjugated polymers, as shown in **Figure 1.8**. According to the energy band diagram, the P3HT-CdSe hybrid PV cells have the potential to provide high open-circuit voltages (V_{oc}), due to the relatively high conduction band of the two materials.[3] The CdSe NCs also show ultrafast photo-induced charge transfer to the polymers, reported to be on the order of picoseconds.[26] This fast charge transfer rate reduces the possibility of charge recombination. Therefore, employing CdSe NCs in PV devices promotes the generation of photocurrents within the active layer under visible light irradiation.[7] In hybrid materials for PV applications, CdSe NRs and tetrapods (TPs) are attractive electron acceptor materials because the long axes of the NRs provide both efficient exciton dissociation and an electron transport pathway. In principle, the dimensions of the NRs and TPs can be optimized for transport across the active layer for collection at the electrodes.[27–31] Controlling the size of CdSe NCs to the nanometer scale increases the polymer-semiconductor interfacial area, improving the power conversion efficiency of the PV devices.

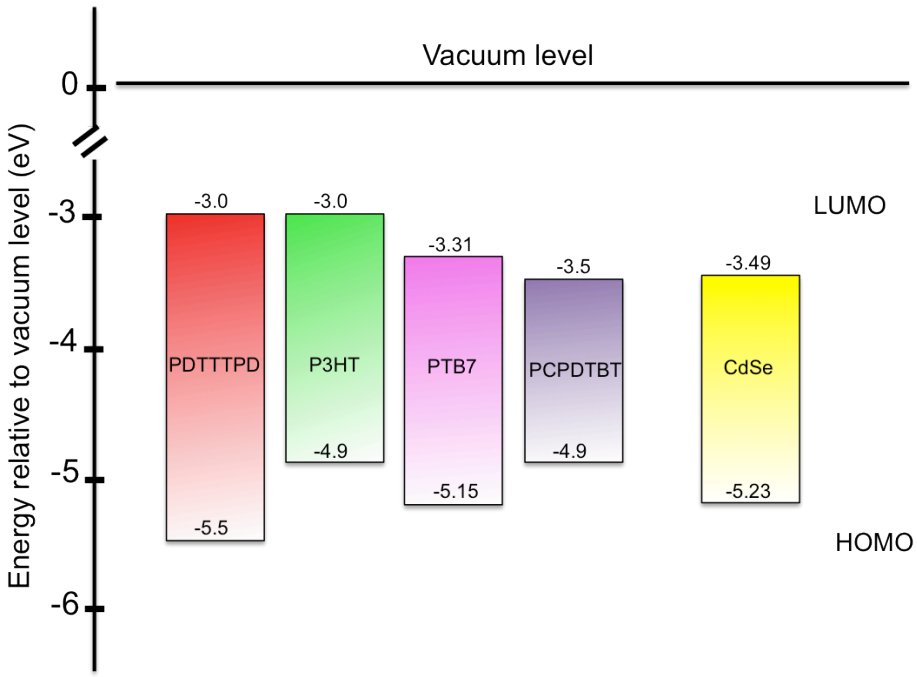

Figure 1.8 Energy band diagram displaying HOMO and LUMO levels of polymeric donor materials, and the valence and conduction band edge of several inorganic acceptors.[3]

Blending the CdSe NCs with polymers has been reported to broaden the light absorption region of the photoactive layer up to ~ 700 nm. In CdSe NC-poly[2,6-(4,4'-bis-(2-ethylhexyl)-4H-cyclopenta[2,1-b;3,4-b']dithiophene)-alt-4,7-(2,1,3-benzothiadia-zole)] (PCPDTBT) blend, 34% of the total absorption comes from the NCs. Dayal and coworkers also reported a significant enhancement in the PCE of BHJ PV devices fabricated from this CdSe-polymer blends. They introduced a low band gap polymer, PCPDTBT, as the electron donor, and CdSe tetrapods as the electron acceptor. The device achieved a PCE of 3.2%.[14] Alivisatos and coworkers reported the highest hole mobility from CdSe NRs blended with P3HT to be 0.1 $cm^2V^{-1}s^{-1}$. The devices made from 90 % CdSe NRs (7 nm x 60 nm) loaded in a P3HT matrix in a pyridine-chloroform

mixed solvent showed an external quantum efficiency over 54% with a PCE of 1.7 %.[21] Greenham and coworkers also reported the performance of PV devices containing 86 % CdSe NCs, where branched CdSe nanoparticles were used as the electron acceptor and were blended with poly(2-methoxy-5-(3',7'-dimethyl-octyloxy)-*p*-phenylenevinylene) (OC_1C_{10}-PPV). The device showed a PCE of 1.8 % under AM1.5 illumination.[19]

Another advantage of CdSe NCs is that they show an MEG characteristic, where in two or more pairs of excitons are generated per one absorbed photon, as described in **Figure 1.9**. Therefore, utilizing these NCs as electron acceptors has the potential to enhance the overall efficiency of the PV cells. This property is also observed in other types of quantum dots such as PbSe, CdSe, InAs, Si, InP, CdTe, and CdSe/CdTe core-shell QDs.[25]

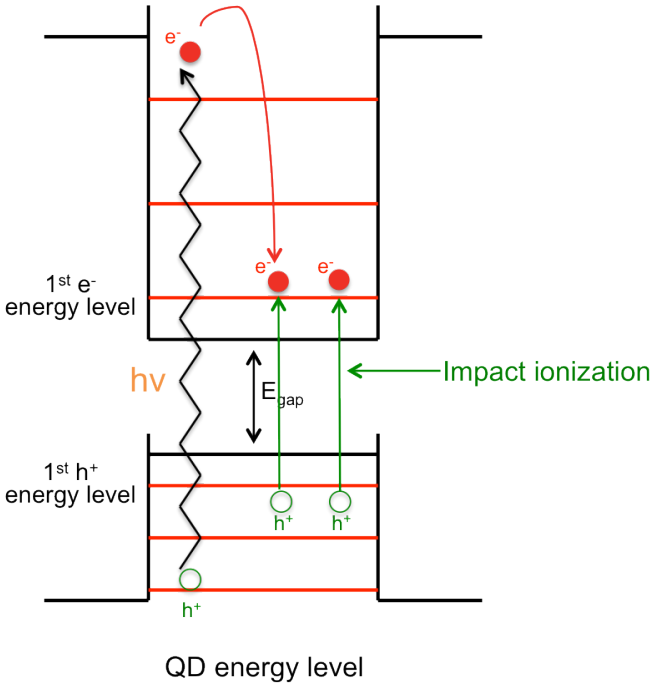

Figure 1.9 Multiple exciton generation in quantum dots.

However, one of the key factors to achieve the best performance from the hybrid organic-inorganic device is the surface chemistry of the NCs and the morphology of the photoactive layer.[3]

1.6 Evolution of CdSe Nanocrystal Synthesis

1.6.1 High Temperature Synthesis

Synthesis of CdSe NRs was first reported in 2000 using dimethyl cadmium, a very dangerous organometallic compound, as a precursor. Later, Peng and coworkers developed a new method, which is less expensive, and less toxic by using cadmium oxide as a precursor to synthesize monodisperse quantum dots and rods of CdTe, CdSe and CdS.[32] Among the tunable parameters in CdSe QD synthesis are the Cd:Se ratio, temperature, and choice of surface binding ligands. Reliable methods have emerged to afford nearly monodisperse nanoparticles of controllable shape and size.[32–35] Synthesis of the NCs typically requires precursors, surfactants, and solvents. In some cases, such as for the synthesis of CdSe NCs, the surfactants also serve as the solvent. The formation of the NCs starts from the nucleation step, where initial seeds are formed by thermolysis of the precursors at high temperature as high as 350 ˚C. In this step, the precursors need to decompose and react rapidly to form active seeds. Subsequently, the second precursor is injected rapidly into the hot solution to yield a super saturated solution. The seeds continue to grow and rearrange the constituent atoms during the hot annealing in the growth step forming crystalline solids, as shown in **Scheme 1.2**.[36] The growth of the NCs

can be monitor from the peak shifting in UV-Vis absorption, where the red shift occurs with an increase in diameter of the NC, **Figure 1.10**.

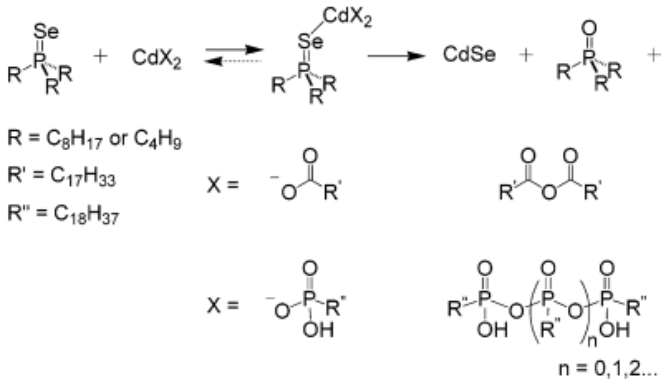

Scheme 1.2 Mechanism of synthesis of CdSe nanocrystal precursor with phosphine ligands.[37]

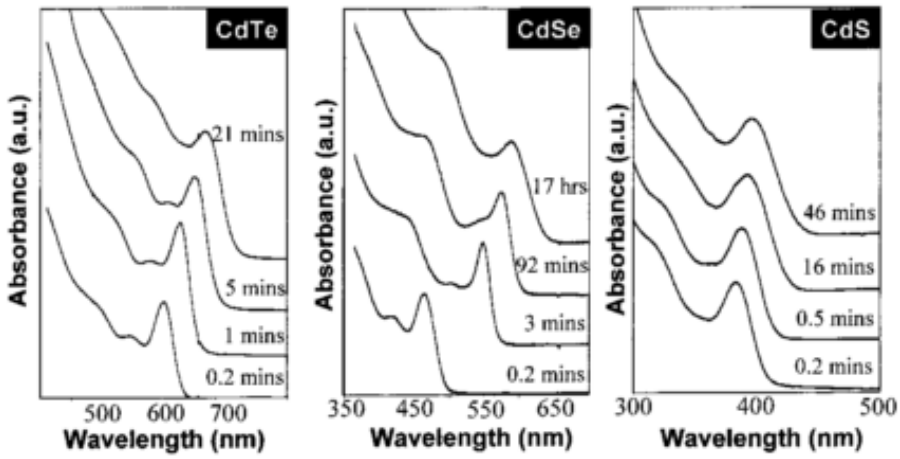

Figure 1.10 UV-Vis absorption spectra follows the size evolution of the nanocrystal, CdTe, CdSe, and CdS.[32]

The mechanism for controlling the size and shape of the NRs was also studied by Peng and Peng.[38] Their results indicate that precursor concentration is an important factor controlling the growth of NRs. The initial Cd to Se precursor ratio is a key factor to control the shape of NCs as well. Higher aspect ratio (AR) NRs can be obtained by increasing the ratio of Cd:Se precursors. At high precursor concentration, the growth of CdSe NRs is anisotropic with a unique *c*-axis (longitudinal axis) leading to the formation of Wurtzite structure, **Figure 1.11**. Increasing temperature of the solution decreases the stability of the intermediate complexes and reduces the number of surfactants bound to the NC surface. Therefore, a higher growth temperature is required in order to form longer rods as well as to limit the formation of branched NCs. However, too high of a temperature may lead to degradation of surfactant molecules and Ostwald ripening during the growth step.[36]

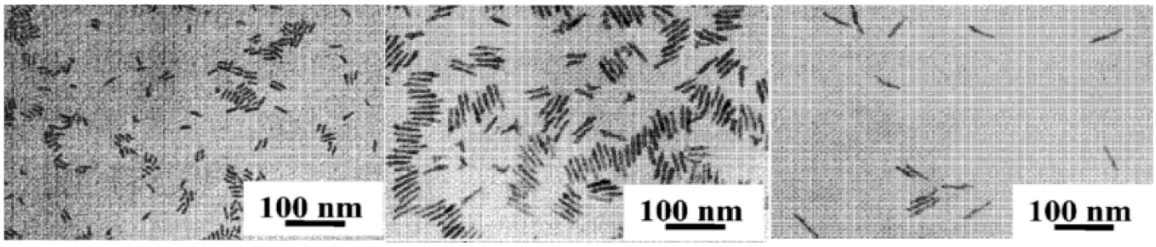

Figure 1.11 TEM images show the influence of the initial ratio of the Cd and Se precursors on the highest average aspect ratio of the resulting rods (from left-to-right, Cd:Se 1:5, 1:2, 5:1).[38]

A small amount of impurities and ligand type can affect the growth kinetics and the shape of the NCs.[39] As shown in **Figure 1.12**, shape of CdSe NCs can be altered by changing the length of alkylphosphonic acid ligands. Using short ligands for the synthesis

leads to formation of branched NRs, whereas long ligands provide mainly high AR NRs. CdSe nanowoires were synthesized using Bismuth as catalyst, and CdSe nanodiscs were formed when oleic acid was used as ligands. Other parameters such as reaction time, injection and growth temperatures, and number of injections can be varied to control size, AR and growth rate of the NRs.[40]

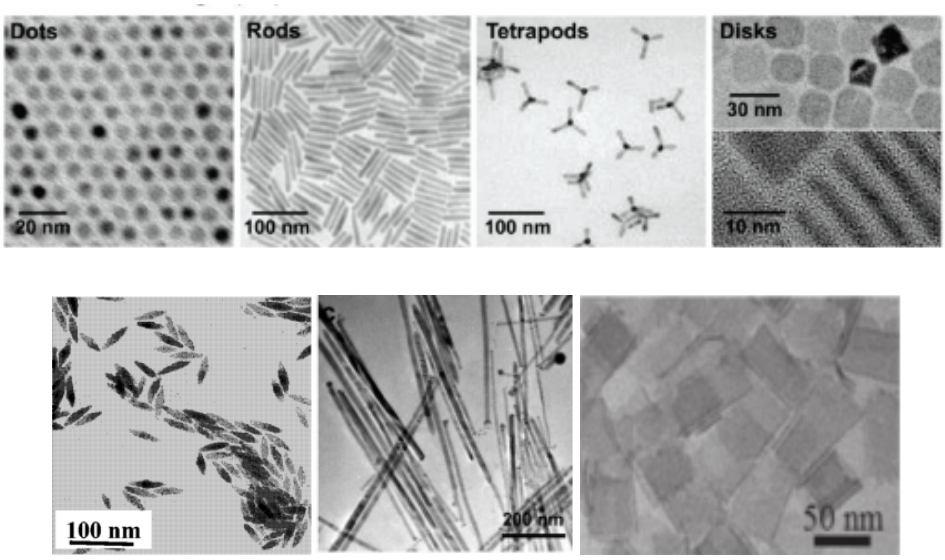

Figure 1.12 TEM images show different geometry of CdSe nanocrystals.[38,41–43]

1.6.2 Solvothermal Synthesis

Another route to synthesize CdSe NCs is a solvothermal method using $Cd(NO_3)$ or $CdCl_2$ and Se as precursors and ethylenediamine as both solvent and growth template. The precursor mixture and solvent template is allowed to react at 140 ˚C for 10-24 hours followed by precipitation. The as-prepared layered precursor is then hydrothermally treated at 120 ˚C for 12 hours to obtain CdSe NCs. The shape and size of the NCs can be controlled by adjusting the ratio of the precursors and temperature during crystallization.[44,45] However, the shapes and sizes of the NCs synthesized from this method are not well controlled. **Figure 1.3** showed two structures of the CdSe NCs,

wurtzite NRs zinc blend NPs, obtained from the solvothermal method using different precursor concentration.

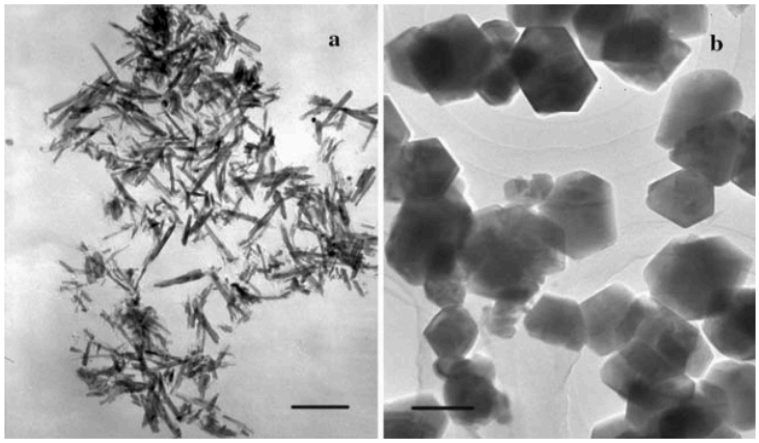

Figure 1.13 TEM images of (a) wurtzite CdSe nanorods, and (b) zinc blend CdSe nanoparticles synthesized by solvothermal method (bar = 100 nm).[45]

1.6.3 Microemulsion Synthesis

An alternative route to synthesize CdSe NCs is the microemulsion method. This technique overcomes several drawbacks from high temperature methods that require extremely dangerous reagents, accurate high temperatures, and high costs. In the microemulsion method, an anionic surfactant such as bis(2-ethylhexyl)sulfosuccinate, and a reducing agent, hydrazine acetate, are used to form water-in-oil microemulsions. The synthesis is done at 100 ˚C using $Cd(NO_3)_2 \bullet H_2O$ and Na_2SeO_3 as precursors, and water and n-heptane as solvents. The size and the shape, NRs or dendrites, of the NCs can be controlled by adjusting the ratio of the water and the surfactant, **Figure 1.14**. However, the details of the mechanism of NC formation from this method are still unclear.[46]

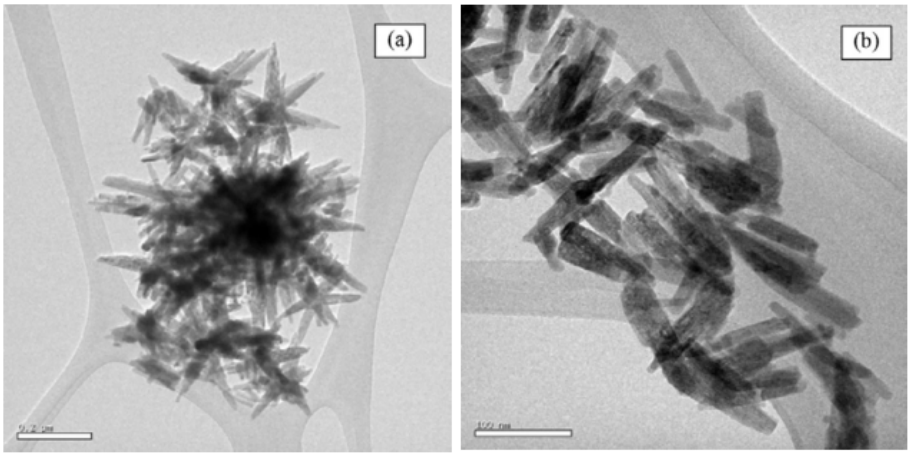

Figure 1.14 TEM images of as-prepared CdSe nanoparticles with different ratio of precursors synthesized from microemulsion method.[46]

1.7 Thesis Overview

There has been an increased interest in development of organic-inorganic solar cells due to high environmental stability and tunable optical properties of inorganic materials. However, recent research has been focused on NCs with complex structures involving multiple synthetic steps and complex methods to develop nanostructured architectures that are not suitable large scale production and require high processing cost.

This thesis describes the development of simple methods for the synthesis of size-controlled, high AR CdSe NRs and for the assembly of NRs into defined structures over large areas. By controlling the density, direction, and the length of the NRs used as well as the thickness of the active layer, the performance of organic-inorganic hybrid solar cells can be improved.

In Chapter 2, the synthesis of high AR CdSe NRs by optimizing the concentration of ligands and precursors is reported. Nearly monodisperse NRs were obtained with

lengths ranging from 16 nm to 120 nm and diameters ranging from 4 nm to 7 nm. The shape of all AR NRs was determined to be Wurtzite structure, which provides dipole moments appropriate for electric field-induced orientation.

In Chapter 3, two techniques for the assembly of NRs were developed. The effect of solvent choice, and electric field strength on the alignment of NRs, were investigated. The vertically ordered assembly of NRs over large areas is reported by combining controlled solvent evaporation techniques and the application of an electric field. The synthesis of oligothiophenes and polythiophenes containing variable functional groups for anchoring onto the NR surface is described. The synthesis of terthiophenes terminated with alkylchains and phosphine oxide functional groups is reported. The process of ligand exchange from the native ligands to functional conjugated polymer ligands and the vertical assembly of the functional NRs are reported.

In Chapter 4, synthesis of random copolymers and block copolymers of P3HT and polythiophene containing multiple functional groups on the side chains or on the chain end is described in details. The effect of molecular weight of the polymer, and location of the functional groups, on solubility and optical properties were studied. The process of ligand exchange on a specific location of the NRs is described. The end-to-end assembly of the functional CdSe NRs is reported by controlling the position of the functional group and the ratio of the two materials.

In Chapter 5, the assembly of polythiophene functionalized CdSe NRs on graphene sheets is described *via* π-π stacking of the polythiophene ligands with the 2-D planar conjugation structure of graphene. The goal of this experiment is to use the graphene as conjugating support to improve performance of the PV devices. Since

graphene shows highest mobility for electron and hole transport at room temperature, the assembly of polythiophene functionalized CdSe NRs is expected to enhance conductivity, improve exciton separation, and reduce possibility of charge recombination within the device.

The goal of this work is to create desired architectures from NR assemblies, where the NRs are in close contact with semiconducting polymer ligands. The controlled directional assembly of p-type/n-type materials will improve charge transfer between the two active layer materials as well as charge transport along the materials, which are both needed to yield high efficiency of organic-inorganic hybrid bulk heterojunction PV devices.

CHAPTER 2

SYNTHESIS OF HIGH ASPECT RATIO CDSE NANORODS

2.1 Introduction

2.1.1 1-Dimensional CdSe Nanocrystals

Due to their high photoluminescence quantum yield, semiconductor CdSe nanocrystals (NCs) have drawn significant interest in research towards biosensors,[15,16] light emitting diodes,[17,18] and photovoltaics (PV).[19–21] By altering the size and shape of the NCs, their optical and electronic properties, such as band gap and conductivity, can be tuned.[22,23] Therefore, 1-dimensional (1D) and 3-dimensional (3D) NCs, such as nanowires, nanorods (NRs), and tetrapods (TPs) are desirable for photovoltaic applications due to their unique inherent shapes. Compared with spherical NCs (0D), the 1D and 3D crystal structures provide a direct pathway for electron transport along the *c*-axis, and therefore are beneficial for use as electron acceptors. In principle, the dimensions of the NRs and TPs can be optimized to facilitate transport of electrons across the active layer for charge collection at the electrodes.[14,20,21,28–31]

In 2002, Alivisatos and coworkers introduced 1D NCs into PV device fabrication to study the effect of elongated NCs on electron transport. In their devices, CdSe NRs (60 nm x 7 nm) blended with poly(3-hexylthiophene) (P3HT) was solution cast from a chloroform-pyridine mixture to form the active layer. TEM images of the films showed better connectivity of the NCs when CdSe quantum dots (QDs) (7 nm x 7 nm) (**Figure 2.1(a)**) were replaced with CdSe NRs (**Figure 2.1(b)**). A development of network

percolation led to higher external quantum efficiency (EQE) and increasing of the optimized film thickness.[21,47]

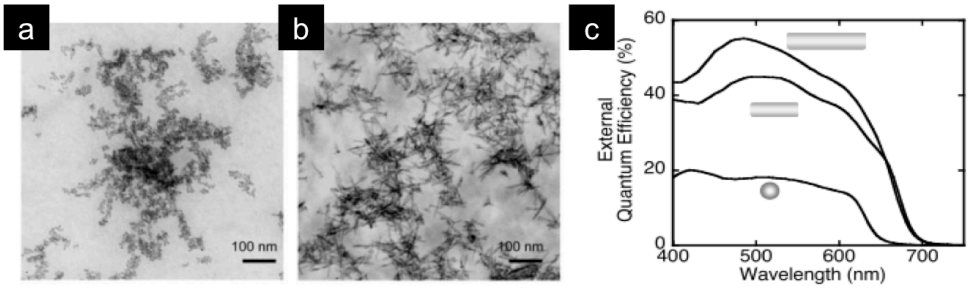

Figure 2.1 TEM images of P3HT-20 wt% CdSe nanocrystal blends and external quantum efficiency spectra of CdSe quantum dots and nanorods.[21]

Dayal *et al.* studied effect of NC shape on the performance of PV devices by blending either CdSe QDs, NRs, or TPs with P3HT. The results showed that the devices fabricated from CdSe TPs and NRs have higher maximum EQE compared to those fabricated from CdSe QDs (43%, 36%, and 5%, respectively).[27] Additionally, they found that the shape of the NCs to strongly effect device performance. When CdSe NCs were blended with P3HT, a PCE of 1.49 % was obtained from TPs, 1.1% from NRs, and 0.066% from QDs. The authors concluded that the NR and TP shape provides a superior conduit for the electrons to mobilize from the dissociation site, as well as an improvement in the active layer morphology that facilitates carrier percolation, resulting in better device performance. An additional advantage of 1D and 3D NCs that provides an enhancement of device performance is that the NRs and TPs lie partially perpendicular to the substrate rather than parallel to the substrate. This orientation of the electron acceptor, where its long axis is perpendicular to the electrode, provides a more direct pathway for electron transport from the active layer to the electrode. A similar result was

observed by Sun and coworkers when CdSe NRs blended with poly(phenylenevinylene) derivative were replaced with TPs, the latter device achieving a PCE of 1.8%.[19]

Banin and coworkers studied confinement effects on the molar absorption coefficient of CdSe NRs. The length of CdSe NRs is larger than the exciton Bohr radius and the quantum confinement, therefore the CdSe NRs with similar diameters showed similar band gaps. However, NRs with different length but similar diameters showed a linear dependence of the molar absorption coefficient on the length of the NRs due to the larger in the volume of the longer NRs.[48] Cunningham *et al.* explored the dependence of the NR aspect ratio (AR) on the cross-sectional absorption. They reported an increase of the anisotropy of the absorption with an increase of the NR AR from 1 to 4 due to changes in dielectric constants and quantum confinements. The anisotropic absorption remained constant for longer NRs (AR 8).[49] Another advantage of 1D CdSe NCs over spherical QDs is their unique ability to form multiple exciton dissociations, due to the combination of ultrafast electron transfer and reduced Auger recombination in 1D CdSe NCs. Compared with QDs, the CdSe NRs generated and transferred more than 21 electrons per electron acceptor molecule under high excitation intensity, when only 4 electrons per electron acceptor were generated from the CdSe QDs.[50]

2.2 Effect of Synthetic Parameters on the Shape and Size of CdSe Nanorods

CdSe NRs were synthesized by the high temperature method reported by Peng and Peng,[32] where cadmium oxide (CdO) and selenium (Se) were used as precursors, and tetradecylphosphonic acid (TDPA) and trioctylphosphine oxide (TOPO) were used as ligands. In this case, TOPO also served as the solvent. The Cd-phosphonic acid precursor

was formed at high temperature (~320 ˚C), and stabilized by aging under nitrogen (N_2) atmosphere for 24 h. The Se-precursor solution was prepared separately, with tributylphosphine (TBP) as the ligand and toluene as the solvent. The Se-TBP precursor was then injected into a hot solution of the Cd-precursor at 320 ˚C. During this step, the seeds of the Cd-Se NCs were generated. The growth process of the NCs was controlled at 250 ˚C, and the NC seeds grew by the Ostwald ripening process. The aging of the Cd precursors at room temperature is a very crucial step in order to obtain high AR NRs. During this step, Cd-TDPA complexes are formed which are more stable than the precursor-seeds without aging.[38] The stable complexes slow down the nucleation and growth process such that it is suitable for the growth of anisotropic nanostructures. Peng and Peng reported the dependence of NR length on the precursor history. Injection of the Se-precursor without the aging step resulted in short NRs with an AR of about 3, whereas aging the precursor at room temperature for 3 days led to longer NRs (AR 6.5) due to the significantly slower growth rate. The CdSe NRs were collected by precipitation in methanol, followed by washing with chloroform ($CHCl_3$) three times. ^{1}H and ^{31}P nuclear magnetic resonance (NMR) spectroscopy of dried NRs indicated the presence of a mixture of ligands (TDPA and TOPO) on the surface of the CdSe NRs. Since the protons of TOPO and TDPA have similar chemical environments, the peaks overlap in the spectrum, making it difficult to use ^{1}H NMR spectroscopy to identify the major ratio of each ligands, as shown in **Figure 2.2**. However, the phosphorous peak in the ^{31}P NMR spectrum of these ligands appear at different chemical shifts (δ_{TOPO} 48 ppm, and δ_{TDPA} 25 ppm), therefore these peaks can be used to determine the ratio of ligands on the surface of the NRs. By comparing the ^{31}P NMR spectrum of dried CdSe NRs with the spectrum of

free ligands, it is obvious that the majority of ligands on the surface of the NRs are TOPO.

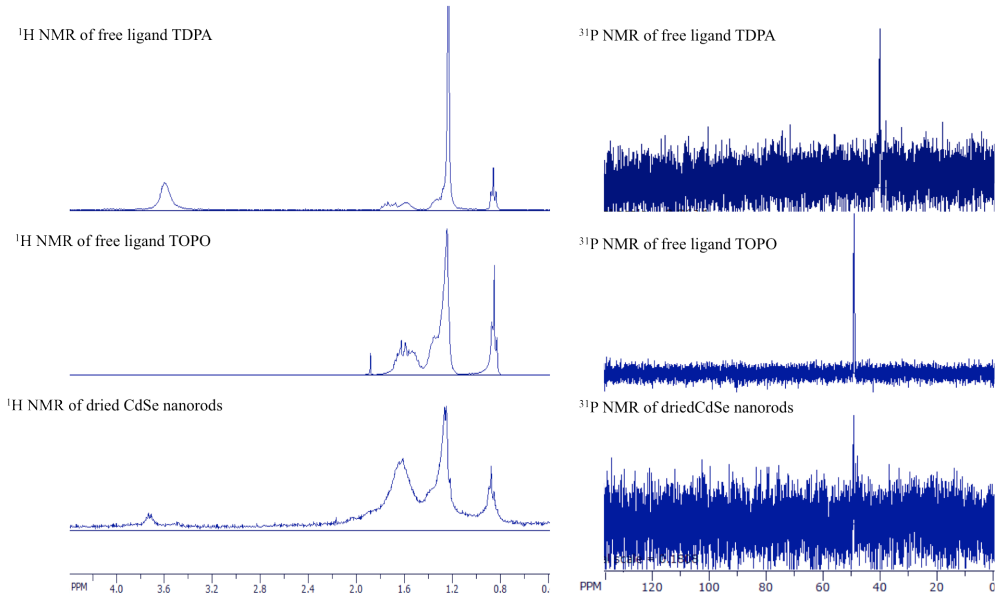

Figure 2.2 ^{1}H and ^{31}P NMR spectra of free ligands (TDPA and TOPO) and dried CdSe nanorods.

The NRs were dispersed in $CHCl_3$ and the optical properties of the CdSe NRs were studied. UV-Vis spectroscopy and photoluminescence of the NR solution showed a maximum absorption peak at 598 nm and a maximum fluorescence peak at 620 nm, **Figure 2.3**.

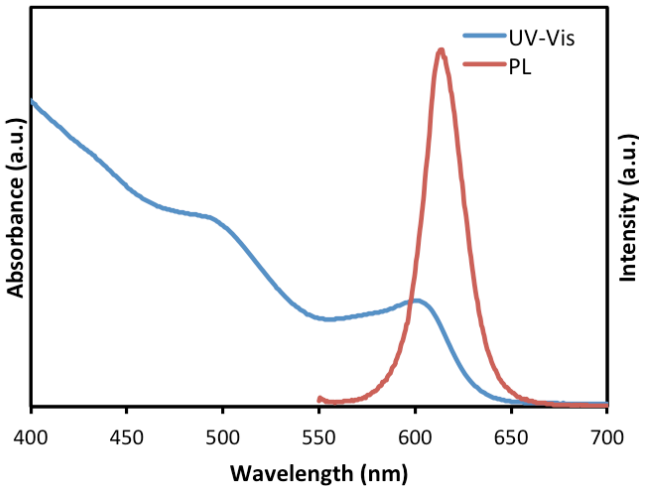

Figure 2.3 Optical properties of CdSe nanorods (16 nm x 4 nm).

TEM images, **Figure 2.4(a)**, revealed monodisperse CdSe NRs with 4 nm in diameter and 16 nm in length (AR 4). However, in some batches, CdSe tripods was observed, having a similar diameter as the NRs and an arm length ~ 7 nm, **Figure 2.4(b)**. The synthesis of branched CdSe NRs was reported by Wang *et al.* by replacing TDPA with hexylphosphonic acid or diethyl-1-tetradecylphosphonate.[51] However, the branching of the NRs obtained from that technique was not controllable, whereas symmetrical CdSe tripods were obtained in this case.

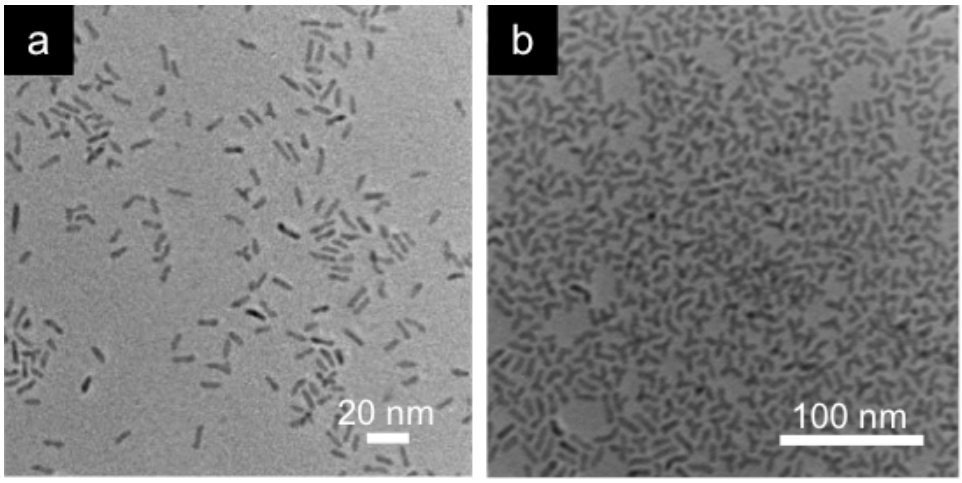

Figure 2.4 TEM images of CdSe nanorods (16 nm x 4 nm) and tripods (7 nm x 4 nm).

2.2.1 Effect of Precursor Concentration

This thesis focuses on CdSe NRs for PV applications, therefore the length of NR is required to suite thickness of the active layer of the PV devices. To increase the length of the NRs, several parameters were studied: (1) the concentration of the Se-precursor, (2) the concentration of the Cd-precursor, (3) the temperature during the growth process, and (4) the concentration of the ligands. Peng and Peng reported the dependence of the shape and size of CdSe NRs on the Cd:Se precursor ratio, finding that an increase of the initial Cd to Se ratio from 0.5:1 to 5:1 resulted in an increase of the NR AR from 6 to 8.

To increase the length (and AR) of the NRs, the Se-precursor solution was injected into the Cd-precursor at multiple time intervals, similarly as reported by Peng and Peng.[38] The Se solution, for subsequent injections, was a mixture of Se and trioctylphosphine (TOP), and was divided into aliquots for drop-wise injections at certain time intervals. Addition of the secondary solution provided an excess of Se in the system,

and suppressed the growth rate of the short axis of the NRs. **Figure 2.5** compares the sizes of the CdSe NRs prepared by multiple injections of the Se solution (**Figure 2.5(b)**) to those prepared by a single Se injection (**Figure 2.5(a)**). The length of the NRs increased from 16 nm in the case of a single Se injection to 62 nm with multiple injections.

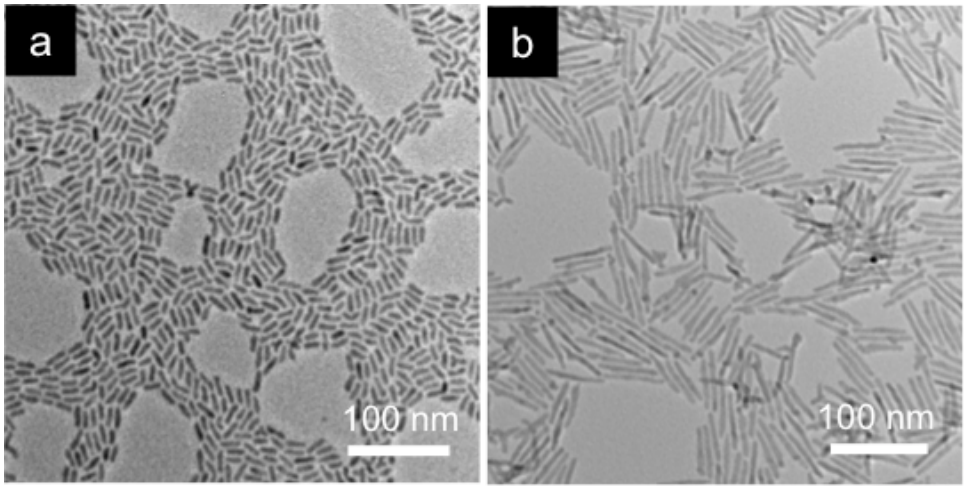

Figure 2.5 TEM images of CdSe nanorods from (a) single Se injection (16 nm x 4 nm), and (b) multiple injections (62 nm x 6 nm).

Given that multiple Se injections resulted in longer NRs, the effect of the duration between each injection during the growth process was studied. As shown in **Figure 2.6**, when the time interval of each injection was increased from 10 minutes to 20 minutes, the length of the CdSe NRs slightly increased from 58 nm to 62 nm, with a slight difference in diameter.

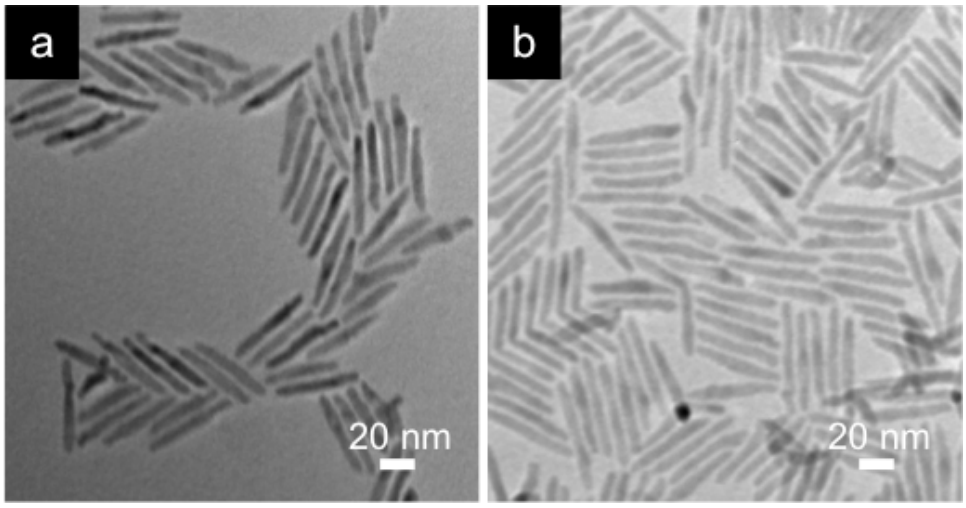

Figure 2.6 TEM images of CdSe nanorods prepared by using different time intervals between Se injections, (a) every 10 min (58 nm x 7 nm), and (b) every 20 min (62 nm x 6 nm).

Another attempt to achieve high aspect ratio NRs was to control the amount of nuclei generated during the first stage of NR synthesis. With the limited amount of initial concentration of Se, less nuclei consumed the remaining Cd and Se in solution, leading to the growth of high aspect ratio NRs. The Se-precursor was reported to be more active (absorbs faster to the growing nuclei) than the Cd-precursor. A high concentration of the Se-precursor in the initial solution accelerates the nucleation process, and as a result, more nuclei were generated. As mentioned above, an increase in the Cd:Se ratio in the initial solution increased the length of the NRs such that the AR increased from 6 to 8. Here, the effect of the Cd-precursor concentration was studied within the multiple Se injection procedure. The dependence of precursor concentration on the length of the NRs was studied by adjusting the concentration of the Cd-precursor. However, TEM images

(**Figure 2.7**) reveal that too high of a concentration of the Cd-precursor at the initial stage led to the formation of tripod and triangular NCs (**Figure 2.7(b)**).

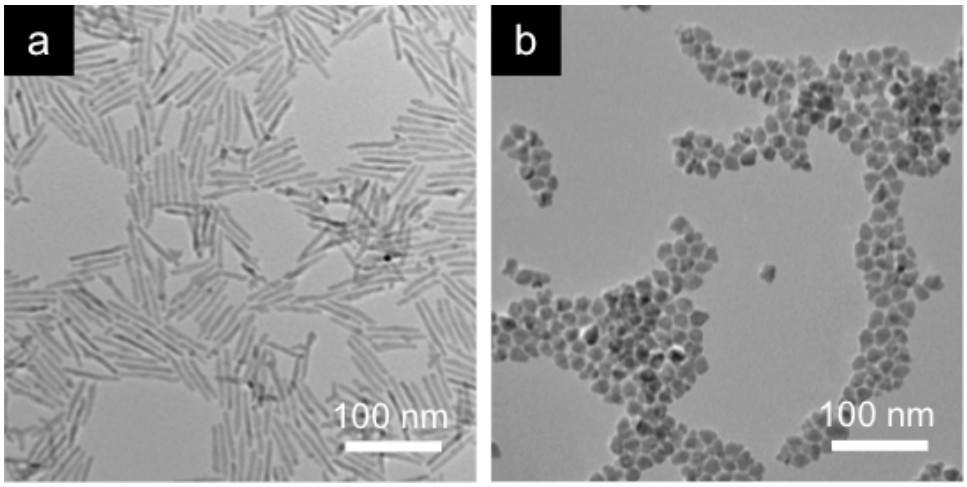

Figure 2.7 TEM images of CdSe nanorods synthesized from multiple injections technique with different Cd:Se ratio (a) 5:1, (b) 7.5:1.

2.2.2 Effect of Growth Temperature

The effect of growth temperature on the size of the NRs was also studied. In these experiments, instead of reducing temperature from the injection temperature (350 ˚C) to 250 ˚C after the Se-precursor injection, the temperature was kept constant at the injection temperature throughout the growth process. The TEM images show that the CdSe NRs synthesized at high growth temperature resulted in polydisperse NRs with several shapes, including rectangular, spherical, bullet-like, and triangular structures (**Figure 2.8**). High temperature accelerated the growth rate of the NCs in all three directions, leading to the loss of control of NR shape.

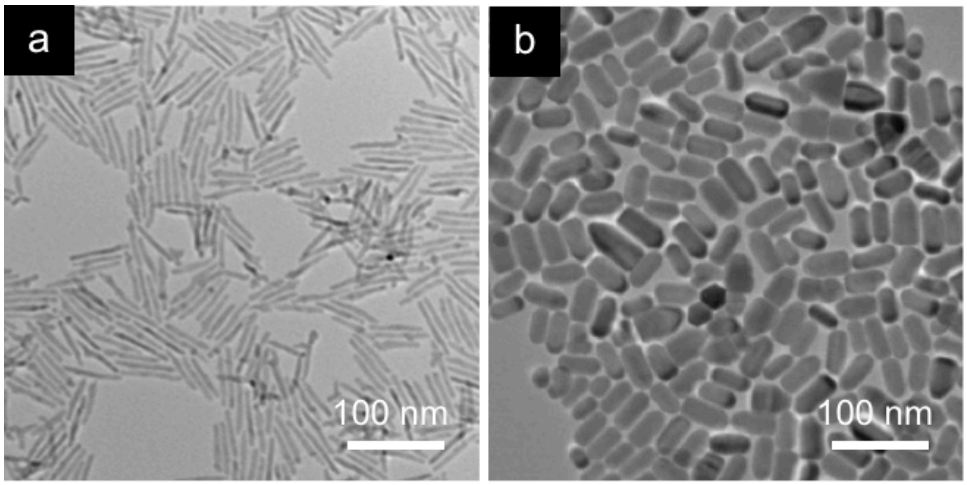

Figure 2.8 TEM images of CdSe nanorods synthesized at different growth temperatures (a) 250 ˚C, (b) 350 ˚C.

2.2.3 Effect of Ligand Concentration

Not only the concentration of the precursors, but also the type and concentration of the ligands play an important role on the NC shape. During the growth process, the terminating facets in the (001) direction of the NCs coordinated with the phosphonic head groups of TDPA. Controlling the ratio of the ligands having different binding abilities also affects the rate of the monomer diffusion along the *c*-axis (longitudinal axis) of the NCs. **Figure 2.9** shows the effect of TDPA concentration on the length of the CdSe NRs. Since TDPA preferentially binds to the surface of the short axis of the NRs (binding energy ~1.2-1.4 eV to the short axis, and ~0.8 eV to the long axis),[52] dense packing of the ligands on the surface suppressed the growth of the NRs in the direction of the short axis. Therefore, increasing the concentration of TDPA led to the formation of higher AR NRs.

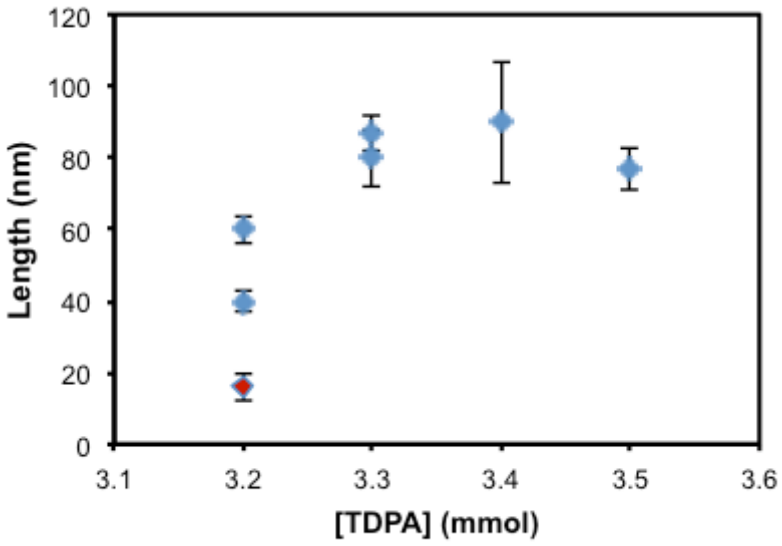

Figure 2.9 Dependence of the length of CdSe nanorods on the concentration of TDPA ligands (a red spot represents the nanorods obtained from a single injection technique).

TEM images show the narrow size distribution of CdSe NRs synthesized using various concentrations of TDPA, with ARs ranging from 4 to 17 (Figure 2.10). The ligand concentration strongly affects only the length of the NRs; while the length of the NRs varied from 40-120 nm, the diameters of the NRs obtained from each set of conditions remained approximately the same (6-7 nm). Increasing the concentration of the ligands also does not affect the shape of the NCs, as the TEM images reveal that monodisperse NRs were obtained from all conditions and other structures were not observed (**Figure 2.10**).

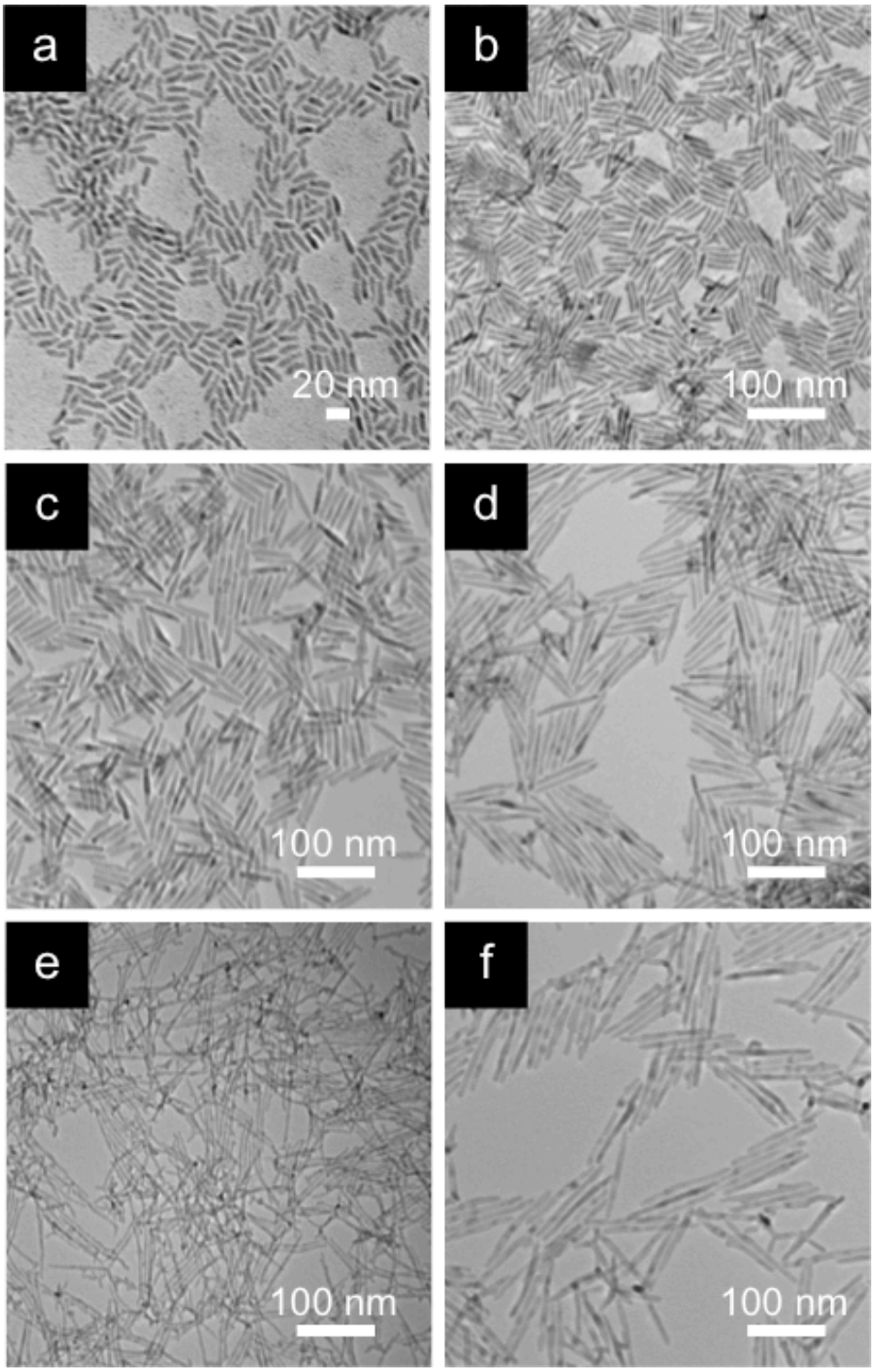

Figure 2.10 TEM images of of CdSe nanorods synthesized using different concentration of TDPA ligands (a) 3.2 mM (single injection), (b) and (c) 3.2 mM (multiple injection), (d) 3.3 mM, (e) 3.4 mM, and (f) 3.5 mM.

2.2.4 Optical Properties of CdSe Nanorods

After optimizing the procedure for obtaining CdSe NRs with different ARs, the optical properties of CdSe NRs with different ARs were studied. In **Figure 2.11**, a UV-Vis absorption spectra of the CdSe NRs show no dependence of the absorption on the length of the NRs when the length of the NRs exceeds the exciton Bohr radius and the quantum confinement.[48] The absorption of CdSe NRs was found only to depend on the NR diameter. The maximum absorption peak of the CdSe NRs having a diameter of 6 nm appears at 635 nm, whereas the maximum absorption peak red shifted for the NRs with a diameter of 7 nm. However, NRs with different lengths showed different PL characteristics (**Figure 2.11(b)**). NRs with smaller diameters showed maximum fluorescence peaks at 626 nm (60 nm x 6 nm) and 672 nm (90 nm x 6 nm), largely blue shifted compared to CdSe NRs with a larger diameter (7 nm). Considering NRs with similar diameters but different lengths, it is obvious that the maximum fluorescence peaks of the longer NRs show a large red shift, ~ 46 nm, when the length increased from 60 nm to 90 nm and from 40 nm to 90 nm. The red shift of the maximum fluorescence peak of the high AR NRs is due to the increased volume of the NRs.

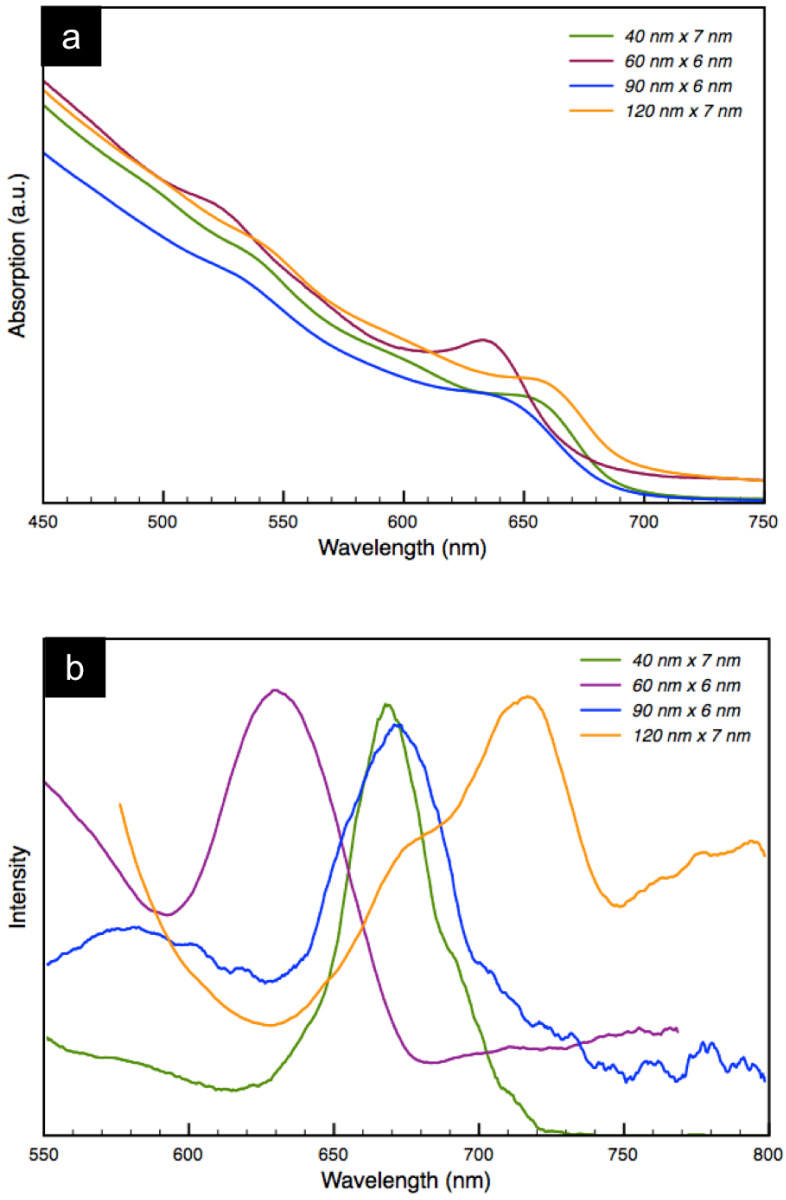

Figure 2.11 UV-Vis absorption (a), and photoluminescence (b) spectra of CdSe nanorods with different aspect ratios.

2.2.5 Crystal Structure of CdSe Nanorods

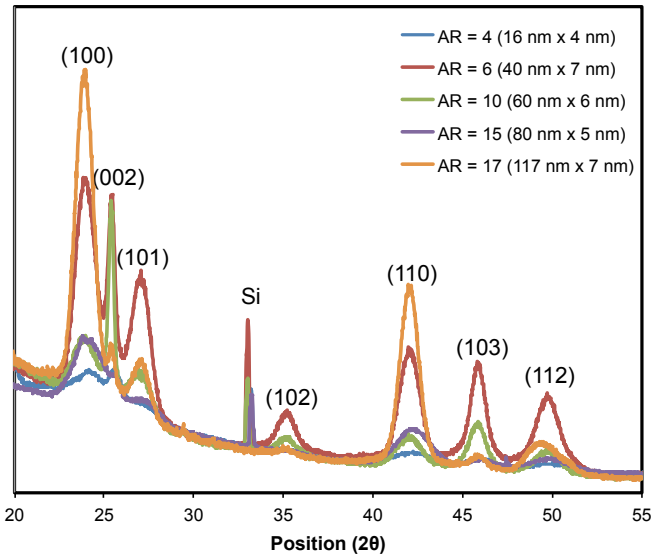

Figure 2.12 XRD patterns of CdSe nanorods with different aspect ratio (AR = 4, 6, 10, 15, and 17).

Powder X-ray diffraction (XRD) was used to characterize the crystal structure of NRs of different length. The samples were prepared by drop-casting the NR solution on clean silicon wafers. XRD patterns of NRs (**Figure 2.12**) having five different ARs showed similar patterns that indexed as Wurtzite structures.[53] The (002) reflection is more intense and significantly narrower than the other peaks, indicating that NR growth occurs along the *c*-axis of the hexagonal lattice. However, the ratios of peak intensities varied, which could arise from a variation in the orientation of NRs in the scattering volume or from stacking faults in the crystal. The strong reflection at $2\theta \sim 32^{\circ}$ is the (100) reflection from the silicon substrate.

2.3 Summary

In summary, the synthesis of high AR CdSe NRs was reported using modified multiple injection procedure. The concentration of ligands, Cd and Se precursors, and the temperature during the growth process were optimized to obtained monodisperse NRs with lengths ranging from 16 nm to 120 nm and diameters ranging from 4 nm to 7 nm. The optical properties of the NRs were studied showing no dependence of the absorption on the length of the NRs only to depend on the NR diameter. The crystal structure of NRs of different length was determined to be Wurtzite structure providing dipole moments appropriate for electric field assisted orientation reported in the next chapter.

2.4 Experimental Section

2.4.1 Materials

Cadmium Oxide (> 99.99%) (CdO), *n*-Tetradecylphosphonic acid (98%) (TDPA), selenium powder (99.999%) (Se), 2,5-dibromothiophene, tetrakis(triphenylphosphine) palladium(0), and *n*-butyllithium (2.5 M in hexane) were purchased from Alfa Aesar. Trioctylphosphine oxide (99%) (TOPO), tributylphosphine (TBP), trioctylphosphine (97%) (TOP), 2-(tributylstannyl)thiophene, 1-bromooctane, diethyl chlorophosphate, lithium diisopropylamide solution (2.0 M in THF) (LDA), and all other reagents were purchased from Sigma Aldrich. Tetrahydrofuran (THF) was distilled over sodium and benzophenone. All other reagents were used as received.

2.4.2 Synthesis of CdSe nanorods

CdSe NRs were synthesized following a previously reported method.[38] Briefly, CdO (0.20 g, 1.56 mmol), TDPA (0.89 g, 3.20 mmol) and TOPO (2.90 g, 7.50 mmol) were added to a 50 mL 3-neck round bottom flask and heated to 100 ˚C under vacuum. After 20 minutes, the flask was heated to 320 ˚C under nitrogen (N_2) atmosphere until the solution turned colorless. The solution was allowed to cool to room temperature, and was kept there for 24 h. In a N_2-filled glove box, a selenium solution was prepared by mixing Se (0.03 g, 0.38 mmol), TBP (0.23 g, 1.14 mmol), TOP (1.45 g, 3.91 mmol) and anhydrous toluene (0.35 mL) in a septum-capped vial. The solution was dissolved by ultra-sonication for 5 minutes, and then rapidly injected into the Cd-precursor solution at 320 ˚C. The temperature was allowed to cool to 250 ˚C and kept at this temperature throughout the growth process. The selenium solution, for subsequent injections, was prepared by mixing Se (0.32 g, 4.05 mmol) and TOP (2.68 g, 7.23 mmol) in a sealed vial. This solution was divided into aliquots (0.6 mL) for drop-wise injections every 20 minutes. After the last injection, the solution was cooled to 50 ˚C and a mixture of anhydrous toluene (5 mL) and anhydrous methanol (MeOH, 10 mL) was added to precipitate the NRs. The NR solution was centrifuged and the NRs washed by dispersion in $CHCl_3$ (3 mL) and subsequent precipitation in anhydrous MeOH (12 mL). The washing step was repeated three times to remove excess surfactant. CdSe NRs were re-dispersed in $CHCl_3$ and kept in a vial under N_2 atmosphere.

2.4.3 Characterization

Powder X-ray diffraction patterns were recorded on a PAN analytical X'Pert Material Research Diffractometer. The dimensions and assemblies of NRs were determined by transmission electron microscopy (TEM) (JEOL 2000FX), with an accelerating voltage of 200 keV and by scanning electron microscopy (SEM) (FEI Magellan 400). TEM samples were prepared by drop-casting a solution of CdSe NRs solution on a copper grid. Grazing-incidence small-angle X-ray scattering (GISAXS) measurements were performed on Beamline 7.3.3 at the Advanced Light Source (ALS) at the Lawrence Berkeley National Laboratory. Absorption and fluorescence measurements of CdSe NR solutions were performed using a Perkin-Elmer Lambda 25 UV/Vis spectrometer and a LS 55 Luminescence spectrometer, respectively. Nuclear Magnetic Resonance (NMR) spectra were obtained on a Bruker DPX-300 NMR spectrometer. Gel permeation chromatography (GPC) was performed relative to polystyrene standards on a Polymer Laboratories PL-220 high temperature GPC equipped with a refractive index detector. 1,2,4-Trichlorobenzene was used as the eluent.

CHAPTER 3

VERTICAL ASSEMBLY OF CDSE NANORODS

3.1 Introduction

3.1.1 Directional Orientation of Nanorods

As discussed in the previous chapter, the optical and electronic properties of CdSe nanocrystals (NCs) such as the band gap and the conductivity can be tuned by adjusting the size and shape of the NCs.[22,23] For photovoltaic applications, one-dimensional and three-dimensional NCs such as nanowires (NWs), nanorods (NRs), and tetrapods (TPs) are suitable to be used as electron acceptors because of their unique inherent shape. As shown in **Figure 3.1**, the longitudinal axes of these crystal structures provide a continuous pathway to transport the generated electrons from the active layer directly to the electrode, reducing the possibility of charge recombination, whereas electron hopping is required when spherical nanoparticles are used as electron acceptors.[20,21,28–30] Vertical arrays of high aspect ratio (AR) semiconductor NWs on the electrode were reported to increase light absorption along the long axis of the NWs and facilitate charge diffusion along the short axis to the donor-acceptor junction, leading to an improvement in the fill factor compared to planar junction devices.[54] Moreover, the dimensions of NWs, NRs, and TPs can be modified to suit the thickness of the active layer to facilitate transportation of the electrons to the electrode.[14,28–30,55]

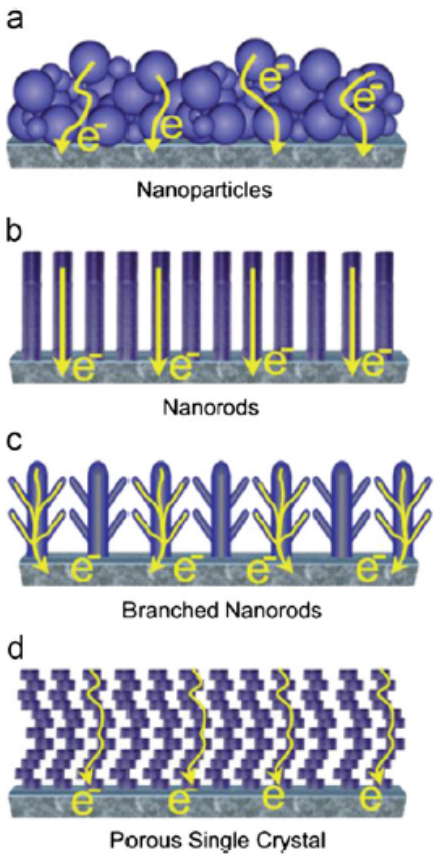

Figure 3.1 Schematic representation of the possible electron path on different nanostructured electron acceptors made with (a) nanoparticles, (b) nanorods, (c) branched nanorods and (d) a porous single crystal.[56]

To improve the performance and facilitate the application of NCs, the long-range ordering of NC assemblies is necessary, with control of the direction and the inter-particle distance. Close packed NRs standing normal to the underlying substrate are expected to improve the efficiency of NR-based photovoltaics (PV), since the density of the NRs per unit area is maximized.[57,58] m

3.1.2 Electric Field Assisted Assembly of Nanorods

According to Alivisatos and coworkers, the CdSe NRs are aligned under an applied EF due to the generation of a dipole moment along the long-axis of the rods.[65] Applying EF to aggregates of rods generates rotation along the short axis, and together with solvent evaporation, the NRs assemble into close-packed hexagonal arrays, the lowest energy configuration. This technique has been reported to assemble CdS NRs (30 nm x 5 nm) by the addition of excess of ligands[58] and CdSe NRs (40 nm x 8 nm) by the addition of poly(methyl mathecrylate). Addition of polymer generates non-favorable interactions of NRs with ligands leading to a self-corralling of NRs in the polymer matrix after solvent evaporation. An EF of 10^7 V/μm was also reported to assemble a small area of vertically aligned CdSe NRs in P3HT.[59]

3.1.3 Controlling Evaporating Rate

Controlling the rate of solvent evaporation as well as temperature of the substrate influences the assembly of NRs, resulting in a high degree of NR ordering on the substrate. At high temperatures, the solubility of the NRs in solution is improved and the shear viscosity of the NR solution decreases, leading to faster self-assembly of the NRs. Alivisatos and coworkers reported the vertical alignment of CdS (30 nm x 4 nm) NRs by evaporation of the solvent at 1 mm/min at 55 ˚C on a variety of substrates. These results suggested that the alignment of NRs is thermodynamically stable. They also reported that while the type of substrate had no effect on the NR assemblies, the roughness of the substrate has a strong effect on the percent alignment of the NRs. The studies also showed that 90 % alignment of the NRs was obtained only when the AR of the NRs was

less than 5, which suggests assemblies are kinetically limited.[60] Modestino *et al.* used a similar technique to assemble CdSe NRs (30 nm x 4 nm) in a P3HT matrix using 1,2-dichlorobenzene as a solvent. They showed that increasing the molecular weight of the polymer matrix decreased the ordering of the system due to the increases viscosity.[66] Cha and coworkers reported a large area of hexagonally packed NRs assembled using a solvent-based approach. The CdSe NRs (24 nm in length) were dissolved in a mixture of good and bad solvents, having different vapor pressures. The long range ordering of the short NRs was obtained by adjusting the gas flow to the solution to control the drying conditions.[62] Xie and coworkers reported the assembly of gold NRs (59 nm x 17 nm) using a two-stage controlled evaporation of a droplet. The evaporation rate was controlled by adjusting the humidity and temperature, resulting in large area monolayer of gold NRs.[67]

3.1.4 Additives-Induced Assembly of Nanorods

Manna and coworkers reported the solution phase assembly of core/shell CdSe/CdS NRs (24 nm x 6 nm) induced by the addition of oleic acid and poly(ethylene glycol) methacrylate. These additives are miscible in the solvent and pull the solvent away from the NRs. This results in an osmotic pressure pulling inward, called a depletion force, that induces NR assembly.[64] Zhao *et al.* reported the assembly of CdSe NRs (21 nm x 4.5 nm) with gold tips by changing the solvent quality for the ligands coating the tips of the NRs. The gold sections were covered with 11-mercapto-undecanoic acid as ligands, which have poor solubility in polar solvents. Addition of dimethylformamide, a poor solvent for the tip ligands, triggers vertical assembly of the NRs. Moreover, the

stability of the assembled lattices was enhanced by hydrogen bonding between the ligands on the gold tips.[63]

While these reports are good examples of additive-induced NR assembly, only monolayers of the vertically aligned short NRs were generate, using NRs whith length between 20 nm and 40 nm, with AR 4 - 5. The height of the vertically aligned NRs is not suitable for the thickness of the active layer (~ 100 nm) of typical PV devices. In this chapter, controlled solvent evaporation and applied electric field techniques are described that provide long-range ordering of hexagonal arrays of high AR CdSe NRs ranging from 16 nm – 90 nm.

3.2 Controlled Solvent Evaporation

The assembly of CdSe NRs after removal of excess native ligands (tetradecylphosphonic acid (TDPA) and trioctylphosphine oxide (TOPO)) was accomplished by controlling the rate of solvent evaporation of the NR solutions. To optimize the solvent system for the assembly, the NRs were dissolved in a mixture of two solvents with different vapor pressures and dielectric constants. A 20-μL droplet of a NR solution was drop-cast onto a copper grid (placed on a glass slide) and slowly dried in a partially sealed chamber, as shown in **Figure 3.2**. During the drying process, the temperature of the NR solution and substrate was held at 45 ˚C. The close-packed hexagonal arrays of the CdSe NRs were formed to minimize interactions between the ligands and the solvents.[68,69]

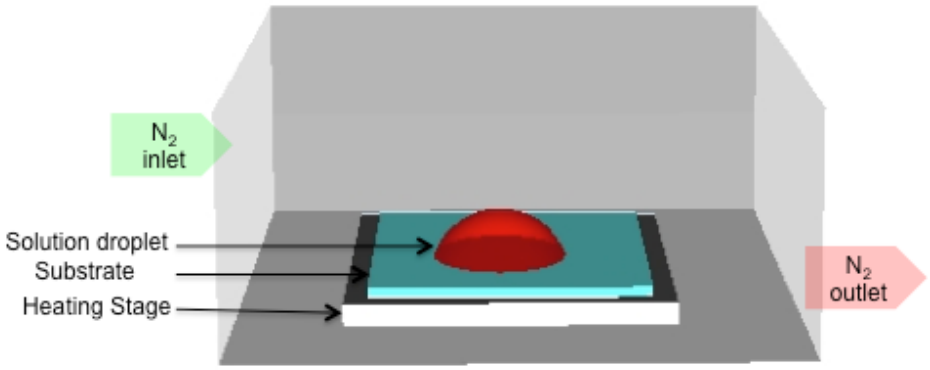

Figure 3.2 Schematic of the experimental set-up for the controlled solvent evaporation technique.

3.2.1 Effect of Solvent System

Figure 3.3 shows NR assemblies prepared from toluene/1,2-dichlorobenzene (DCB) mixtures at various ratios. Toluene has a higher vapor pressure (28.5 torr) than DCB (1.76 torr). In order to obtain long-range ordering of vertically aligned NRs, both the solvent volatility and the dielectric constant (ε) must be optimized. Solvents with high volatility and large ε lead to small domain sizes, whereas solvents with low volatility and low ε provide large areas of ordered arrays.[68] In our work, the best results were obtained with a mixture of toluene (ε = 2.38) and DCB (ε = 9.93) with a volume ratio of 7:3. Using these conditions, long-range (~ 4 μm^2/domain) ordering of NRs was obtained. The distance between each NR within the close-packed array was ~ 2 nm, as measured from TEM images, corresponding to approximately the length of the ligands attached to the NRs, confirming the close-packing of the NRs. For solvent mixtures with a high volume fraction of toluene, evaporation occurs too rapidly, not allowing sufficient time for assembly to occur. In solvent mixtures with a large volume fraction of DCB, electrostatic

interactions between rods are screened due to the large dielectric constant of the solvent, inhibiting the assembly.[68] For other solvent mixtures, including chloroform ($CHCl_3$):isopropanol, $CHCl_3$:DCB, toluene:dimethylsulfoxide, the NRs formed much smaller hexagonal arrays, with a majority of the NRs packed with a nematic- or smectic-type ordering and oriented parallel to the substrate, as shown in **Figure 3.4**.

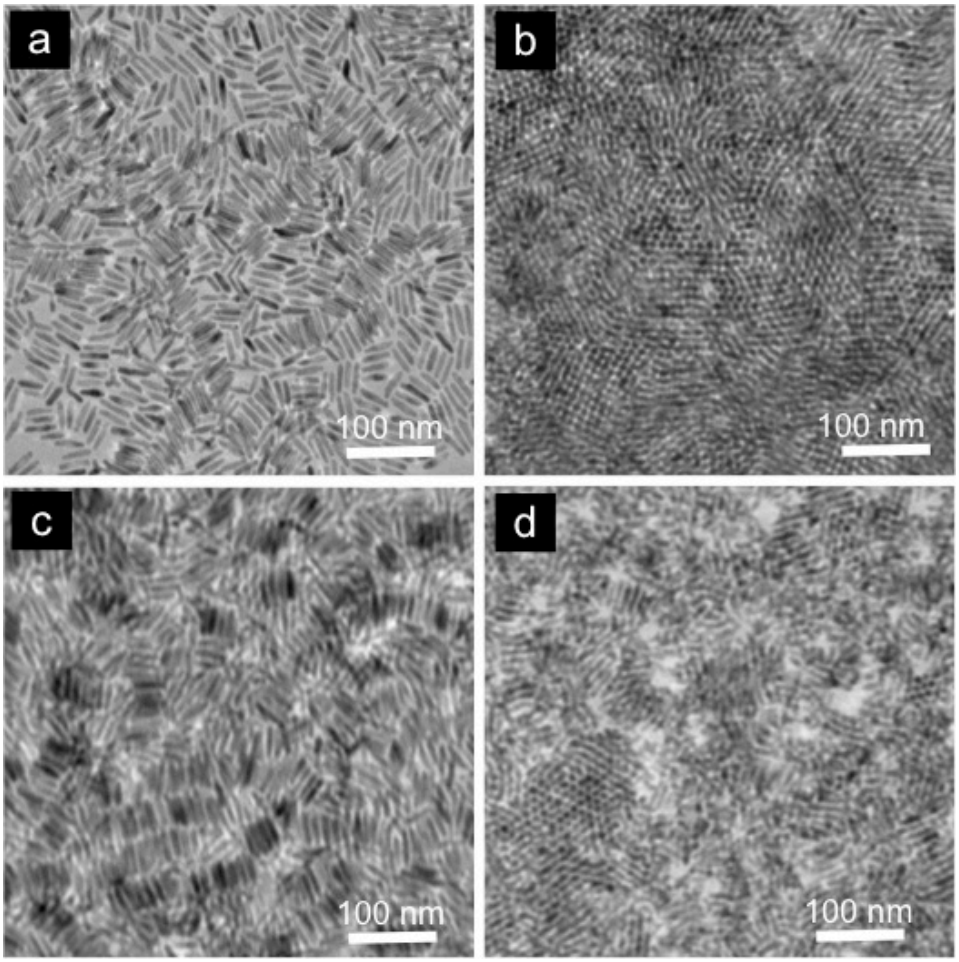

Figure 3.3 TEM images of CdSe nanorods (AR = 6, 40 nm x 7 nm) assembled from (a) toluene (b) toluene:DCB 7:3, (c) toluene:DCB 1:1, (d) toluene:DCB 3:7 on copper grids.

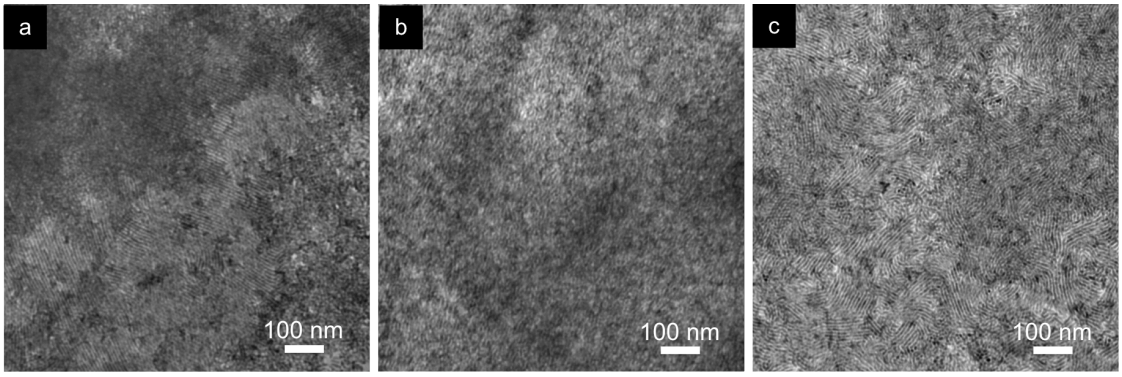

Figure 3.4 TEM images of CdSe nanorods (AR = 6, 40 nm x 7 nm) assembled from various solvent mixtures (a) $CHCl_3$:isopropanol 6:4 (b) toluene:dimethylsulfoxide 6:4, and (c) $CHCl_3$:DCB 7:3 on copper grids.

From observation of NRs assembled on lacey copper grids, it is clearly seen that the assembly occurs in the solution instead of on the substrate, as continuous vertical arrays were observed between the copper grids and holes. As the solvent evaporates, the concentration of NRs increases, leading to aggregation and assembly into a hexagonal close-packed NR array. The growth of the hexagonal arrays increases with time by the addition of free rods from the solution onto the array, followed by a deposition of the NR arrays onto the substrate due to gravity and van der Waals interactions.[70] This mechanism was confirmed by the presence of the continuous hexagonal arrays of the NRs covering the holes and the lacey grids (white dashed line in **Figure 3.5(a)** and **(b)**). Additionally, the cracks in the hexagonal arrays were observed in some areas, which probably occurred when the arrays were placed on the substrate, **Figure 3.5(c)** and **(d)**.

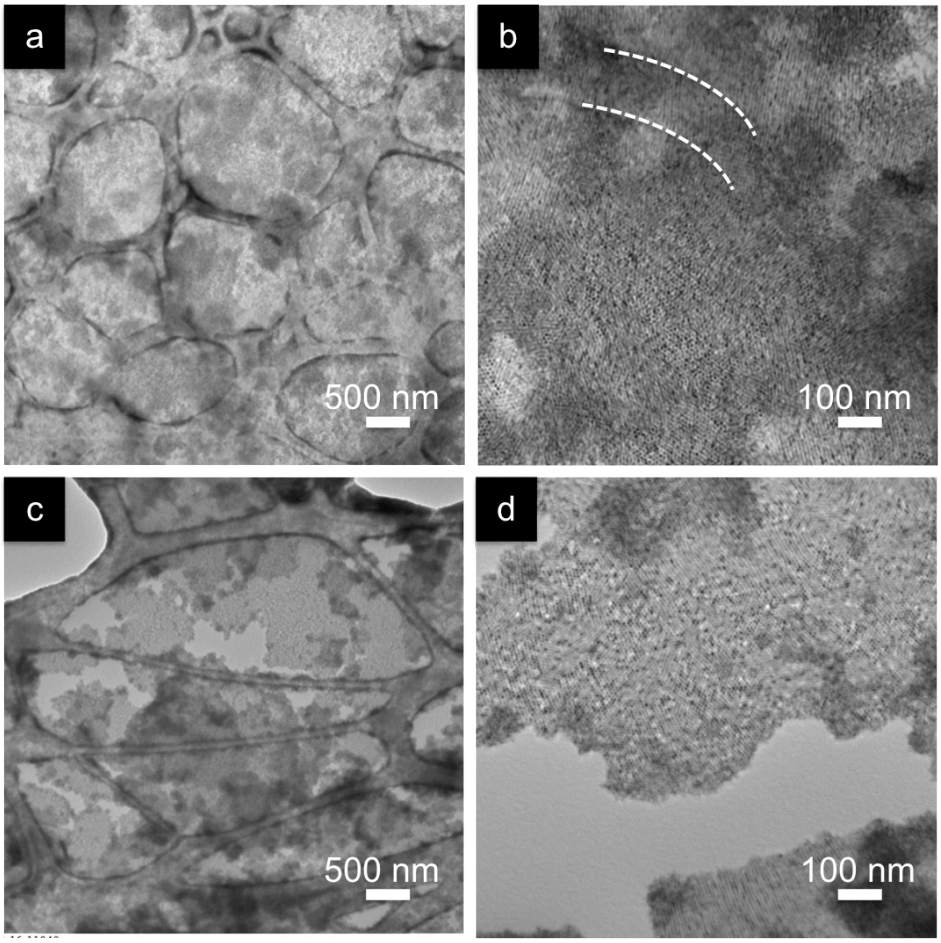

Figure 3.5 TEM images of CdSe nanorods (AR = 6, 40 nm x 7 nm) assembled on lacey copper grids showing the continuous arrays of the hexagonally packed NRs (a) – (b), and the cracks in the arrays (c) – (d). White dashed lines indicate the copper grid.

3.2.2 Effect of Nanorod Aspect Ratio

The effect of NR AR on the assemblies was also studied. As shown in **Figure 3.6**, long-range ordering (over 5 μm^2) of vertically aligned NRs was obtained for the NRs with AR < 10 (16 nm x 4 nm and 40 nm x 7 nm), whereas NRs with AR > 10 tend to form nematic structures. The darker areas in the TEM images (an inset of **Figure 3.6(b)**)

are multiple layers of the hexagonally-packed NRs. When the AR of the NRs was increased, the area of the hexagonally packed arrays decreased due to a substantial decrease in the rotational diffusion constant.[60]

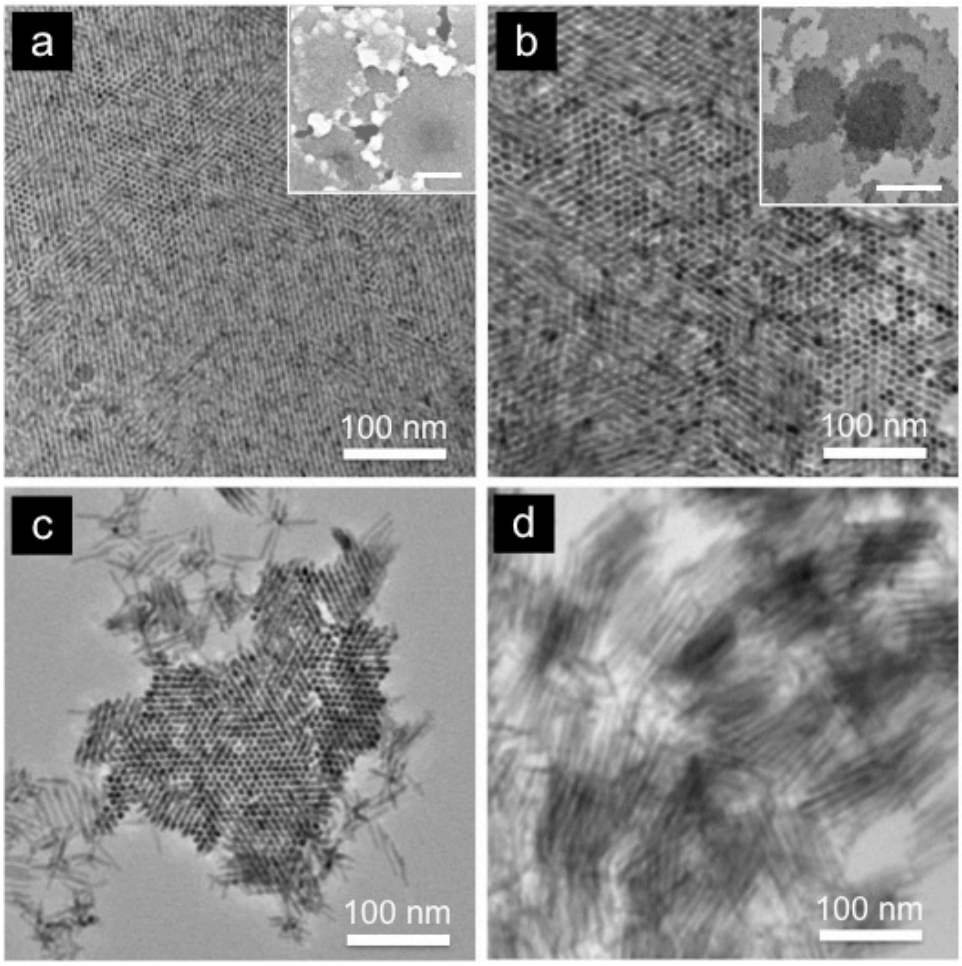

Figure 3.6 TEM images of CdSe nanorods assembled on substrates by the controlled solvent evaporation technique (a) AR 4 (16 nm x 4 nm), (b) AR 6 (40 nm x 7 nm), (c) AR 10 (60 nm x 6 nm), (d) AR 15 (90 nm x 6 nm). Insets are low magnification SEM and TEM images with scale bars representing 500 nm.

Grazing-incidence small angle x-ray scattering (GISAXS) was used to examine larger area assemblies of CdSe NRs than possible by TEM. CdSe NRs with different ARs (4, 6, 10 and 15) assembled on silicon wafers were characterized, giving the 2D scattering patterns shown in **Figure 3.7(a)**. Scattering patterns of the short NRs with AR 4 (16 nm x 4 nm) and AR 6 (40 nm x 7 nm) show sharp peaks at q = 0.103 $Å^{-1}$ and 0.064 $Å^{-1}$, respectively. These peaks correspond to center-to-center distance between adjacent NRs of 6.1 and 9.3 nm, respectively. The average center-to-center distances of NRs with AR 10 and 15 were found to be 8.3 and 8.4 nm, which correspond to inter-NR distances of 2.3 and 2.4 nm, respectively. These results are consistent with values obtained from the TEM images (**Figure 3.6**). The higher order reflections observed for NRs with ARs of 4 and 6 are indicative of longer range laterally ordered NRs. The broadening of the reflections of the higher AR NRs is consistent with their less dense packing.

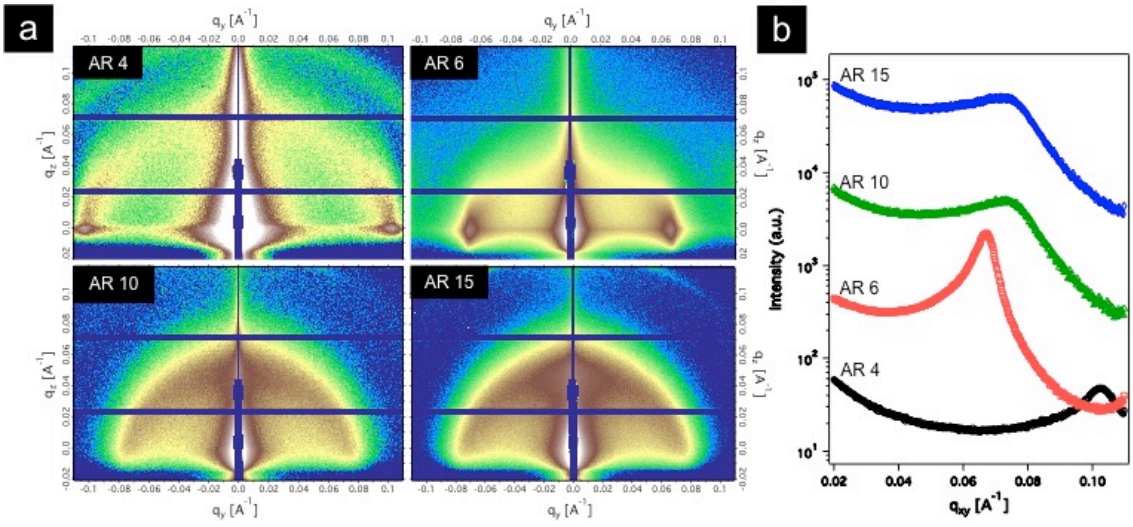

Figure 3.7 GISAXS patterns and in-plane cut profiles of CdSe nanorod assemblies on Si substrates (a) AR 4 (16 nm x 4 nm), (b) AR 6 (40 nm x 7 nm), (c) AR 10 (60 nm x 6 nm), (d) AR 15 (90 nm x 6 nm).

3.3 Electric Field Assisted Technique

To improve the vertical orientation of high AR NRs, a 20-µL droplet of NR solution was drop-cast onto a copper grid placed on an electrode. Two sheets of aluminum (1" x 2") were used as conducting electrodes and connected to a power source (Standford Research Systems, Model PS350). A DC EF was applied during solvent evaporation. The strength of EF was controlled by adjusting the thickness of the Teflon spacer and the voltage applied to the electrodes. The experimental set-up is illustrated in **Figure 3.8**.

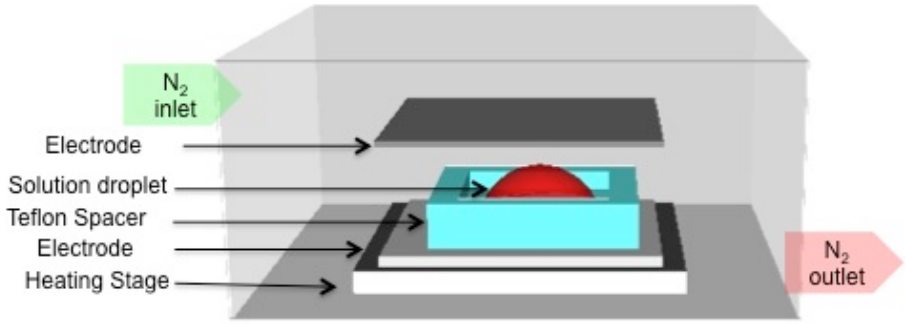

Figure 3.8 An experimental set-up for an applied external electric field technique.

3.3.1 Effect of Electric Field Strength

CdSe NRs with a Wurtzite crystal structure have a permanent dipole moment along the long-axis of the rod that increases linearly with NR volume.[65] In a uniform EF, the dipole moment results in a torque acting on the NRs, orienting the NRs in the direction of the applied field[57,58,65] ($T = P \times E$, where T is the torque, P is the unscreened dipole moment of the NRs, and E is magnitude of the EF). The insets of **Figure 3.9(a)** and **3.9(b)** clearly show that by applying an EF (1 V/µm) during the drying process, the

long-range hexagonal packing of CdSe NRs is enhanced. When the AR of the NRs is decreased from 6 to 4, the lateral area of grains of close-packed NR domains increased from ~ 1-4 μm^2 to ~ 9-25 μm^2, fully covering surface of the 1 cm × 1 cm substrate (**Figure 3.9(a)** and **3.9(b)**). Even with the increased dipole moment of the longer NRs ($P_{AR\sim4}$ ~ 103 D, $P_{AR\sim15}$ ~ 548 D), the alignment was poor due to the low EF strength of 1 V/μm. Consequently, a stronger EF (16 V/μm) was applied, resulting in a larger area of vertical oriented NRs with AR 10, and some ordered areas of AR 15 NRs (**Figure 3.9(c)** and **3.9(d)**).

The impact of EF strength on the long range ordering of hexagonal array of NRs has been studied with NRs with AR 6. Low magnification TEM images of assemblies formed by the application of different EF strengths are shown in **Figure 3.10,** which compare the areas of continuously packed vertically aligned NRs. It is evident that increasing EF during solvent evaporation increased the area of the hexagonally packed arrays. When the EF was increased from 0.5 to 1.5 and 4 V/μm, the area of the arrays of the oriented NRs (the grey area in **Figure 3.10(b)** and the dark area in **Figure 3.10(c)**) grew significantly, from ~ 1 μm^2 to ~ 25 μm^2.

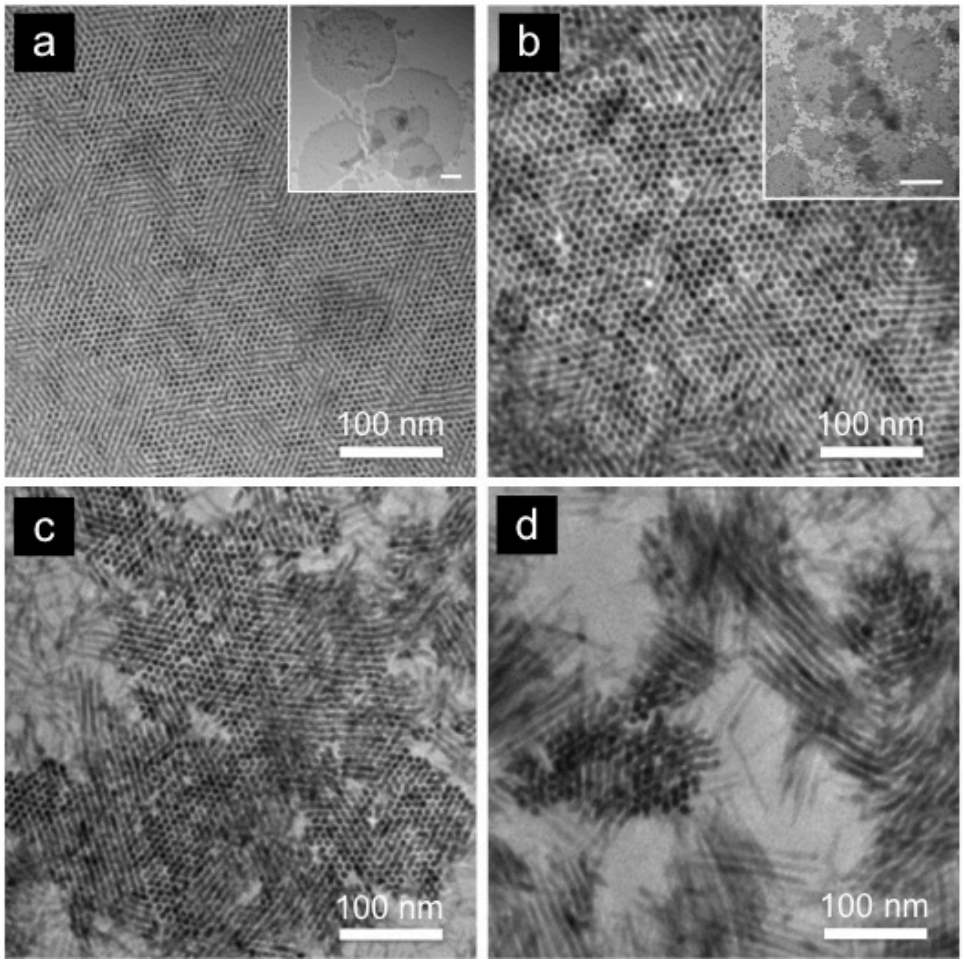

Figure 3.9 TEM images of CdSe nanorod assemblies under an applied electric field (a) AR 4 (16 nm x 4 nm, 1 V/µm), (b) AR 6 (40 nm x 7 nm, 1 V/µm), (c) AR 10 (60 nm x 6 nm, 16 V/µm), (d) AR 15 (90 nm x 6 nm, 16 V/µm). Insets are low magnification TEM images with scale bars representing 1 µm.

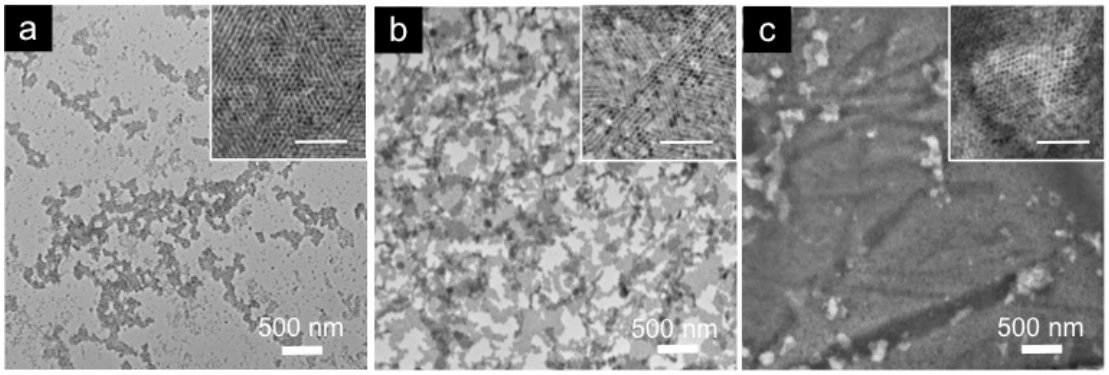

Figure 3.10 Low magnification TEM images of CdSe nanorod (AR 6, 40 nm x 7 nm) assemblies formed by using various electric field strengths (a) 0.5 V/µm, (b) 1.5 V/µm (c) 4.0 V/µm. Insets are high magnification TEM images with scale bars representing 100 nm.

3.3.2 Effect of Nanorod Concentration

Increasing the concentration of the NR solution did not affect the hexagonal assembly of the NRs (**Figure 3.11(a)**). The substrate was fully covered with multilayers of the vertical aligned NRs. A cross-sectioned image obtained by scanning electron microscopy (SEM), **Figure 3.11(b)**, shows that increasing the concentration of the NR solution from 2 mg/mL to 10 mg/mL (when other conditions were constant, *i.e.* the EF strength, and the solvent system) led to the multilayers (~ 20 layers) of the vertically packed NRs, compared with the monolayers and bilayers obtained from more dilute solutions.

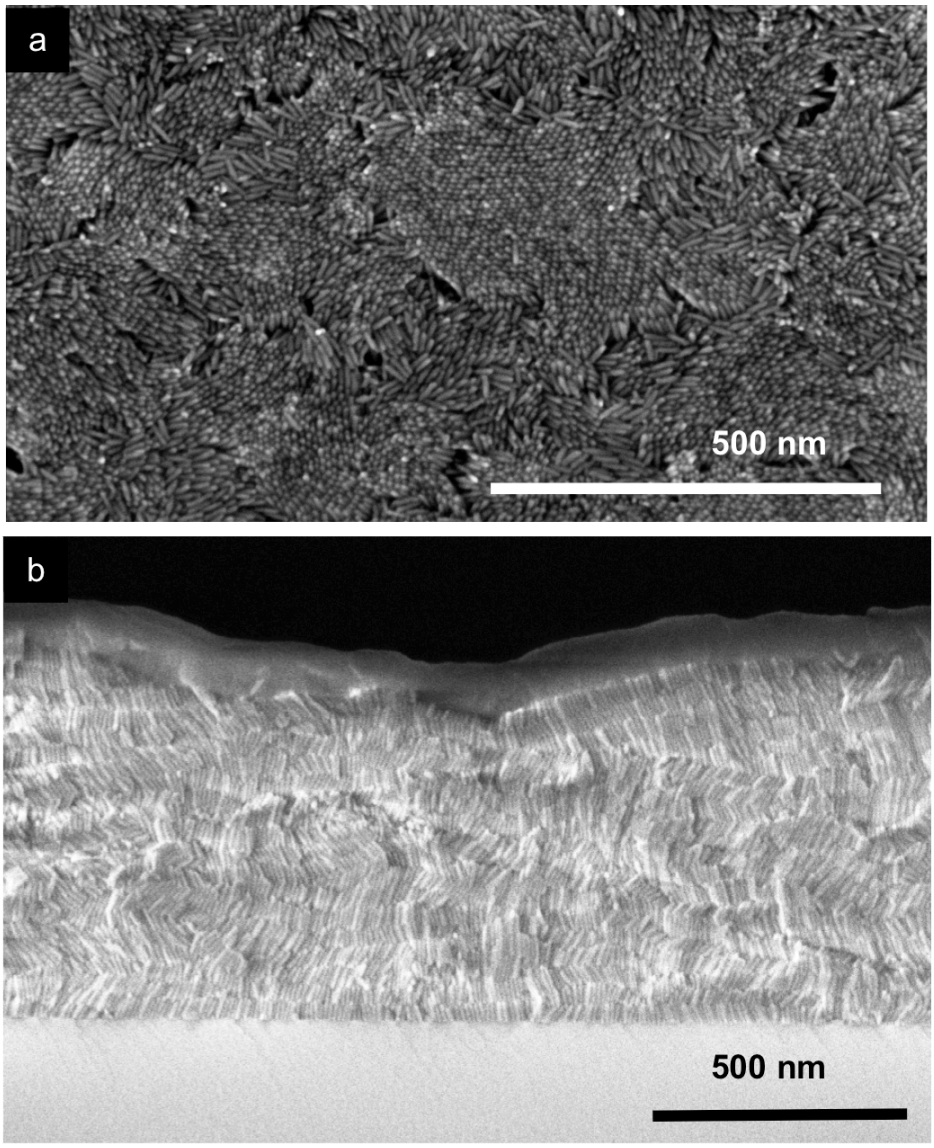

Figure 3.11 SEM images, (a) top view, and (b) cross-section view, of multilayers of CdSe nanorod (40 nm x 7 nm) assemblies under an applied electric field of 2 V/μm.

3.3.3 Assembly of CdSe Nanorod with Different Aspect Ratios

Mixing CdSe NRs with different ARs is expected to induce vertical assembly of the longer NRs. In this experiment, the low AR CdSe NRs, that formed long range ordering with the use of the low strength EF, were mixed with the higher AR NRs. Upon

drying under the applied EF, the TEM images revealed phase separation of the NRs with the different ARs. It is clearly seen in the case of the AR 4 and AR 8 mixture that both AR 4 and 8 NRs formed large arrays of hexagonal packing, as shown in **Figure 3.12(a)**. However, strong phase separation was observed, where the light area of the image is the shorter NRs and the darker area is the longer NRs, with the NRs tilted along the grain boundaries. The strong phase separation is probably due to the large difference in diameters of the two groups of NRs (4 nm for AR 4 and 6 nm for AR 8). When CdSe NRs with AR 6 were mixed with AR 10 NRs, the size of the resulting hexagonal arrays was smaller compared to arrays formed from a solution of NRs with a single AR. The phase boundaries were not clearly observed when the NRs having similar diameters and different ARs were mixed. Instead, the TEM images showed only slight vertical orientation of the NRs (**Figure 3.12(b)** and **3.12(c)**). High-resolution SEM images clearly show phase separation of the vertically aligned NRs with different ARs and the tilted NRs along the boundaries, **Figure 3.13**.

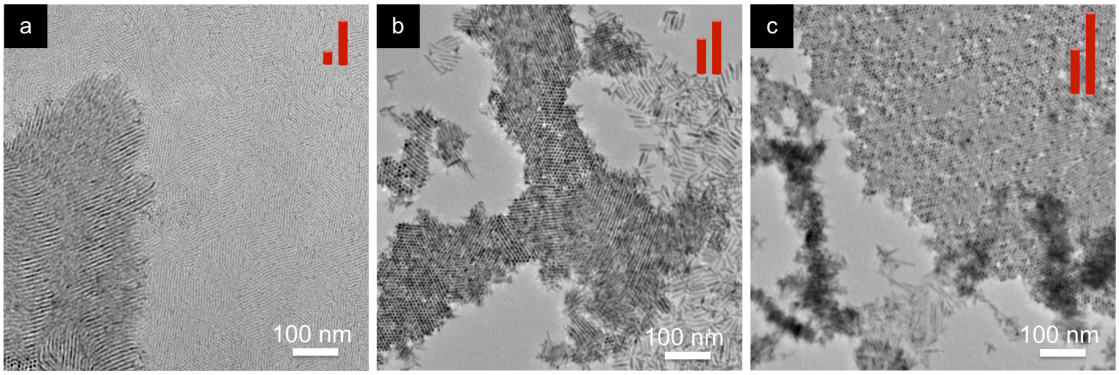

Figure 3.12 TEM images of mixtures of CdSe nanorod assemblies, (a) AR 4 and AR 8 (16 nm x 4 nm and 50 nm x 6 nm), (b) AR 6 and AR 10 (40 nm x 7 nm and 60 nm x 6 nm), and (c) AR 8 and AR 15 (50 nm x 6 nm and 90 nm x 6 nm), under an applied electric field of 2 V/μm.

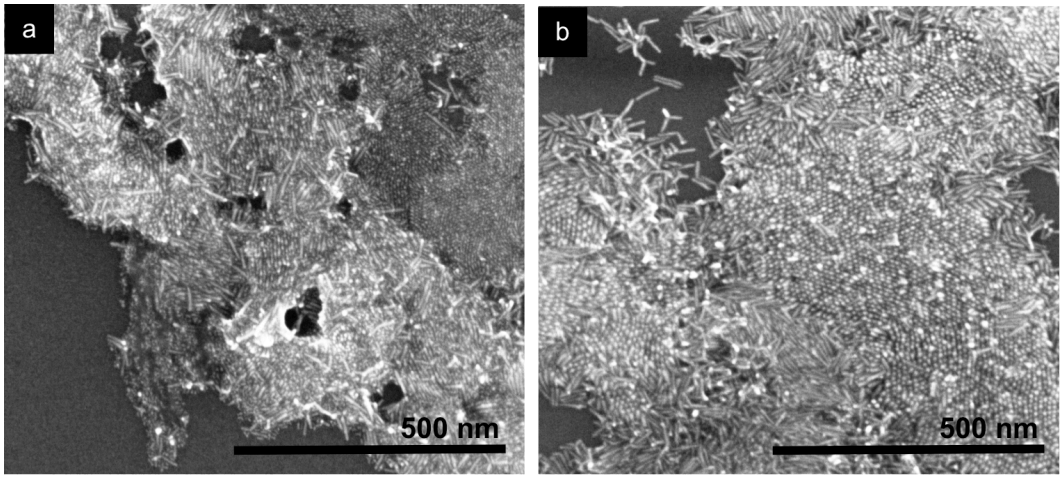

Figure 3.13 SEM images of CdSe nanorod assemblies under an applied electric field of 2 V/μm, (a) AR 4 and AR 10 (16 nm x 4 nm and 60 nm x 6 nm), and (b) AR 6 and AR 10 (40 nm x 7 nm and 60 nm x 6 nm).

3.4 Vertical Assembly of Oligothiophene and Polythiophene Functionalized CdSe Nanorods

Several research groups have studied PV devices with active layers composed of blends of semiconducting polymers and inorganic NCs blend. Greenham and coworkers reported PV devices containing 86 % CdSe NCs and OC_1C_{10}-PPV. These devices produced a power conversion efficiency (PCE) of 1.8 % under AM1.5 illumination.[19] Huynh *et al.* reported a PCE of 1.7 % obtained from PV devices having of 90 wt% CdSe NRs blended with P3HT,[21] and Dayal *et al.* reported a blend of 90 wt% CdSe TPs and PCPDTBT, which gave a PCE of 3.13%.[14] However, these studies relied on a physical blend of two materials, leading to low electron mobility within the polymer matrix due to the lack of the direct contact points between the polymers and NC surfaces.

3.4.1 Ligand Exchange Process

After synthesis, the NCs are typically bonded with native ligands that are electrical insulating layers that block charge transfer at the NC-polymer interface. These layers reduce the electron mobility and increase the possibility of charge recombination, resulting in lower efficiency PV devices. The ligand exchange process is a crucial step to remove the electrical insulating layers and increase interactions between the ligands and the NC surfaces, which leads to an improvement of the dispersion of the NCs in the polymer matrix. Two types of ligand exchange methods, grafting-to and grafting-from, provide direct attachment of the desired ligands by replacing the native ligands. The grafting-from technique requires polymerization to grow directly from the precursor-functionalized NC surfaces, resulting in polymer ligands with a broad polydispersity. On the other hand, the grafting-to technique is the attachment of pre-synthesized polymer chains containing functional groups that are suitable to form intimate contacts with the NC surfaces, such as thiols, amines, carboxylates, and phosphonic acids. These functional groups contain metal-coordinating groups (electron-donating groups) that coordinate to electron-poor metal atoms at the NC surface. The polymers are purified by Soxhlet extraction to the desired molecular weight distribution before functionalization of the NC surfaces. Pyridine is a common solvent, as it is used as an intermediate ligand in the ligand exchange process. The insulating layers of the native ligands are replaced easily by the introduction of excess pyridine and refluxing at 110 ˚C. These pyridine layers are then removed by thermal annealing and replaced with the conjugated polymers having functional groups with higher binding affinity to the NC surface, such as thiols and phosphonic acids. However, treatment of the NR surface with pyridine leads to the

aggregation and the side-packing of NRs after the removal of pyridine, as shown in **Figure 3.14**, which prevented the vertical orientation of NRs after functionalization with polythiophene ligands. Therefore, the one-step direct ligand exchange was employed throughout the experiments, without the use of pyridine to avoid NR aggregation.

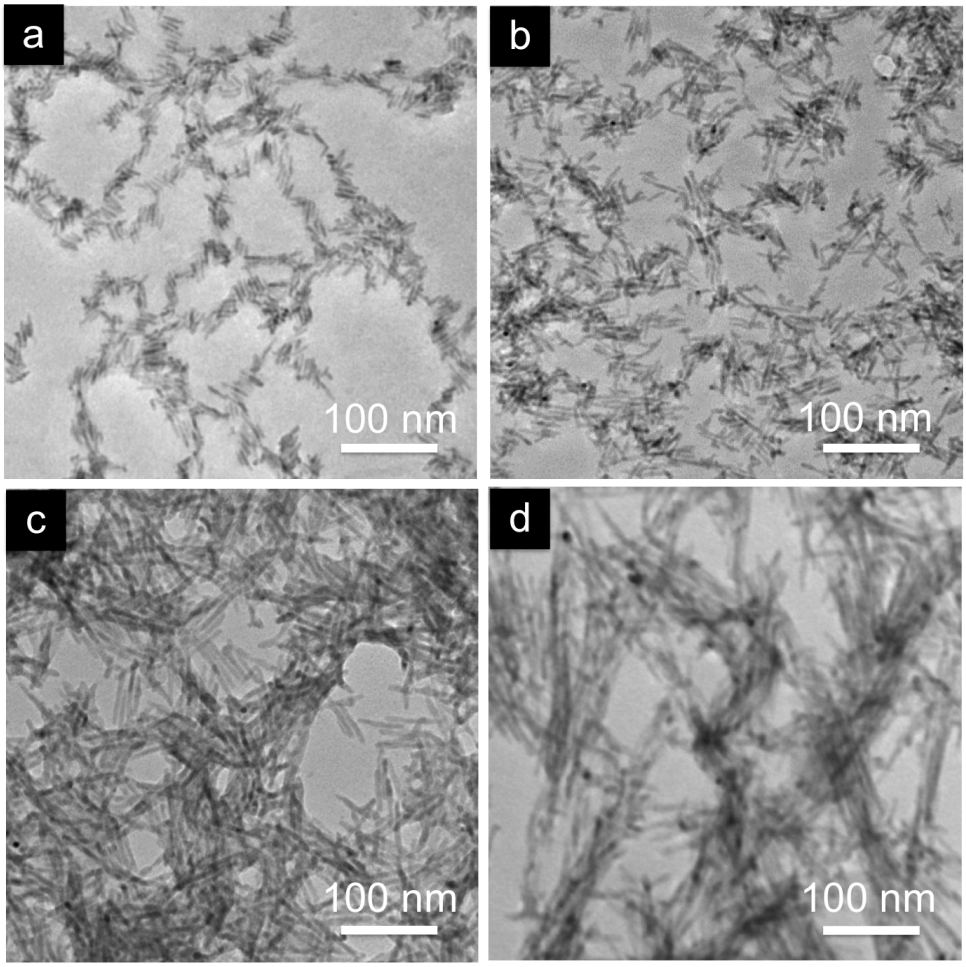

Figure 3.14 TEM images of CdSe nanorod assemblies after ligand exchange process with pyridine. (a) AR 4 (20 nm x 4 nm), (b) AR 6 (40 nm x 7 nm), (c) AR 10 (60 nm x 6 nm), and (d) AR 17 (120 nm x 7 nm).

3.4.2 Semiconducting Polymers on Nanocrystal Surface

Additional experiments were performed using CdSe NRs functionalized with polythiophene, with a p-type polymer anchored to the n-type NRs, with the ultimate objective using the NR arrays in photovoltaic devices. Functional polythiophene and oligothiophene were selected as semiconducting polymer candidates due to their suitable electronic properties, appropriate energy levels and hole mobilities, and environmental stability.[3] Terthiophene (Th_3) and P3HT (Mw 5000 g/mol) were end-functionalized with diethylphosphonate for attachment to the NR surface. Ligand exchange on NRs, from TDPA/TOPO coverage to oligo- or polythiophene coverage, was performed by mixing CdSe NRs (40 nm x 7 nm, 2 mg/mL in $CHCl_3$) and PO-Th_3 (2 mg/mL in DCB) (1:1 by volume), and stirring the solution at 65 ˚C overnight. The terthiophene-CdSe solution was isolated by centrifugation to remove free ligands, and used without further purification. ^{1}H NMR spectroscopy of the dried NRs confirmed the exchange of ligands on the NR surface from TDPA/TOPO to oligothiophene (**Figure 3.15**).

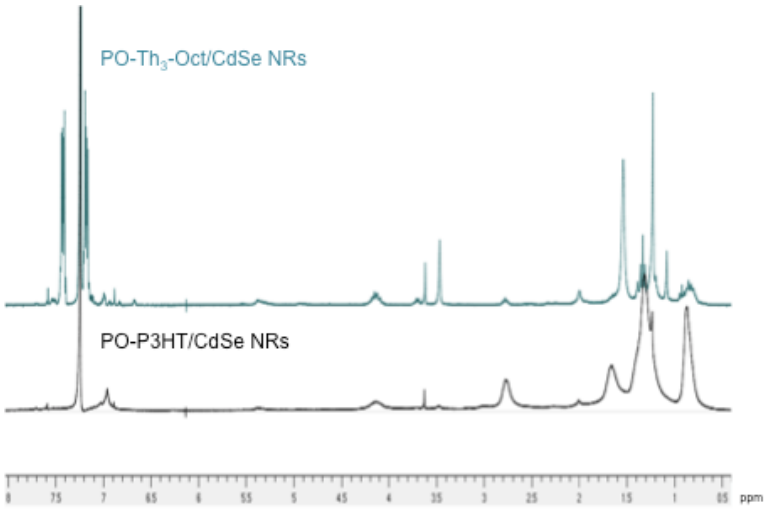

Figure 3.15 ^{1}H NMR spectra after ligand exchange to PO-Th_3 and PO-P3HT.

Figure 3.16 shows the optical properties of PO-Th_3 and PO-P3HT in $CHCl_3$ before and after functionalization of the CdSe NRs. Significant quenching of polymer fluorescence is observed for both oligothiophene and polythiophene functionalized CdSe NRs, indicating the interactions and charge transfer between the semiconducting polymer or oligomer and the NRs. Charge transfer and fluorescence reduction occurs in such systems when photogenerated excitons are dissociated at the polymer/NR interface before luminescence occurs.[30]

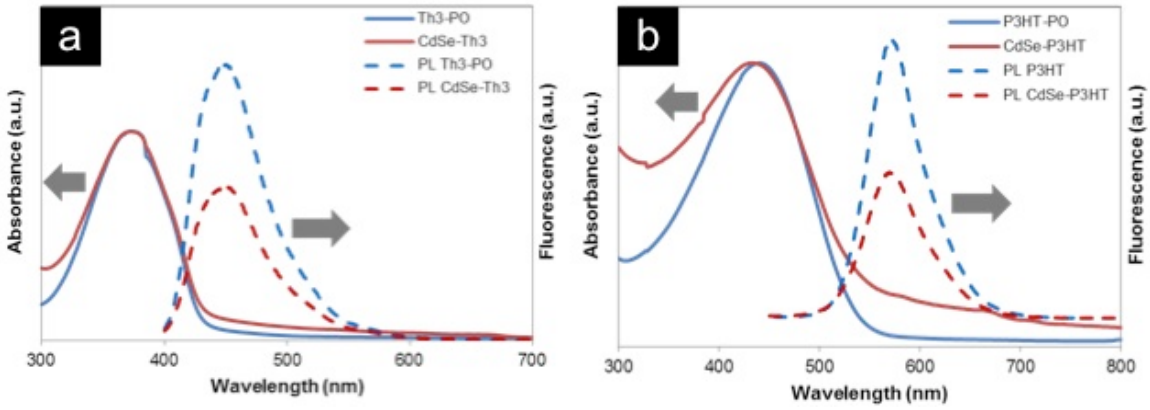

Figure 3.16 Optical properties of (a) PO-Th_3, (b) PO-P3HT in $CHCl_3$, before and after functionalization on CdSe nanorod surface.

To order and orient the oligothiophene- and polythiophene-functionalized NRs, a solution of terthiophene-CdSe NRs in toluene:DCB (7:3 v/v) was drop-cast onto a copper grid placed on a conducting substrate held at 45 ˚C with an applied DC EF 2 V/μm. A monolayer of vertically aligned oligothiophene-functionalized CdSe NRs was obtained, as shown in **Figure 3.17**. However, when the TDPA/TOPO ligands were replaced with PO-P3HT, achieving oriented NRs was more difficult. As shown in **Figure 3.17(b)**, only

small areas of vertically aligned NRs surrounded by partially aligned NRs, were observed after drying under an applied EF of 3 V/μm, a stronger field than that needed to align terthiophene-CdSe NRs. Additionally, the thickness of the film after drying is less uniform compared to the terthiophene-CdSe film, as some darker areas are observed in the TEM image indicating multiple layers of NRs, as shown in **Figure 3.17**. Moreover, the lateral area of close-packed hexagonal ordering was smaller than that seen for the terthiophene-CdSe NR assemblies, suggesting that the P3HT ligands inhibit the assembly of NRs, as observed by Modestino and coworkers.[66] This may arise from the higher viscosity of the P3HT-Cdse NRs or entanglements of the polymer ligands as the concentration increases during solvent evaporation. These results suggest that either a much slower solvent evaporation, to allow the polymer functionalized NRs to pack or the use of a stronger EFs that might exceed the dielectric breakdown of the solution may improve the assemblies.

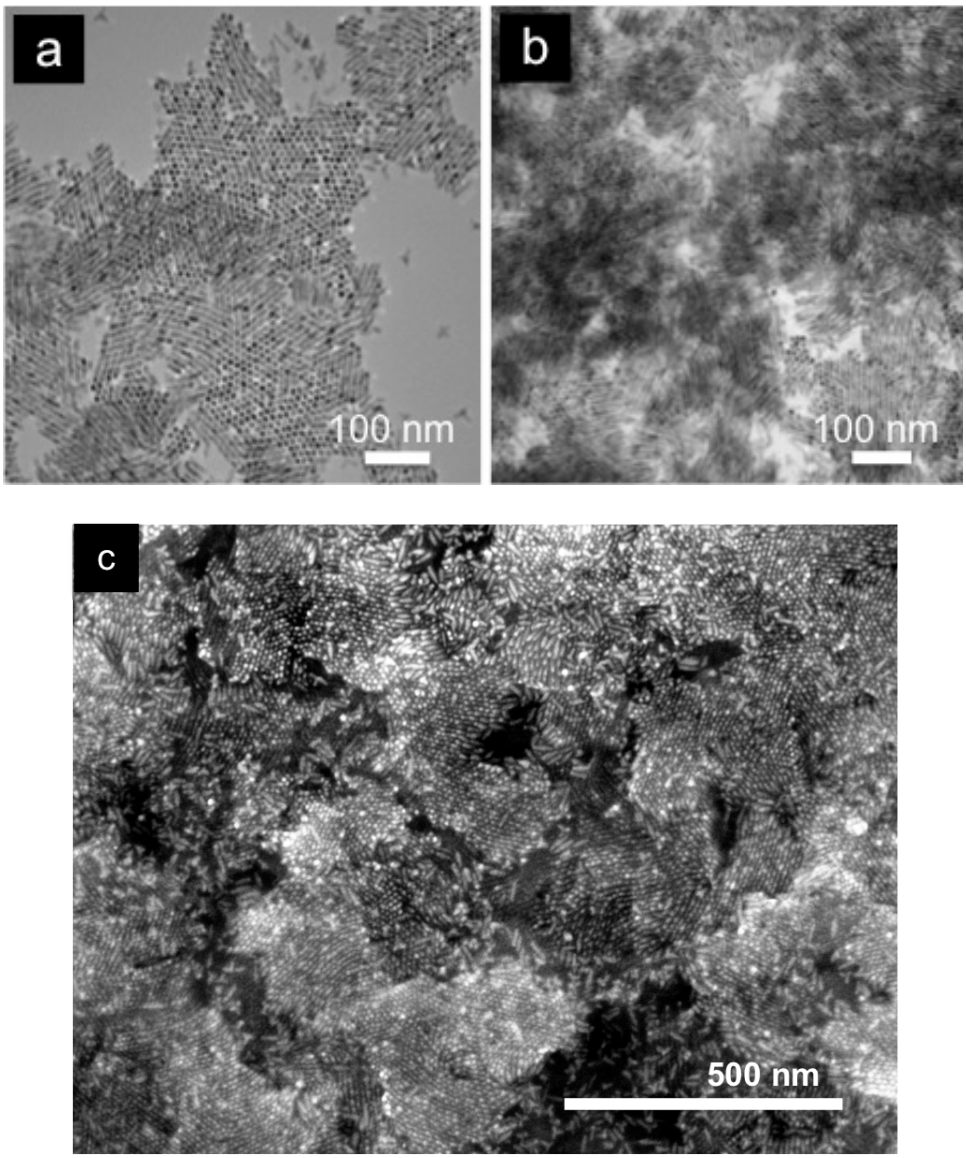

Figure 3.17 (a) TEM image of terthiophene-CdSe nanorod assemblies using electric field of 2 V/µm, (b) and (c) TEM and SEM images of P3HT-CdSe nanorod assemblies using electric field of 3 V/µm.

3.4.3 Assembly of the Nanorods Functionalized on the Pre-Formed P3HT Fibrils

Besides using functionalized P3HT as ligands, pre-formed fibrils of this polymer were used as a template to assemble the CdSe NRs along the fibrils. Several research

groups have studied the assembly of the inorganic NCs on the surface of one-dimensional (1D) templates such as carbon nanotubes,[71] block copolymers,[72] viruses,[73] and crystalline polymer fibrils,[74–76] by chemical bonding or electrostatic interactions.

CdSe NRs were assembled along the pre-crystallized thiol-terminated P3HT nanowires using a previously reported technique.[75] Conjugated polymers crystallized into 1D nanowires improve the hole-transporting properties along the fibril direction due to π-π stacking of the conjugated backbone. The pre-formed P3HT fibrils contain thiol functional groups at the chain end of the polymers that bind to the NR surfaces. **Figure 3.18(a)** and **(b)** show CdSe NRs assembled on the functional P3HT fibrils. After the deposition of the NRs along the surface of the P3HT fibrils, the nanocomposite solution was drop-cast onto a copper grid and dried under EF. **Figure 3.18(c)** reveals the vertical orientation of the NRs assembled along the fibrils. The ability to control the orientation and direction of both n-type and p-type materials has the potential to improve charge transport to the electrodes and enhance the performance of the PV devices.

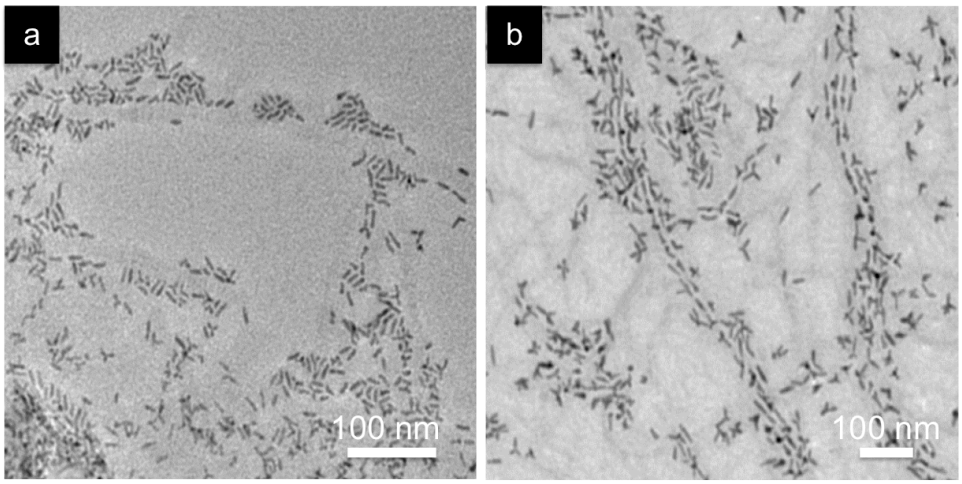

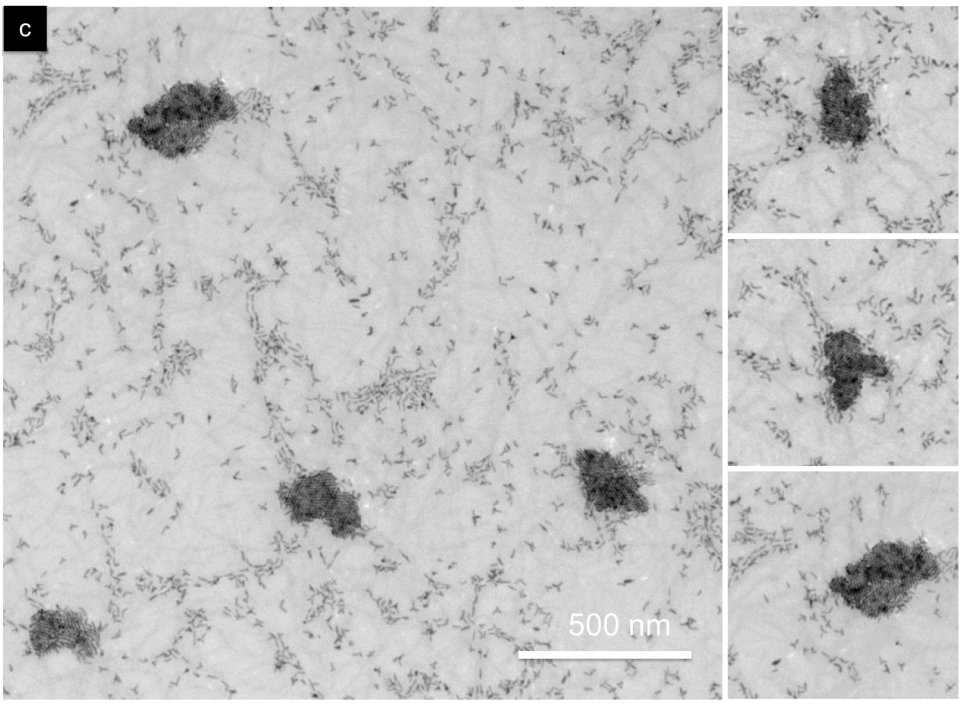

Figure 3.18 TEM images of CdSe nanorod assemblies on the pre-formed P3HT fibrils (a) 16 nm x 4 nm, (b) 40 nm x 7 nm, and (c) with an apply of electric field of 2 V/μm.

3.5 Summary

In summary, the assembly of high AR CdSe NRs into oriented, ordered hexagonal arrays over 1 cm^2 was described. Combining an applied EF with controlled solvent evaporation afforded long-range order of CdSe NRs oriented normal to the underlying substrate. A continuous array of vertically packed NRs (AR 4 and 6) over millimeter length scales was achieved by using an external field as low as 1 V/μm. Moreover, NRs with ARs greater than 15 were successfully oriented using this methodology. Vertically oriented assemblies of CdSe NRs functionalized with oligo- and polythiophene were also

obtained indicating a pathway toward the generation of photovoltaic devices by this self-assembly route.

3.6 Experimental Section

3.6.1 Materials

2,5-dibromothiophene, tetrakis(triphenylphosphine) palladium(0), and *n*-butyllithium (2.5 M in hexane) were purchased from Alfa Aesar. 2-(tributylstannyl)-thiophene, 1-bromooctane, diethyl chlorophosphate, lithium diisopropylamide solution (2.0 M in THF) (LDA), and all other reagents were purchased from Sigma Aldrich. Tetrahydrofuran (THF) was distilled over sodium and benzophenone. All other reagents were used as received.

3.6.2 Characterization

Nuclear Magnetic Resonance (NMR) spectra obtained from a Bruker DPX-300 NMR spectrometer was used to confirm the structure of polymers. UV-Vis absorption and photoluminescence spectrum of polymer solutions and assembled CdSe NR solutions were performed using Perkin-Elmer Lambda 25 UV/Vis spectrometer and a LS 55 Luminescence spectrometer, respectively. The NRs assemblies were determined with a JEOL 2000FX transmission electron microscope (TEM) with 200 keV accelerating voltage. Gel permeation chromatography (GPC) was carried out with a Polymer Laboratories PL-220 high temperature GPC. The polymer solutions were run at 135 °C using 1,2,4-trichlorobenzene as eluent, and polystyrene standards.

3.6.3 Synthesis of diethyl (5''-octyl-[2,2':5',2''-terthiophen]-5-yl)phosphonate (PO-Th_3)

Terthiophene and 5-octyl-2,2':5',2''-terthiophene (Th_3-Oct) were synthesized according to procedures previously reported.[77,78] In a 100 mL 2-neck round bottom flask, 5-octyl-2,2':5',2''-terthiophene (1.18 g, 3.29 mmol) was dissolved in THF (30 mL) and cooled to -78 ˚C. LDA (2.47 mL, 4.94 mmol) was added drop-wise and the reaction stirred at -78 ˚C for 1 h. Diethylchlorophosphate (0.71 mL, 4.94 mmol) was added drop-wise and the reaction stirred at -78 ˚C for 1 h, then warmed to room temperature and stirred overnight. The reaction was quenched by adding a few drops of water, then extracted with diethyl ether and washed with 1M HCl. The product was purified by column chromatography (silica/ 40% EtOAc/Hexanes), and obtained as a yellow liquid (0.71 g, 44 %yield).

^{1}H NMR ($CDCl_3$, 300MHz, ppm): δ = 7.51 (m, 2H), 7.13 (m, 2H), 7.01 (m, 2H), 4.14 (m, 4H), 2.76 (t, 2H), 1.65 (m, 2H), 1.32 (m, 10H), 1.23 (bs, 6H), 0.91 (t, 3H), ^{13}C NMR ($CDCl_3$, 300MHz, ppm): δ = 146.16, 138.59, 137.64, 137.50, 133.95, 127.06, 125.80, 124.56, 123.88, 123.23, 61.33, 33.66, 31.85, 29.71, 22.66, 22.15, 16.35, 16.26, 14.12, 13.81, ^{31}P NMR ($CDCl_3$, 300MHz, ppm): δ = 11.35

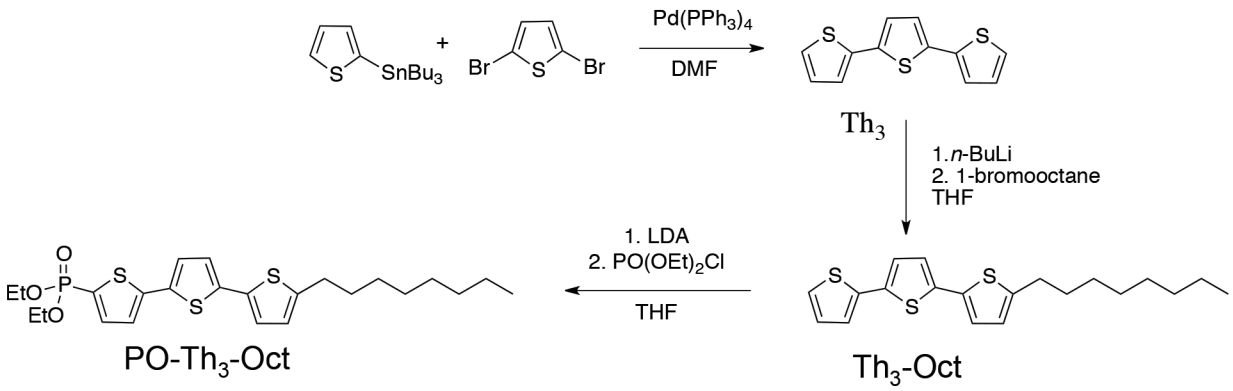

Figure 3.19 Schematic shows synthesis of diethylphosphonate terminated 5-octylterthiophene.

3.6.4 Synthesis of diethylphosphonate terminated P3HT (PO-P3HT)

P3HT-H/Br was synthesized according to a published procedure.[79] GPC-TCB, M_w 5000 g/mol, PDI 1.06, diethylphosphonate-terminated P3HT was synthesized following the procedure described above. FT-IR was used to confirm the presence of functional end-group, **Figure 3.20**.

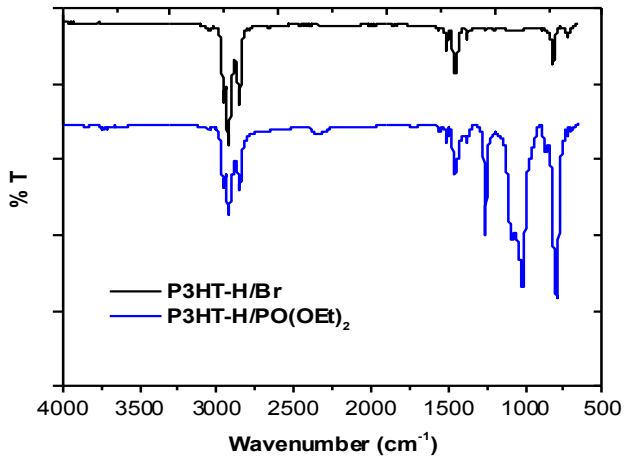

Figure 3.20 FT-IR spectra of H/Br-P3HT and PO-P3HT.

CHAPTER 4

END-TO-END ASSEMBLY OF POLYTHIOPHENE-FUNCTIONALIZED CDSE NANORODS

4.1 Introduction

4.1.1 End-to-End Assembly of Nanorods

Recently, organic-inorganic hybrid photovoltaic (PV) devices have attracted interest due to the facile processability, light weight, and the low cost of their large scale production. The incorporation of nanocrystals (NCs) into these devices is beneficial, as NCs impart fast charge separation between NCs and conjugated polymers as well as excellent energy transport through the NCs to the respective electrodes.[80] The close contact of the polymer ligands with the NC surface facilitates exciton dissociation at the NC-polymer interface upon the absorption of the photons. In the previous chapter, two techniques providing long range ordering of vertically aligned CdSe nanorods (NRs) were described. CdSe NRs hexagonally packed perpendicular to the substrate facilitate electron transfer along the NR longitudinal axis to the electrode, while the optical properties of the assembled NRs remain the same.

Altering the optical properties, such as UV-Vis absorption, of NCs has been realized by the end-to-end assembly of gold NRs, due to the strong surface plasmon resonance between closely packed Au NRs.[81–84] Moreover, these properties can be tuned by adjusting inter-particle spacing with linkers and by varying the degree of polymerization, broadening their applications in sensors and optical devices. The end-to-

end assembly of NRs has been accomplished using chemical and physical bonds, such as by the coupling ligands preferentially bound at the tips of NRs using bifunctional linkers,[85,86] the use of bifunctional tip ligands,[87,88] the coalescence of NR tips,[89] and the attachment of polymer tethers at the ends of NRs.[81,90] For example, Caswell *et al.* reported end-to-end linked gold NRs by coupling of streptavidin with disulfide – containing molecules coated on the gold NR surfaces.[85] A similar technique was reported by Salant *et al.,* where gold-tipped CdSe NRs were functionalized with biotin disulfide specifically at the tips of the NRs. The addition of avidin, having four functional sites, led to the end-to-end assembly of the NRs *via* avidin-biotin interactions.[86] Singamaneni and coworkers studied the mechanism and dynamics of the end-to-end assembly of gold NRs using aminothiols as linkers. These bifunctional groups bound at both ends of the gold NRs, forming chain-like structures from the NRs. They found that adjusting the concentration, pH, and zeta-potential of the solution controlled the dynamics and behavior of the assemblies.[82] Additionally, Manna and coworkers reported end-to-end assembly of NRs through the coalescence of gold NCs on the tips of CdSe NRs. CdSe NRs were functionalized with gold NCs at both ends, then coalescence induced by the addition of iodine to destabilize the gold domains and form larger gold particles bridging two NRs.[89] Another example of the end-to-end assembly of gold NRs was reported by Kumacheva and coworkers, where thiol-terminated polysterene was tethered to both ends of gold NRs. Due to the hydrophobicity of the polystyrene, addition of water resulted in dense packing of the polymer chains between NRs, forming an end-to-end assembly. This process was reversible by addition of a better solvent for the polymer, dimethyl-formamide, which resulted in good solubility of the NRs in solution.[90]

In this chapter, the synthesis of poly(3-hexylthiophene) (P3HT) containing multiple functional groups along the chain is discussed. These anchoring groups provide close contacts between the polymers and the NR surfaces. By controlling the ratio of NRs to polymer, the end-to-end assembly of CdSe NRs was obtained utilizing functional P3HTs (thiols, amines, and phosphonates) as linkers. Direct attachment of the NRs to the polymers promotes efficient charge transfer between the two materials. Moreover, the end-to-end assembly of NRs has the potential to improve the interpenetrating network of nanocomposites within the active layer of the device, which would enhance the performance of p-type/n-type hybrid solar cells.

4.2 End-to-End Assembly of CdSe Nanorods Using Dithiol-Ligands

CdSe NRs (35 nm x 6 nm) were synthesized following a method previously reported by Peng and Peng.[32] The NRs were washed several times with chloroform and methanol to remove excess native ligands (trioctylphosphine oxide (TOPO) and tetradecylphosphonic acid (TDPA)), re-dispersed in toluene, and diluted to a concentration of 0.1 mg/mL. Due to the large size of the functional groups in the native ligands (phosphonic acid and phosphine oxide), these ligands preferentially cover the longitudinal faces of the NRs. Moreover, the binding energies of the ligands on these faces are higher than the binding energy of the NRs on the tips of the NRs (1.23 – 1.37 eV and 0.85 eV, respectively),[52] making the NR end facets ligand deficient and allowing replacement of the tip ligands with stronger end-specific functional molecules.

In this chapter, an end-to-end assembly of CdSe NRs using P3HTs as linkers was described. A simple, one-step ligand exchange process, was employed to replace the

native ligands on CdSe NRs with 1,3-propanedithiol. By adding a small amount of dithiol ligands to the CdSe NR solution (CdSe:SH = 40:1 v/v), the thiol head groups bound primarily to the end facets of the NRs. When both thiol groups of the dithiol molecules attached to the tips of two adjacent NRs, these molecules acted as linkers producing the end-to-end assembly of NRs, as shown in **Figure 4.1**.

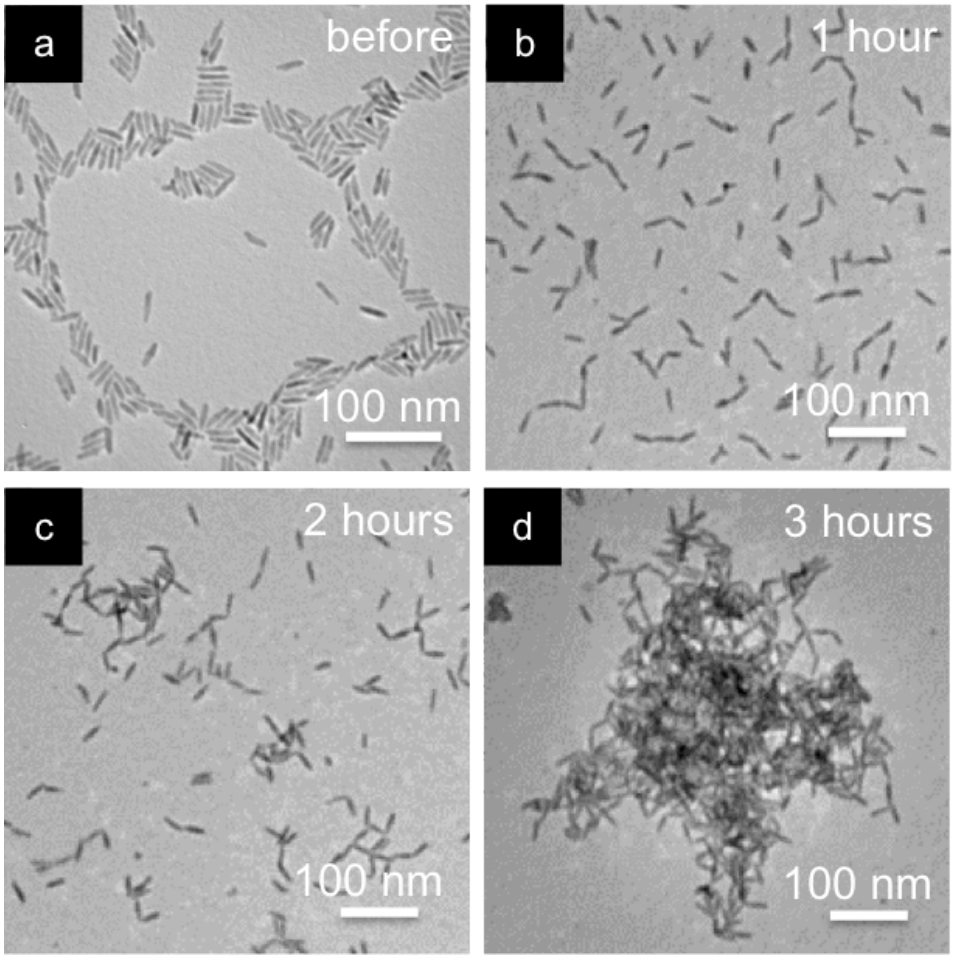

Figure 4.1 TEM images of the end-to-end assembly of CdSe nanorods over time by using 1,3-propanedithiol as tip ligands (a) before addition of 1,3-propanedithiol, and after (b) 1 hour, (c) 2 hours, and (d) 3 hours of the ligand exchange process.

Before addition of 1,3-propanedithiol, the NRs were fully covered with native ligands and separated from each other or formed side-by-side stacks due to dipole interactions and van der Waals attraction.[91] Following the growth of the NR assembly over time, two steps were identified. First, one end of the dithiol molecules bound to an end facet of the NR tips and replaced the native ligands due to its stronger binding energy, leaving NRs dispersed, as shown in **Figure 4.1(a)**. Next, the free end of the dithiol molecules bound to the tips of adjacent NRs, forming an end-to-end assembly, shown schematically in **Figure 4.2**.

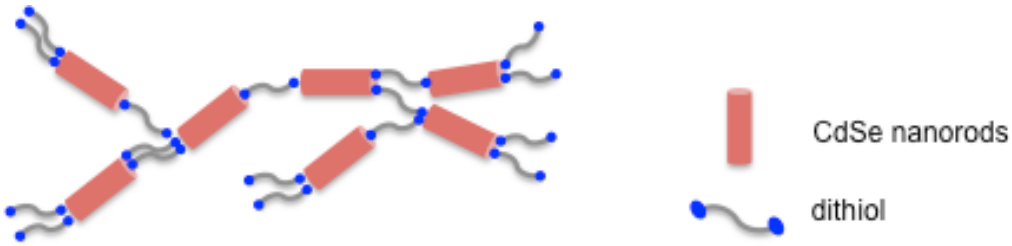

Figure 4.2 Schematic showing the end-to-end assembly of CdSe nanorods using 1,3-propanedithiol as a bifunctional linker.

The end-to-end distance between the NRs in the end-to-end assemblies is less than 1 nm, as observed from TEM, **Figure 4.1(b) – (d)**, which is plausible for a single layer of propanedithiol or a bilayer with a disulfide-linkage. The growth of the assembly proceeded in solution by linking together adjacent NRs. Dimers, trimmers, and oligomers of the NRs were observed after 1 hour of the ligand exchange process, **Figure 4.1(b)**. This process evolved afforded extensive chains, branches, and small aggregates, as observed from TEM images after 2 and 3 hours of the ligand exchange process, **Figure 4.1(C)** and **(d)**. The results are consistent with previous reports of the dimerization of

gold NRs in water:acetonitrile, using 1,2-phenylenedimethanethiol as linker,[83] and the polymerization of gold NRs by addition of non-solvent for the tip ligands (polystryrene),[81] which clearly demonstrate the selective functionalization of thiol end-group on the tip of NRs. When the amount of 1,3-propanedithiol was increased from 10 μL to 500 μL, the NRs aggregated and precipitated, as shown in **Figure 4.3**. Addition of excess dithiol ligands led to ligand replacement not only on the tips of the NRs but also on the longitudinal surfaces of the NRs. These side ligands formed disulfide linkages with the adjacent NRs, resulted in the aggregation as shown in **Figure 4.3(c) and (d)**.

The absorption spectra of the NRs after end-to-end assembly showed a slight red shift (5 nm) compared to the free NR solution (λ_{max} at 652 nm and 647 nm, respectively) (**Figure 4.4**). However, this shift is not as large as the absorption shift of gold NRs after chain formation. A large shift in UV-Vis absorption of chain-like gold NRs is due to the strong surface plasmon resonance energy in both transverse and longitudinal directions, which can be used as an evidence for the end-to-end assembly of gold NRs.[84,90,92,93] In contrast, CdSe NRs do not show this characteristic. Therefore, only a small shift was observed after the assembly. An increased amount of dithiol ligands did not show a significant shift of the maximum absorption peak, however, it caused faster aggregation of the NRs. This implies that only CdSe NR solution having an optimal amount of the replacing ligand generated chain-like structures.

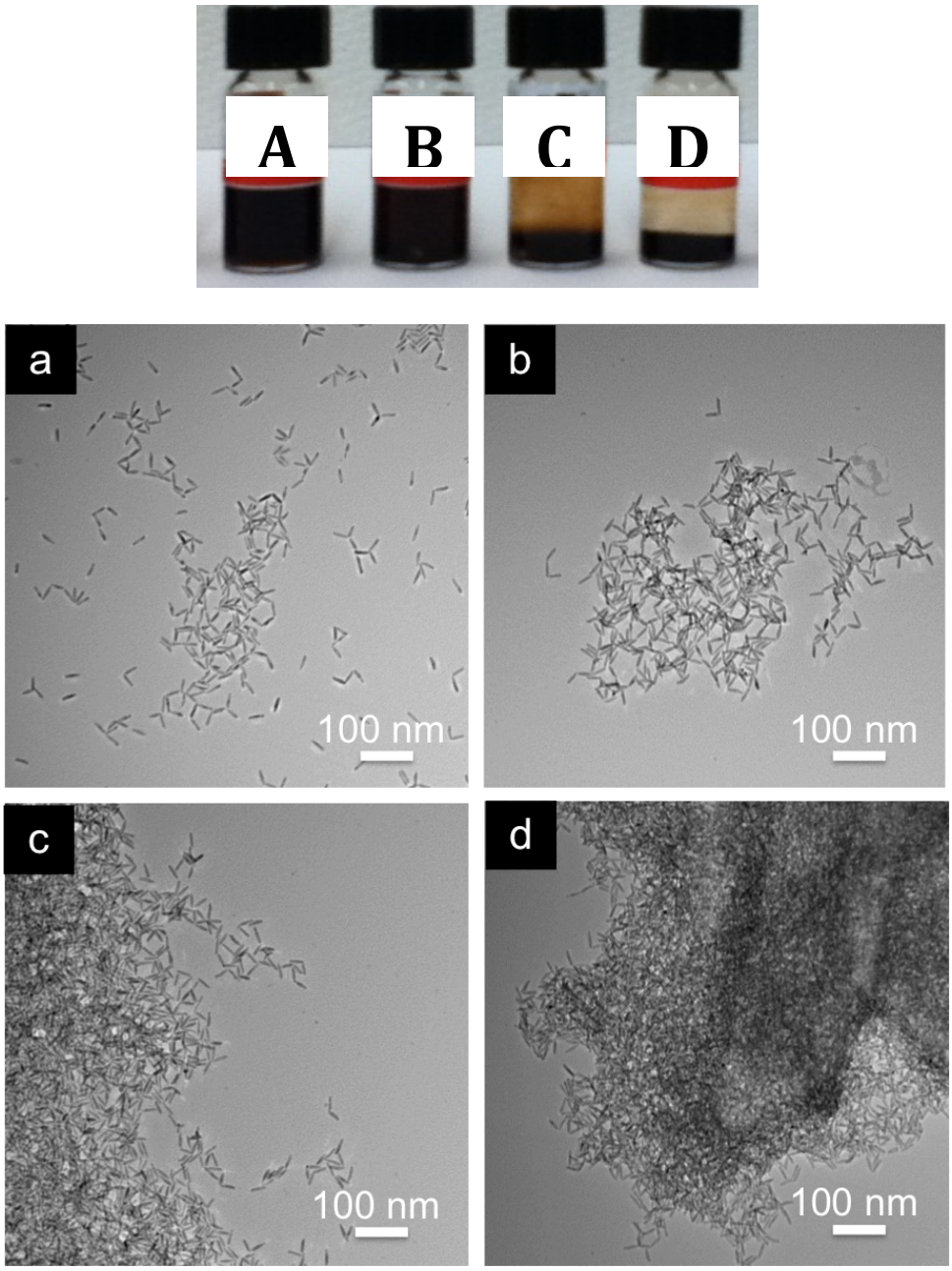

Figure 4.3 Photographs of CdSe nanorods precipitated in solutions with increasing amounts of 1.3-propanedithiol. TEM images of the CdSe nanorods forming end-to-end assemblies with different amounts of 1,3-propanedithiol, (a) 10 µL, (b) 50 µL, (c) 100 µL, and (d) 500 µL.

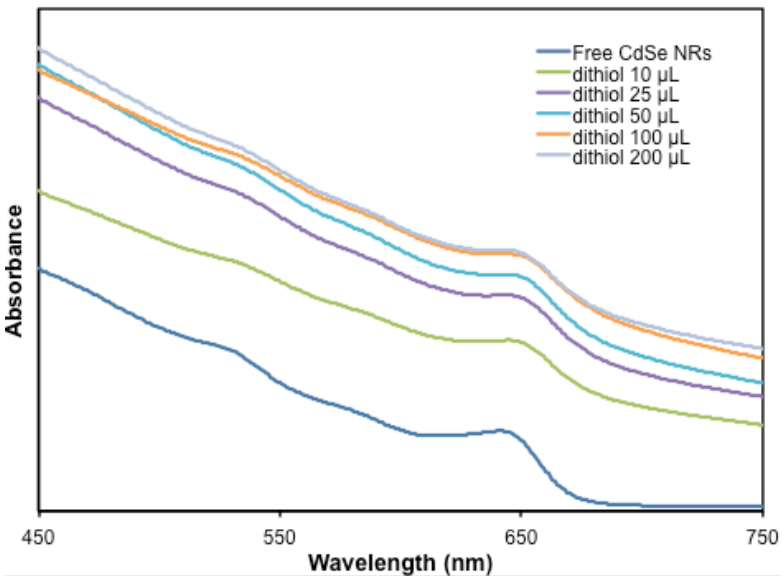

Figure 4.4 UV-Vis absorption spectra of CdSe nanorods after end-to-end assembly with different amount of 1,3-propanedithiol.

The experiments were extended by changing the structure of the dithiol linker from the flexible 1,3-propanedithiol linker to the rigid linkers, benzene-1,4-dithiol and *p*-terphenyl-4,4”-dithiol. The ratio of CdSe:linkers was identical (40:1). TEM images after the ligand exchange process revealed the assembly of NRs in a similar fashion (**Figure 4.5**). All samples showed the end-to-end structures, however, the flexibility and the packing density of the chain-like NR assemblies were obviously different. When the flexible linker, 1,3-propanedithiol, was used, the packing of the chain-like NRs was looser compared to assemblies prepared with the rigid linkers, benzene-1,4-dithiol and *p*-terphenyl-4,4”-dithiol.

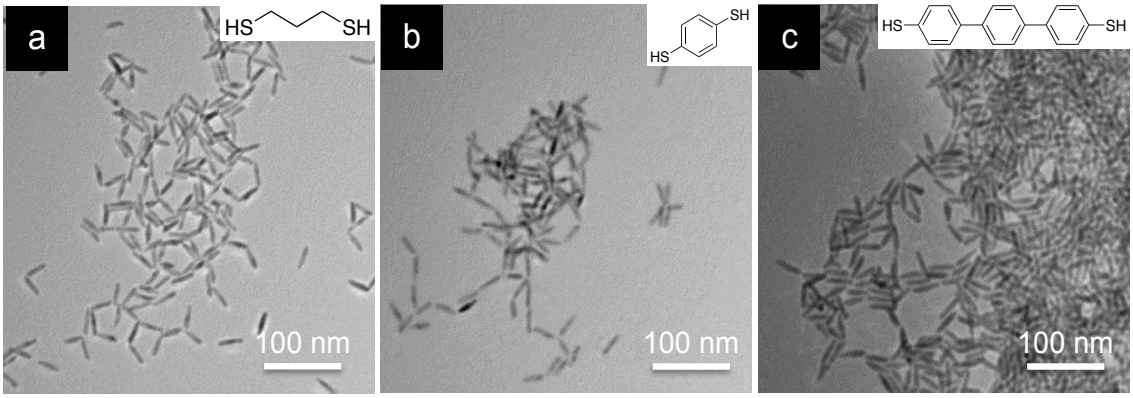

Figure 4.5 TEM images of the CdSe nanorods forming end-to-end assemblies using different types of bifunctional linkers, (a) 1,3-propanedithiol, (b) benzene-1,4-dithiol, and (c) *p*-terphenyl-4,4′′-dithiol.

4.3 Synthesis and Characterization of Functional Polythiophenes

4.3.1 End-Functionalized Side Chains of Polythiophenes

Given that end-to-end assemblies of CdSe NRs can be controlled by changing the tip ligand, we then installed functional groups on P3HT to tune its interactions with the NR surface in the middle of the NRs. P3HT with phosphonate-terminating groups (Mn 7600 g/mol, PDI 1.13) and random copolymers of P3HT and 30% P3HT containing functional groups (Mn 12000 g/mol, PDI 1.38) (thiol, amine and phosphonate) on the alkyl side-chains were synthesized, (**Figure 4.6 and 4.7**). These functional groups have different binding affinities to the CdSe NR surface,[52] which affect the density of the polymers between the NR tips.[30]

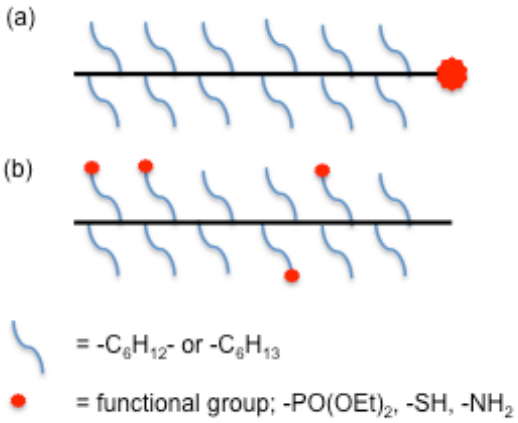

Figure 4.6 Schematic showing sites of functional groups (a) at chain-end of the polymer, and (b) at the end of the hexyl side-chains.

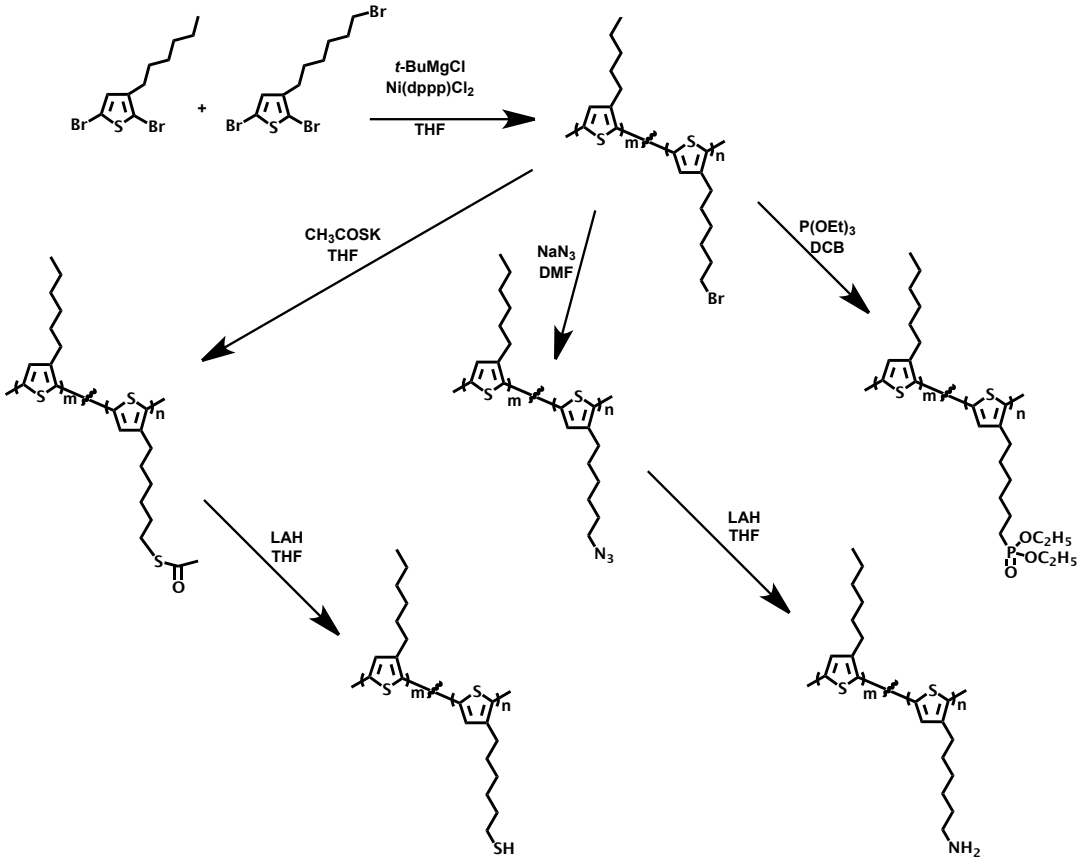

Figure 4.7 Synthesis of PO-P3HT, P3HT-*rnd*-P3(SH)HT, P3HT-*rnd*-P3(PO)HT, and P3HT-*rnd*-P3(NH_2)HT.

The polymers containing different functional groups did not show a significant change in either UV-Vis absorption or fluorescence due to the presence of the hexyl spacers between the thiophene backbones and the functional groups. (**Figure 4.8**) The functional P3HT derivatives contain more anchoring groups than the dithiol ligands, and therefore an increased number of close contacts between the NRs and polymer.

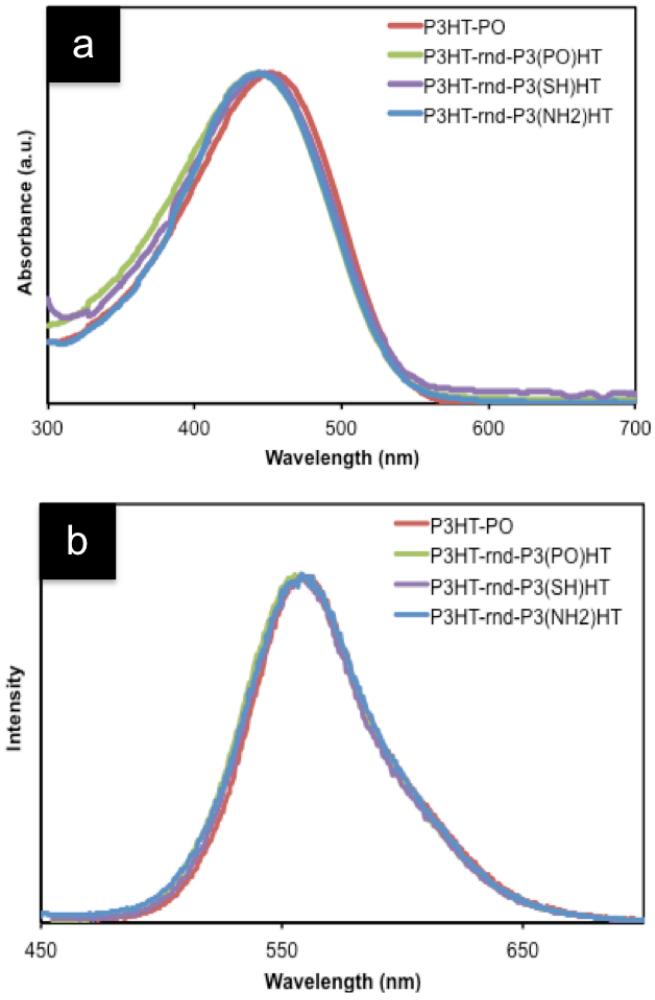

Figure 4.8 UV-Vis absorption (a) and fluorescence spectra (b) of the functional P3HT copolymer solutions in chloroform.

4.3.2 End-to-End Assembly with Polythiophene Ligands

The one-step ligand exchange process using functional P3HT copolymers as ligands was performed slightly differently from the previous discussed procedure using 1,3-propanedithiol due to the difference in size and solubility of the ligands. The polymer solutions were prepared in 1,2-dichlorobenzene (DCB) at with a concentration of 1 mg/mL. The NR and P3HT solutions were mixed in a ratio of 2:1 v/v, and the mixture stirred overnight at 70 ˚C to dissolve the P3HTs. After the ligand exchange process, the NRs were collected by centrifugation to remove free native ligands (TOPO, TDPA) and excess polymer, then re-dispersed in toluene. TEM images of the NRs drop-cast from solution after the ligand exchange process showed the end-to-end assembly of the NRs facilitated by all types of functional P3HT copolymers, similar to the structures observed with the dithiol linkers (**Figure 4.9**).

Since the tip of the NRs (*i.e.* the (0001) facet) is more reactive due to its higher surface energy and less native ligand coverage than the sides of the NRs ((0110) and (1120) facets), the tip ligands are easily replaced by molecules having functional groups with comparable or stronger binding energies, such as phosphonates, amines, and thiols.[52] Interestingly, two types of the end-to-end structures were observed from the functional P3HT copolymer mediated assemblies, depending on the position of the functional groups. Two possible structures leading to the assemblies in **Figure 4.9** are described schematically in **Figure 4.10**.

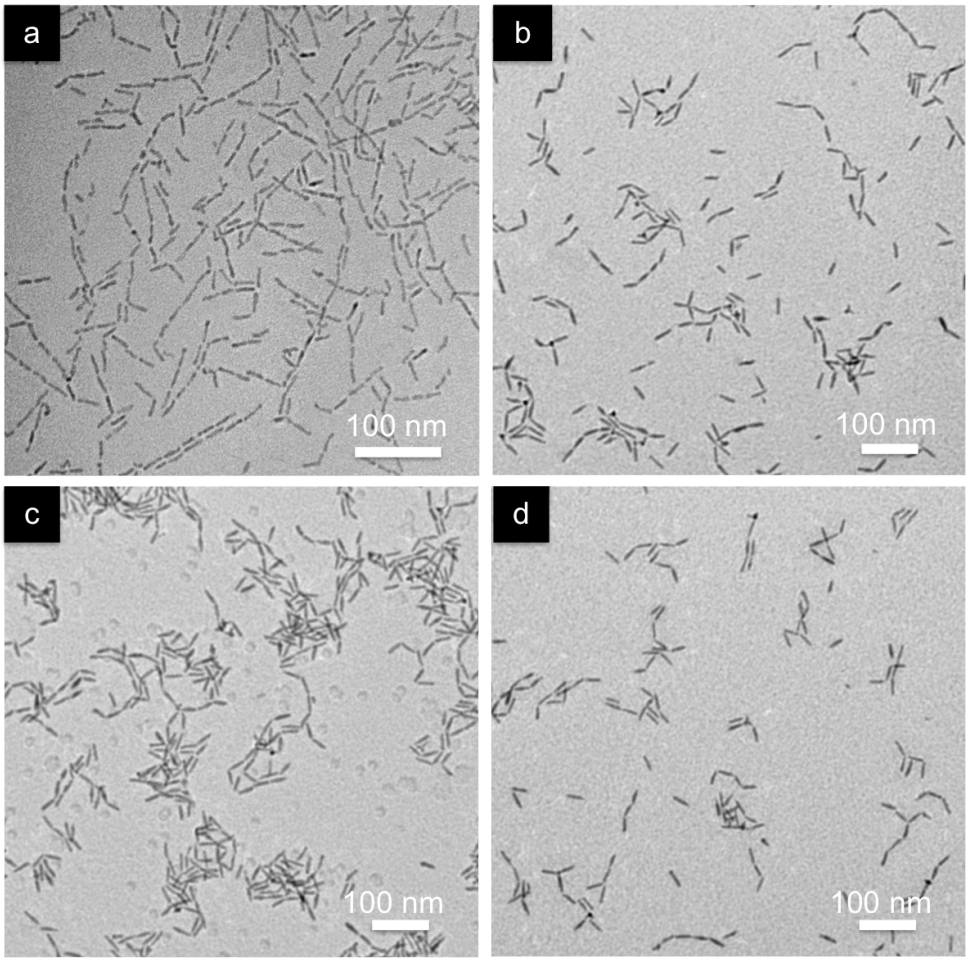

Figure 4.9 TEM images of end-to-end assemblies of CdSe nanorods functionalized with (a) PO-P3HT, (b) P3HT-*rnd*-P3(PO)HT, (c) P3HT-*rnd*-P3(SH)HT, and (d) P3HT-*rnd*-P3(NH_2)HT.

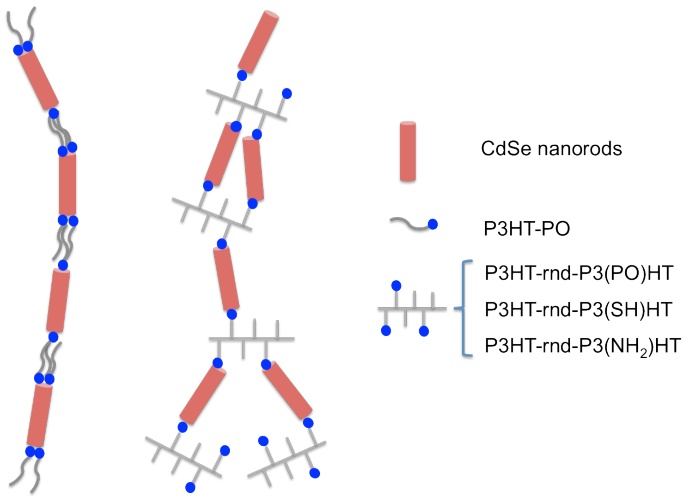

Figure 4.10 Proposed structures of end-to-end assemblies of nanorods with functional polymers as the tip ligands.

When the phosphonate-terminated P3HT was used to functionalize the tips of the NRs, the phosphonate groups bound to the NR tips and the P3HT chains freely moved at the NR ends. These polymer chains crystallized with the P3HT chains on the same NR end and on the adjacent NRs, leading to strong π-π stacking interactions, affording rigid linkers between the ends of adjacent NRs. These crystalline linkers led to the straight end-to-end assemblies of NRs, shown in **Figure 4.9(a)**. On the other hand, when P3HT having functional side chains were used as ligands, the functional groups on the hexyl side chains of the same polymer attached to one or two adjacent NRs. This hindered the crystalline packing of the P3HT chains, resulting in flexible connections and branched end-to-end assemblies, **Figure 4.9(b) - (d)**.

The optical properties of the NRs before and after the ligand exchange process with the functional P3HT were then studied. UV-Vis absorption spectra of P3HT functionalized CdSe NRs in **Figure 4.11** clearly show the combination of the absorption

spectra of both P3HT and CdSe NRs (λ_{max} at 450 nm and 628 nm, respectively). This is additional evidence for the direct attachment of the polymers on the NR tips. Fluorescence spectra of the nanocomposites in **Figure 4.11** show nearly complete quenching of the P3HT fluorescence at 554 nm, indicating efficient charge transfer from P3HT to the CdSe NRs.[30] These results suggest that using conjugated polymers containing multiple anchoring group as linking sites improves the rate of charge transfer from the polymer to the NRs, as well as the charge transport along the NR end-to-end assemblies.

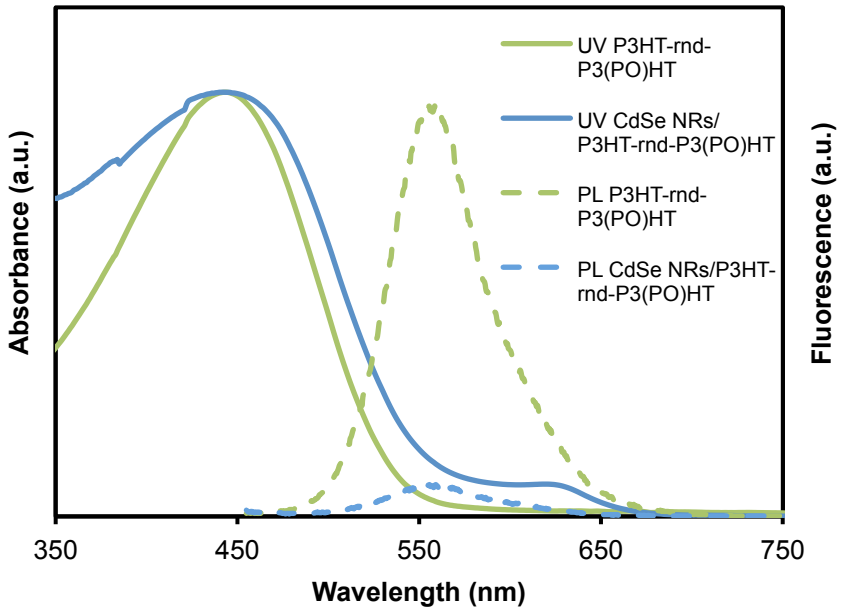

Figure 4.11 Optical properties of P3HT-*rnd*-P3(PO)HT solutions before (solid lines) and after functionalization onto CdSe NR tips (dashed lines).

4.4 Summary

In summary, P3HT functionalized CdSe NRs with three binding groups (phosphonate, thiol, and amine) either at the chain ends or on the side chains of the polymers has been synthesized. A facile one-step ligand exchange process was employed to replace the native ligands at the tips of the NRs with the functional P3HT, leading to the end-to-end assembly of the NRs. Two types of end-to-end assemblies of the CdSe NRs were obtained using the functional P3HTs as linkers, depending on the number and the positions of the functional groups on the polymer chains. These types of the NR arrangement have the potential to improve charge transfer between p-type/n-type nanocomposites, as well as charge transport along NR end-to-end assemblies, which will benefit organic-inorganic hybrid photovoltaic devices.

4.5 Experimental Section

4.5.1 Materials

Sodium azide (NaN_3, 99% min) was purchased from Alfa Aesar. Tris(dibenzylidene acetone)dipalladium ($Pd_2(dba)_3$) and 1,3-bis(diphenylphosphino)-propane nickel (II) chloride ($Ni(dppp)Cl_2$ 99% were purchased from Strem Chemicals. Tri-*t*-butylphosphine solution (1.0 M in toluene), lithium aluminum hydride (LAH) (1.0 M in THF), potassium thioacetate (CH_3COSK, 98%), triethyl phosphite ($P(OEt)_3$, 98%), *t*-butylmagnesium chloride (*t*-BuMgCl, 2.0 M in diethyl ether), and all other reagents were purchased from Sigma Aldrich. Tetrahydrofuran (THF) was distilled over sodium and benzophenone. All other reagents were used as received.

4.5.2 Characterization

The assemblies of NRs were imaged on a transmission electron microscope (TEM) (JEOL 2000FX), using accelerating voltage of 200 keV. Absorption and fluorescence measurements of CdSe NR solutions were performed on a Perkin-Elmer Lambda 25 UV/Vis spectrometer and a LS 55 Luminescence spectrometer, respectively. Nuclear Magnetic Resonance (NMR) spectra were obtained from a Bruker DPX-300 NMR spectrometer. Gel permeation chromatography (GPC) was performed with a Polymer Laboratories PL-220 high temperature GPC operated at 135 ˚C equipped with a refractive index detector. 1,2,4-Trichlorobenzene was used as the eluent, and the system was calibrated with PS standards.

4.5.3 Ligand Exchange of CdSe Nanorods

CdSe NRs (35 nm x 6 nm) were precipitated into MeOH to remove excess ligands and centrifuged. The supernatant containing excess ligands was discarded, and the precipitate was re-dispersed in chloroform. This washing process was repeated 5 times. The NRs were re-dispersed in toluene at a concentration of 2 mg/mL. A solution of 1,3-propanedithiol 0.1 wt% in toluene (25 μL) was added to 1 mL of 0.1 mg/mL CdSe NR solution (40:1 v/v). The solution was stirred overnight at room temperature. For the P3HT copolymer ligands, the polymers were dissolved in 1,2-DCB at a concentration of 1 mg/mL. The P3HT solution was mixed with the CdSe NR solution at a ratio of 2:1 v/v, and the mixture stirred at 70˚C overnight. After assembly, the NRs were collected by centrifugation at 13000 rpm for 10 min and re-dispersed in toluene. TEM samples were prepared by drop-casting the solution onto copper grids.

4.5.4 Synthesis of Poly(3-hexylthiophene)-random-poly(3-bromohexylthiophene) (P3HT-rnd-P3BrHT)

The synthesis procedure was modified from a procedure previously reported by Zhai *et al*.[94] 2,5-Dibromo-3-hexythiophene (4.90 g, 15.00 mmol) and 2,5-dibromo-3-bromohexylthiophene (2.03 g, 5.00 mmol) were added to a 100 mL 3-neck round bottom flask and dissolved in THF (60 mL). *t*-BuMgCl (10.00 mL, 20.00 mmol) was added with a syringe to the reaction. The mixture was refluxed for 1 h, and additional 60 mL of THF was added. Ni(dppp)Cl_2 (0.18 g, 0.33 mmol) was added, and the mixture was stirred at room temperature for 1 h before precipitation into MeOH. The product was purified by Soxhlet extraction. (MeOH, hexanes, chloroform). TCB GPC: Mn 12000 g/mol, PDI 1.38.

4.5.5 Synthesis of Poly(3-hexylthiophene)-random-poly(3-hexylthiolthiophene) (P3HT-rnd-P3(SH)HT)

In a 3-neck round bottom flask, P3HT-*rnd*-P3BrHT (0.40 g, 3.00 mmol) was dissolved in THF (40 mL), and potassium thioacetate (2.00 g, 17.5 mmol) was added to the solution. The mixture was stirred at 65 ˚C overnight followed by precipitation into MeOH.[94]

4.5.6 Synthesis of Poly(3-hexylthiophene)-random-poly(3-hexylphosphonic acid diethyl ester thiophene) (P3HT-rnd-P3(PO)HT)

In a 3-neck round bottom flask, P3HT-*rnd*-P3BrHT (0.40 g, 3.00 mmol) and triethyl phosphite 6.00 mL, 35.00 mmol) were dissolved in DCB (30 mL). The solution was stirred at 165 ˚C overnight before precipitation into MeOH.

4.5.7 Synthesis of Poly(3-hexylthiophene)-random-poly(3-hexylamine thiophene) (P3HT-rnd-P3(NH_2)HT)

In a 3-neck round bottom flask, P3HT-*rnd*-P3BrHT (0.40 g, 3.00 mmol) was dissolved in DMF (100 mL). The solution was heated to dissolve the polymer at 153 ˚C. Sodium azide (2.00 g, excess) was added to the reaction and the mixture was refluxed overnight before quenching by addition of MeOH. The solution was then precipitated into MeOH.[94]

CHAPTER 5

ASSEMBLY OF POLYTHIOPHENE-FUNCTIONALIZED CDSE NANORODS ON GRAPHENE

5.1 Introduction

5.1.1 Graphene in Solar Cells

Graphene is a two-dimensional crystal composed of a single layer of sp^2-hybridized carbon atoms. The 2D graphene sheet has attracted interest in physics, chemistry, and material science due to its unique mechanical and electronic properties, which are suitable for many applications, including transistors, sensors, and electrodes.[95–98] Graphene-based materials also draw interest in energy related applications, such as solar cells,[99–102] capacitors,[103–106] and lithium-ion batteries.[107,108] Recently, introduction of graphene into photovoltaic (PV) devices has been reported to improve the PV device performance when graphene was employed as a transparent conducting electrode or as an acceptor material. [96,109–111] One of the benefitial properties of graphene is its extremely high electron mobility (2×10^5 $cm^2v^{-1}s^{-1}$)[112] compared to silicon. Additionally, a single layer of graphene is nearly transparent (it absorbs only ~ 2% of incident light)[113] and has robust mechanical properties, making it an ideal material to be used as an electrode in PV devices. Graphene has been reported as both an electron and a hole transporter,[114–119] as well as an interfacial layer,[120,121] and as a Schottky junction layers.[122–125] Moreover, due to the unique structure of the graphene, it is used as a template in organic-inorganic graphene-based PV devices *via* π-π stacking.[126–128]

5.1.2 Graphene as Electrodes

The mechanical properties and high optical transparency of graphene makes it a beneficial material for use as flexible electrodes in PV cells. Zhou and workers reported the use of graphene as flexible transparent conducting electrodes, fabricated by chemical vapor deposition (CVD). The graphene was first deposited onto a silicon substrate, then transferred onto a transparent substrate (glass or polyethylene terephthalate), as shown in **Figure 5.1**. This technique provided smooth and continuous graphene films (minimum surface roughness ~ 0.9 nm) and offered a sheet resistance as low as 230 Ω/sq with 72% transparency. PV cells fabricated with copper phthalocyanine/fullerene/batho-cuproine active layer and a graphene anode afforded a power conversion efficiency (PCE) of 1.18%, which is comparable to a similar device with an ITO electrode (1.27%).[129]

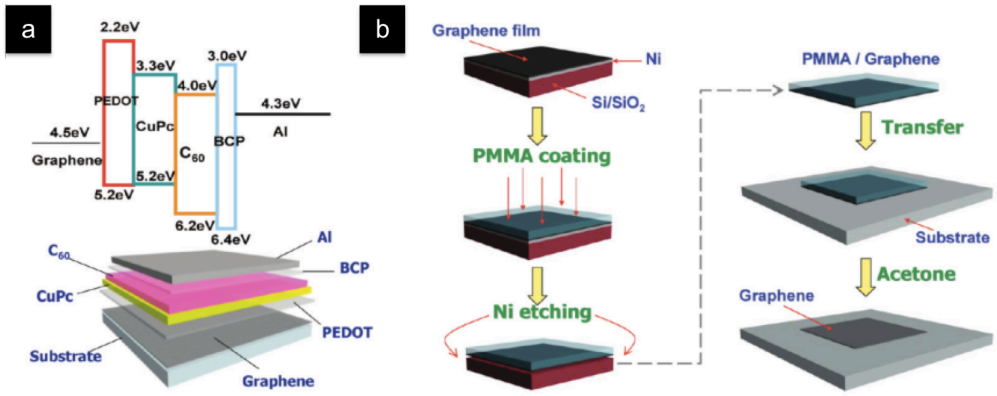

Figure 5.1 Schematic representation of (a) the energy level alignment and construction of an heterojunction organic solar cell fabricated with graphene as the anodic electrode, and (b) the CVD graphene transfer process onto transparent substrates.[129]

A similar technique was used to generate graphene electrodes with controlled thicknesses by adjusting the flow rate of hydrogen gas during the CVD process. A device with ZnO/CdS/CdTe as the active layer, as shown in **Figure 5.2(a)**, resulted in a PCE of 4.17%.[130] Park and cowokers reported crystalline ZnO nanowires (NWs) grown directly on a graphene substrate using a hydrothermal method. In their work, the graphene exhibited a sheet resistance of 300 Ω/sq with 92% transparency. A device having PbS quantumdots (QDs) or P3HT as the active layer materials gave a PCE of 4.2%, as shown in **Figure 5.2(b)**.[131]

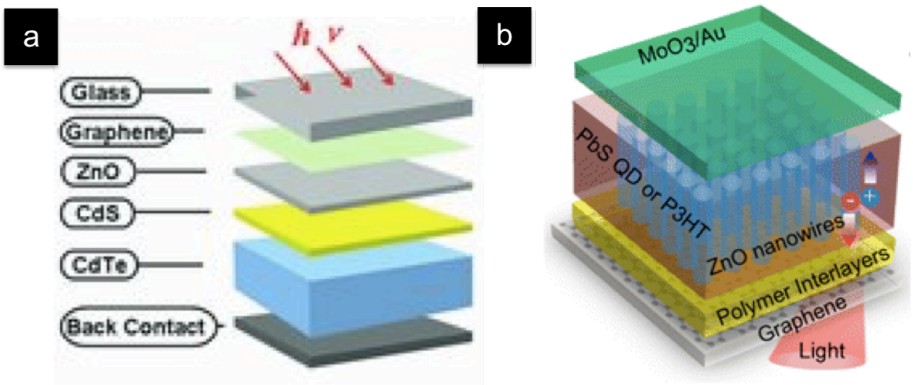

Figure 5.2 Schematic diagram of (a) a glass/graphene/ZnO/CdS/CdTe/graphite paste solar cell,[130] and (b) a graphene/PEDOT:PEG(PC)ZnO/PbS or P3HT/MoO_3 solar cell.[131]

Not only graphene, but also reduced graphene oxide (rGO) was reported as an electrode material in hybrid solar cells. Zhang and coworkers synthesized rGO by a two-step reduction of graphene sheets, using hydrazine vapor to generate rGO with a sheet resistance of 420 Ω/sq and 61% transparency. This rGO sheet was used as an electrode in a device having electrochemically-deposited ZnO nanorods (NRs) as the n-type material

and poly(3-hexylthiophene) (P3HT) as the p-type material. The inorganic-organic hybrid solar cell afforded a PCE of 0.31%.[111]

5.1.3 Graphene in Active Layers

Due to the high charge mobility of graphene, it has been reported as an active layer material in PV devices as well.[132,133] The energy level and work function of graphene can be altered by chemical functionalization or a doping with other semiconducting materials.[122,124,125,134] Chen and coworkers reported the use of graphene as an acceptor material in a PV device. In their work, a graphene oxide sheet was functionalized with phenyl isocyanate to reduce the hydrophilicity of the graphene. These functional groups were then removed by thermal annealing at 160 ˚C for 20 minutes. A device having functionalized graphene and poly(3-octylthiophene) as the active layer gave a PCE of 1.4%.[132] A Schottky junctional solar cell fabricated from a CdSe nanobelt and a graphene sheet was reported by Qin and coworkers that afforded a PCE of 1.25%. They developed a patterning method using electron beam lithography to prepare graphene.[135]

One of the most beneficial properties of graphene is its high electron mobility, which makes it suitable for use as an electron transport layer. Jiang and coworkers reported the use of rGO in dye-sensitizer solar cell, where rGO was used as a 2-dimensional electron transport layer. Comparing the efficiency of the devices having TiO_2 nanoparticles (NPs) - 2D rGO nanocomposites with those having TiO_2 NPs - 1D carbon nanotube (CNT) nanocomposites as electron transport layers, they found that 2D rGO performed faster electron transfer from the TiO_2 NPs to rGO and faster electron

transport along rGO to the collection electrode due to better attachment and intermolecular connection of TiO_2 NPs onto 2D rGO sheets, resulting in a reduction of charge recombination at interface, as shown in **Figure 5.3**.[136]

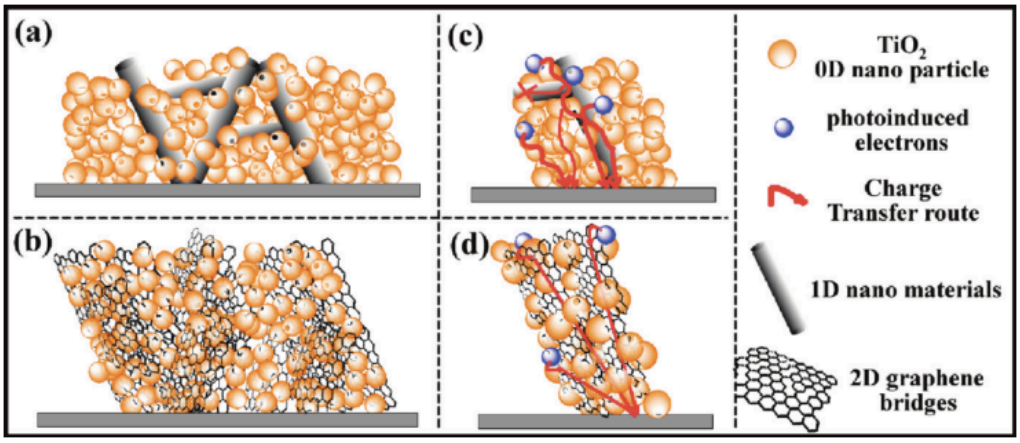

Figure 5.3 Schematic illustrations of 1D (carbon nanotube) and 2D (reduced graphene oxide) nanocomposite electrodes.[136]

5.1.4 Graphene as Templates

Dai and coworkers reported fullerene-grafted graphene prepared by a lithiation reaction. Additionally, reduced graphene oxide was prepared by treating graphene with hydrazine followed by reaction with n-butyllithium and C_{60}. The C_{60} attached on the rGO acted as a nucleation site for C_{60} aggregates. The rGO-C_{60} composite was used as an electron acceptor in a P3HT-based PV device, giving a PCE of 1.22%.[137] Gong and coworkers report the use of graphene oxide as a supporting layer for the synthesis of CdS NPs using a solvothermal method. The GO-CdS nanocomposite was used as photocatalyst in the production of H_2, providing a higher H_2-production rate than pure CdS NPs. They concluded that graphene served as both an electron collector and

transporter, decreased the probability of charge recombination, and lengthened the lifetime of the photogenerated charges from CdS NPs.[138] As mention above, graphene is a honeycomb lattice of sp^2-hybridized carbon atoms capable of π-π stacking and functionalization *via* hydrogen bonding.[139] Dai and coworkers reported noncovalent functionalization of the sidewall of single-walled carbon nanotubes (SWNTs) with pyrene derivatives containing the functional anchoring groups, 1-pyrenebutanoic acid and succinimidyl ester, which absorbed strongly on the surface of SWNTs *via* the π-π stacking of pyrene and on the basal plane of SWNTs, as shown in **Figure 5.4**. The functional groups on pyrene enabled protein immobilization on nanotubes.[140]

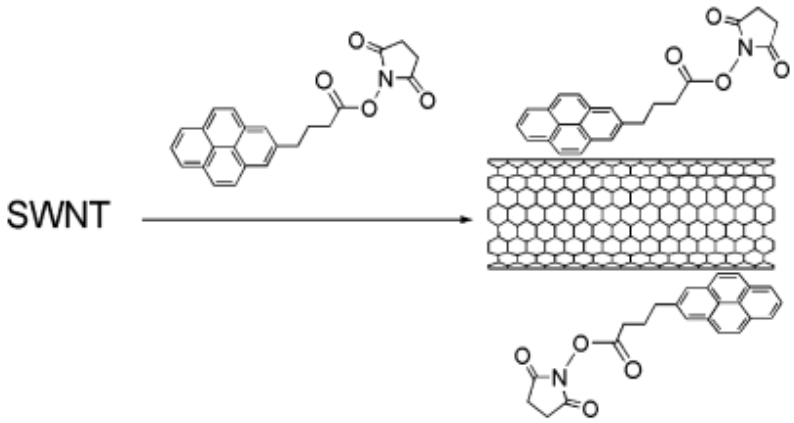

Figure 5.4 Schematic shows interactions of carbon nanotubes with pyrene derivatives.[140]

5.2 Polythiophene-Coated CdSe Nanorods

In this chapter, the assembly of polythiophene functionalized CdSe NRs on graphene is discussed. Block copolymers of poly(3-hexylthiophene) (P3HT) and P3HT containing functionalized groups on the alkyl chains were synthesized (Mn 13500 g/mol,

PDI 1.35) using a similar procedure to those described in the previous chapter. Two types of anchoring groups, phosphonate and thiol, were functionalized onto a small percent of the hexyl side chains of P3HT to avoid crosslinking while providing sites to bind to the NR surface with different binding affinities, as shown in **Figure 5.5**.[52]

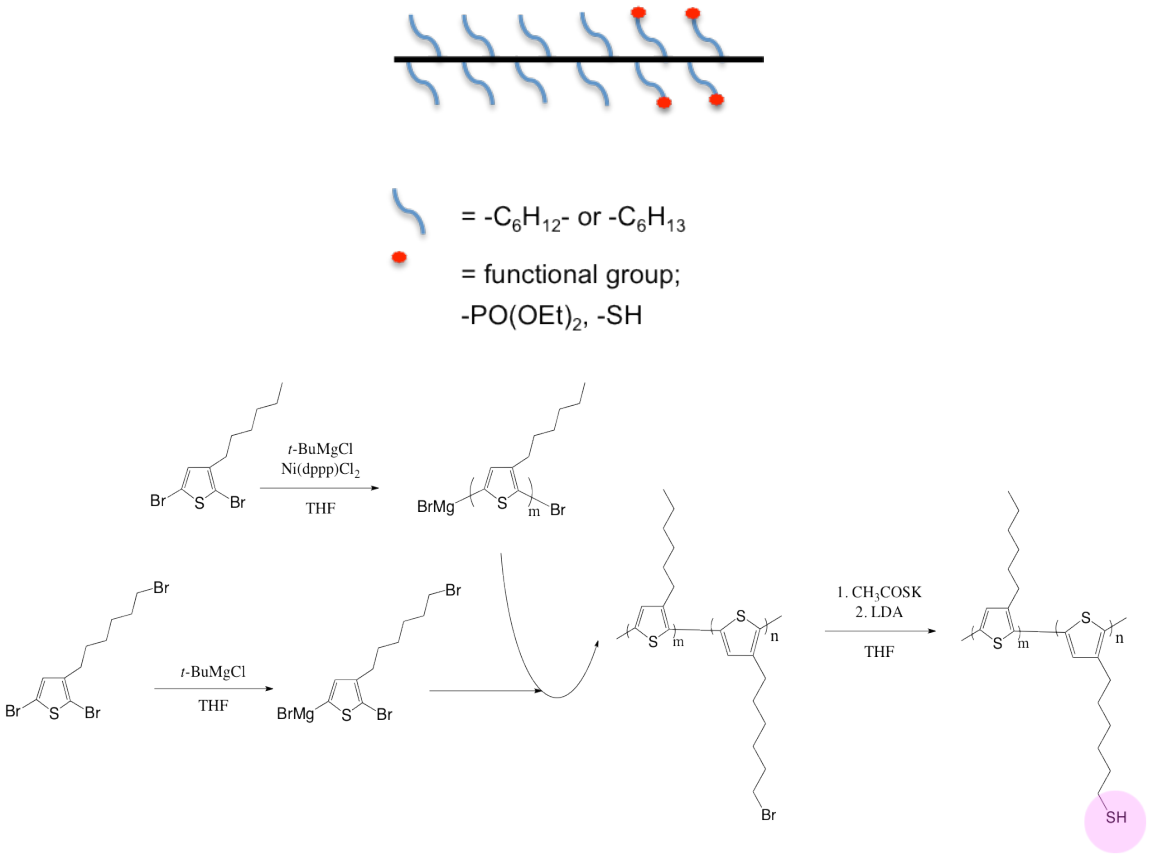

Figure 5.5 The top schematic shows the position of functional group at the end of the hexyl side-chains of the P3HT block copolymers and the bottom schematic describes the synthesis of P3HT-*b*-P3(SH)HT.

^{1}H NMR spectroscopy was used to characterize the percent incorporation of functional groups on P3HT, revealing 15 mol% of functional 3-hexyl thiophene units incorporated

in the block copolymers. **Figure 5.6** shows the ^{1}H NMR spectra of the block copolymers. It is clear that after the reaction of Br-P3HT with potassium thioacetate followed by the reduction of the thioacetate group, the peak at 3.40 ppm (-CH_2-Br) disappeared while a peak 2.15 ppm (-CH_2-SH) appeared, confirming the conversion of the bromide to a thiol.

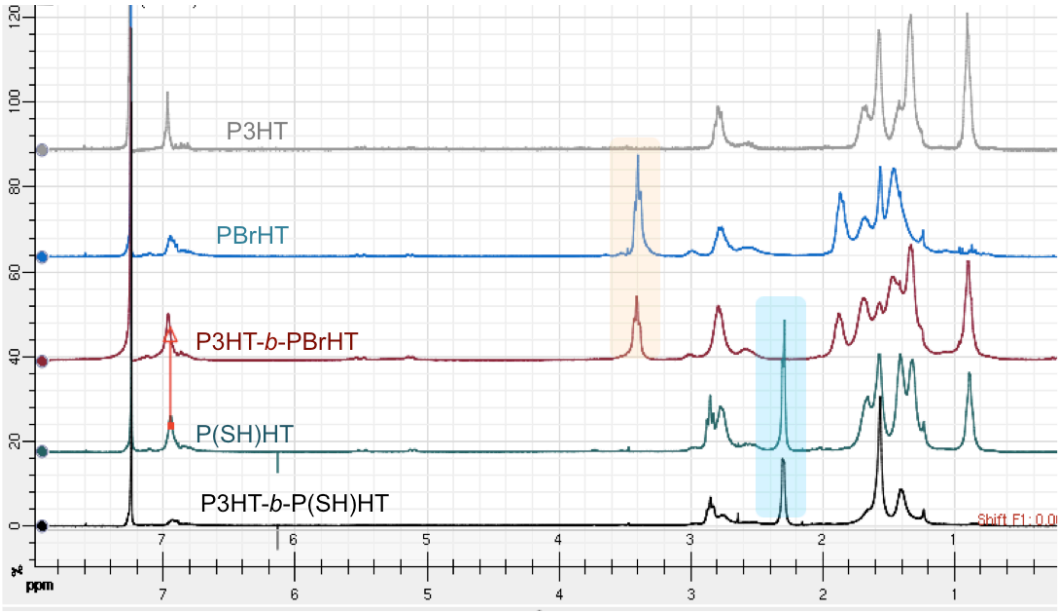

Figure 5.6 ^{1}H NMR spectra of poly(3-hexylthiophene) homopolymer and block copolymer before and after functionalization with thiol.

The optical properties of the block copolymers containing multiple functional groups (thiol or phosphonate) did not show a significant change in either their UV-Vis absorption or fluorescence, similar to what was observed in the case of random polymers described in the previous chapter.

5.3 Assembly and Characterization of Polythiophene Functionalized CdSe Nanorods on Graphene

A one-step ligand exchange process was employed to replace the native ligands (TOPO, TDPA) with functionalized P3HT block copolymers. The polymer solutions were prepared in 1,2-dichlorobenzene (DCB) at a concentration of 1 mg/mL. The CdSe NR (35 nm x 6 nm) solution and the P3HT solutions were mixed in a ratio of 10:1 v/v, and the mixture was stirred overnight at 70 ˚C to dissolve the P3HT. After the ligand exchange process, the NRs were collected by centrifugation to remove free native ligands (TOPO, TDPA) and excess polymer then re-dispersed in toluene. A similar procedure was applied to CdSe NPs (4 nm) to functionalize the surface with P3HT. TEM images of the NPs and the NRs drop-cast from solution after the ligand exchange process showed good dispersion in both cases, as shown in **Figure 5.7**, suggesting full coverage of P3HT block copolymers on the surfaces. Additionally, UV-Vis absorption spectra of solutions of CdSe NPs and CdSe NRs functionalized with P3HT-*block*-P3(SH)HT solutions showed a combination of the absorption spectra of P3HT and CdSe NRs, as observed in the case of random copolymers in the previous chapter, which is additional an evidence for the direct attachment of the polymers on the NR surfaces.

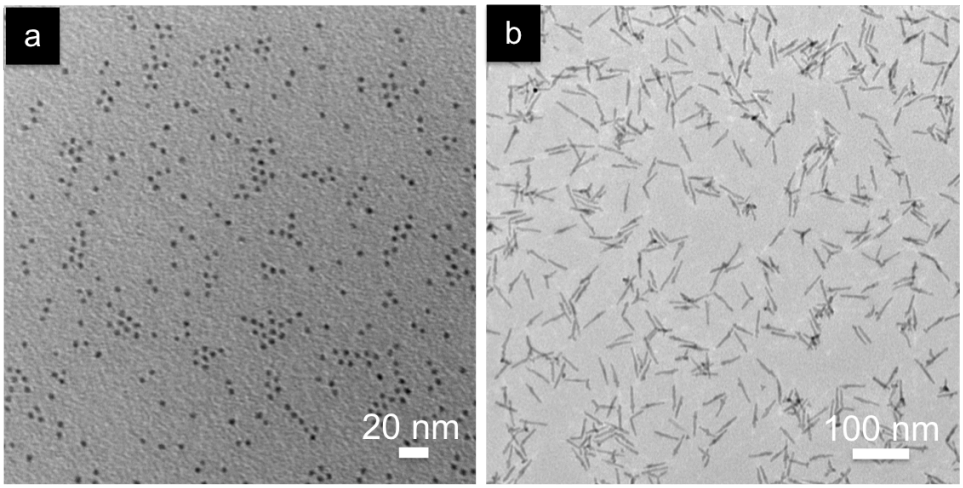

Figure 5.7 TEM images of (a) CdSe nanoparticles and (b) CdSe nanorods functionalized with P3HT-*block*-P3(SH)HT.

Lobez and Afzali reported the assembly of carbon nanotubes (CNTs) using side-chain functionalized poly(thiophene)s. In their work, the CNTs were wrapped with poly(thiophene)s *via* π-π stacking of the CNTs and the thiophene backbone, leaving free side chains to interact with the substrate.[141] Using a similar approach, CdSe NRs were coated with thiol-functionalized P3HT block copolymers described in the previous section. The thiol-containing block bound to the NR surface, while the P3HT block was free to assemble on reduced graphene oxide *via* π-π interactions, as shown in **Figure 5.8**.

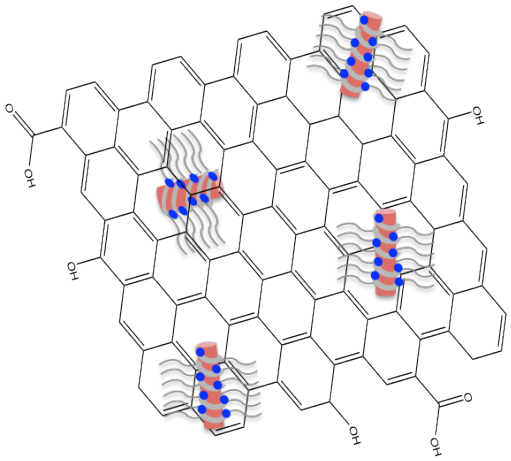

Figure 5.8 Schematic illustrating the assembly of P3HT-*block*-P3(SH)HT functionalized CdSe NRs on graphene.

Reduced graphene oxide was prepared by Hummer's method and re-dispersed in toluene.[142] The P3HT functionalized CdSe NP and NR solutions were prepared in DCB at a concentration of 2 mg/mL. The CdSe NR solution and the graphene solution were mixed at a ratio of 10:1 v/v, and the mixture stirred overnight at room temperature. After the assembly process, the P3HT-functionalized CdSe NRs on the graphene were collected by centrifugation and re-disperse in toluene. TEM images of the functionalized CdSe NPs and CdSe NRs drop-cast from solution after the assembly process showed the attachment of the NPs and NRs on graphene, as shown in **Figure 5.9(a)** and **(b)**. A control experiment was carried out using the CdSe NRs without functionalization with P3HT. The TEM image from this experiment, **Figure 5.9(c)**, shows no decoration or direct attachment of the NRs on graphene due to the lack of π-π stacking interactions between the two materials.

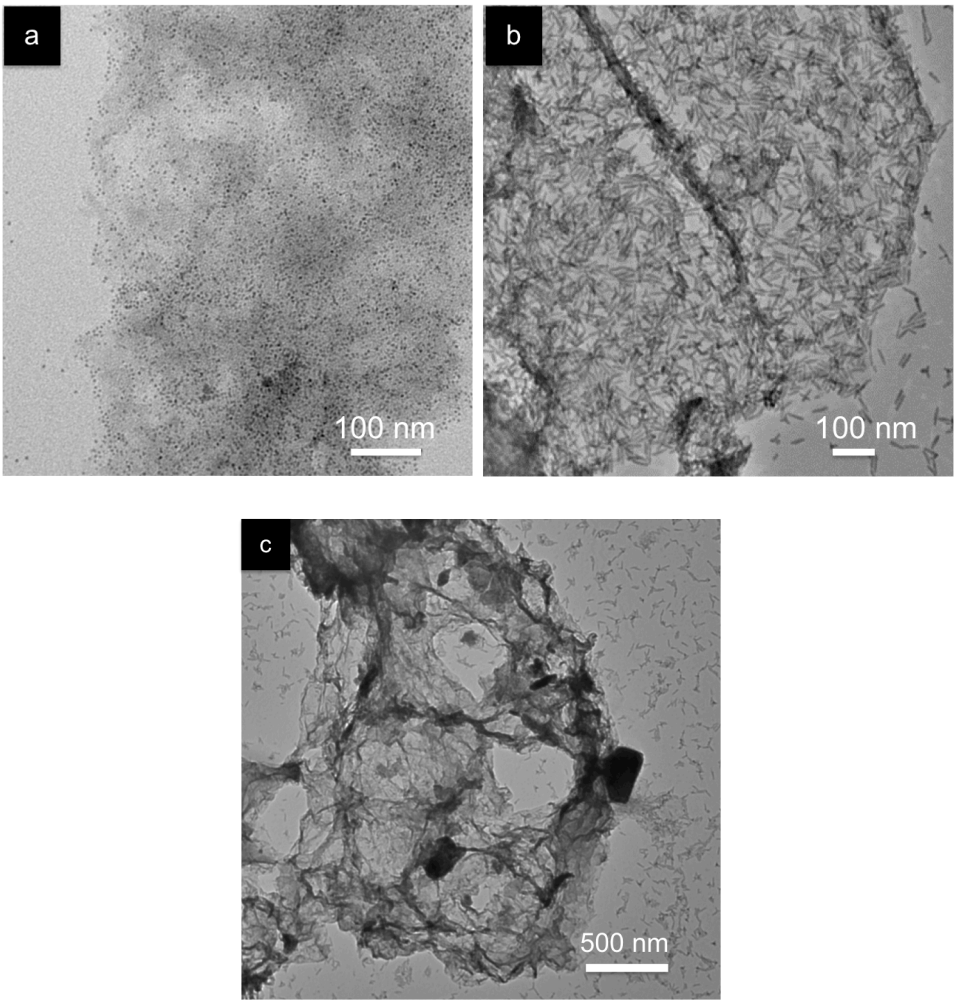

Figure 5.9 TEM images of (a) CdSe nanoparticles, (b) CdSe nanorods functionalized with P3HT-*block*-P3(SH)HT assemble on graphene, and (c) a controlled experiment.

The assembly of CdSe NPs and NRs on graphene not only prevented the aggregation of the NPs and NRs, but also improved charge transfer between the nanocomposites due to the increased number of contact points between graphene and the functionalized CdSe NRs. The fluorescence of the P3HT-*block*-P3(SH)HT before and after functionalization on the CdSe NR surface was studied. **Figure 5.10** shows quenching of 90% of the polymer's emission intensity after functionalization on the CdSe NR surface, and total

quenching when the functionalized NRs were assembled on graphene, suggesting efficient charge transfer between the three materials upon light irradiation.

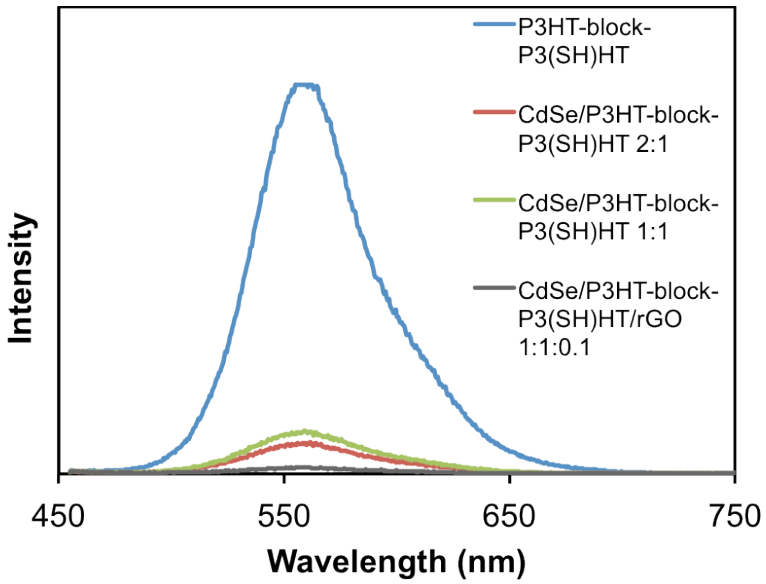

Figure 5.10 Fluorescence spectra of P3HT-*block*-P3(SH)HT solutions before and after functionalize onto CdSe nanorod surface, and after assembly on graphene.

5.4 Summary and Future Outlook

In summary, block copolymers of P3HT and 15 mol% of P3HT containing functionalized groups, phosphonate and thiol, on the hexyl chains were synthesized. A one-step ligand exchange process was employed to coat the NR surface with functionalized P3HT block copolymers. The polythiophene covered CdSe NRs were assembled on graphene *via* π-π interactions as observed by TEM. UV-Vis absorption spectra and complete quenching of fluorescence of the nanocomposite solutions confirmed the direct attachment of the polymers on the NR surfaces and improvement of charge transfer between the nanocomposites and graphene due to the increased number of

contact points between three materials. These composite materials have potential to benefit inorganic-organic hybrid PV applications.

REFERENCES

(1) Lee, A.; Zinaman, O.; Logan, J. Opportunities for Synergy Between Natural Gas and Renewable Energy in the Electric Power and Transportation Sectors Opportunities for Synergy Between Natural Gas and Renewable Energy in the Electric Power and Transportation Sectors. *NREL Tech. Rep.* **2012**.

(2) Coakley, K. M.; McGehee, M. D. Conjugated Polymer Photovoltaic Cells. *Chem. Mater.* **2004**, *16*, 4533–4542.

(3) Wright, M.; Uddin, A. Organic—inorganic Hybrid Solar Cells: A Comparative Review. *Sol. Energy Mater. Sol. Cells* **2012**, *107*, 87–111.

(4) Liu, F.; Gu, Y.; Jung, J. W.; Jo, W. H.; Russell, T. P. On the Morphology of Polymer-Based Photovoltaics. *J. Polym. Sci. Part B Polym. Phys.* **2012**, *50*, 1018–1044.

(5) Ma, W.; Yang, C.; Gong, X.; Lee, K.; Heeger, A. J. Thermally Stable, Efficient Polymer Solar Cells with Nanoscale Control of the Interpenetrating Network Morphology. *Adv. Funct. Mater.* **2005**, *15*, 1617–1622.

(6) Louis, A.; Sanchez, C.; Curie, M. Synthesis and Characterization of Mesostructured Titania-Based Materials through Evaporation-Induced Self-Assembly. *Chem. Mater.* **2002**, *14*, 750–759.

(7) Kamat, P. V. Quantum Dot Solar Cells. Semiconductor Nanocrystals as Light Harvesters. *J. Phys. Chem. C* **2008**, *112*, 18737–18753.

(8) Chen, D.; Nakahara, A.; Wei, D.; Nordlund, D.; Russell, T. P. P3HT/PCBM Bulk Heterojunction Organic Photovoltaics: Correlating Efficiency and Morphology. *Nano Lett.* **2011**, *11*, 561–567.

(9) Park, J. H.; Kim, J. S.; Lee, J. H.; Lee, W. H.; Cho, K. Effect of Annealing Solvent Solubility on the Performance of Poly(3-hexylthiophene)/Methanofullerene Solar Cells. *J. Phys. Chem. C* **2009**, *113*, 17579–17584.

(10) Chen, H.-Y.; Yang, H.; Yang, G.; Sista, S.; Zadoyan, R.; Li, G.; Yang, Y. Fast-Grown Interpenetrating Network in Poly(3-Hexylthiophene): Methanofullerenes Solar Cells Processed with Additive. *J. Phys. Chem. C* **2009**, *113*, 7946–7953.

(11) Kim, J. S.; Lee, J. H.; Park, J. H.; Shim, C.; Sim, M.; Cho, K. High-Efficiency Organic Solar Cells Based on Preformed Poly(3-Hexylthiophene) Nanowires. *Adv. Funct. Mater.* **2011**, *21*, 480–486.

(12) He, X.; Gao, F.; Tu, G.; Hasko, D.; Hüttner, S.; Steiner, U.; Greenham, N. C.; Friend, R. H.; Huck, W. T. S. Formation of Nanopatterned Polymer Blends in Photovoltaic Devices. *Nano Lett.* **2010**, *10*, 1302–1307.

(13) Varghese, O. K.; Paulose, M.; Grimes, C. A. Long Vertically Aligned Titania Nanotubes on Transparent Conducting Oxide for Highly Efficient Solar Cells. *Nat. Nanotechnol.* **2009**, *4*, 592–597.

(14) Dayal, S.; Kopidakis, N.; Olson, D. C.; Ginley, D. S.; Rumbles, G. Photovoltaic Devices with a Low Band Gap Polymer and CdSe Nanostructures Exceeding 3% Efficiency. *Nano Lett.* **2010**, *10*, 239–242.

(15) Goldman, E. R.; Clapp, A. R.; Anderson, G. P.; Uyeda, H. T.; Mauro, J. M.; Medintz, I. L.; Mattoussi, H. Multiplexed Toxin Analysis Using Four Colors of Quantum Dot Fluororeagents. *Anal. Chem.* **2004**, *76*, 684–688.

(16) Goldman, E. R.; Medintz, I. L.; Whitley, J. L.; Hayhurst, A.; Clapp, A. R.; Uyeda, H. T.; Deschamps, J. R.; Lassman, M. E.; Mattoussi, H. A Hybrid Quantum Dot-Antibody Fragment Fluorescence Resonance Energy Transfer-Based TNT Sensor. *J. Am. Chem. Soc.* **2005**, *127*, 6744–6751.

(17) Colvin, V. L.; Schlamp, M. C.; Alivisatos, A. P. Light-Emitting Diodes Made from Cadmium Selenide Nanocrystals and a Semiconducting Polymer. *Nature* **1994**, *370*, 354–357.

(18) Schlamp, M. C.; Peng, X.; Alivisatos, A. P. Improved Efficiencies in Light Emitting Diodes Made with CdSe(CdS) Core/shell Type Nanocrystals and a Semiconducting Polymer. *J. Appl. Phys.* **1997**, *82*, 5837.

(19) Sun, B.; Marx, E.; Greenham, N. C. Photovoltaic Devices Using Blends of Branched CdSe Nanoparticles and Conjugated Polymers. *Nano Lett.* **2003**, *3*, 961–963.

(20) Huynh, W. U.; Peng, X.; Alivisatos, A. P. CdSe Nanocrystal Rods/Poly(3-Hexylthiophene) Composite Photovoltaic Devices. *Adv. Mater.* **1999**, *11*, 923–927.

(21) Huynh, W. U.; Dittmer, J. J.; Alivisatos, A. P. Hybrid Nanorod-Polymer Solar Cells. *Science* **2002**, *295*, 2425–2427.

(22) Brus, L. E. Electron–electron and Electron-Hole Interactions in Small Semiconductor Crystallites: The Size Dependence of the Lowest Excited Electronic State. *J. Chem. Phys.* **1984**, *80*, 4403.

(23) Alivisatos, A. P. Perspectives on the Physical Chemistry of Semiconductor Nanocrystals. *J. Phys. Chem.* **1996**, *100*, 13226–13239.

(24) Yu, P.; Nedeljkovic, J. M.; Ahrenkiel, P. A.; Ellingson, R. J.; Nozik, A. J. Size Dependent Femtosecond Electron Cooling Dynamics in CdSe Quantum Rods. *Nano Lett.* **2004**, *4*, 1089–1092.

(25) Nozik, A. J. Nanoscience and Nanostructures for Photovoltaics and Solar Fuels. *Nano Lett.* **2010**, *10*, 2735–2741.

(26) Huang, J.; Huang, Z.; Yang, Y.; Zhu, H.; Lian, T. Multiple Exciton Dissociation in CdSe Quantum Dots by Ultrafast Electron Transfer to Adsorbed Methylene Blue. *J. Am. Chem. Soc.* **2010**, *132*, 4858–4864.

(27) Dayal, S.; Reese, M. O.; Ferguson, A. J.; Ginley, D. S.; Rumbles, G.; Kopidakis, N. The Effect of Nanoparticle Shape on the Photocarrier Dynamics and Photovoltaic Device Performance of Poly(3-hexylthiophene):CdSe Nanoparticle Bulk Heterojunction Solar Cells. *Adv. Funct. Mater.* **2010**, *20*, 2629–2635.

(28) Dayal, S.; Kopidakis, N.; Rumbles, G. Photoinduced Electron Transfer in Composites of Conjugated Polymers and Dendrimers with Branched Colloidal Nanoparticles. *Faraday Discuss.* **2012**, *155*, 323–337.

(29) Liu, J.; Tanaka, T.; Sivula, K.; Alivisatos, A. P.; Fréchet, J. M. J. Employing End-Functional Polythiophene to Control the Morphology of Nanocrystal-Polymer Composites in Hybrid Solar Cells. *J. Am. Chem. Soc.* **2004**, *126*, 6550–6551.

(30) Zhang, Q.; Russell, T.; Emrick, T. Synthesis and Characterization of CdSe Nanorods Functionalized with Regioregular Poly (3-Hexylthiophene). *Chem. Mater.* **2007**, *19*, 3712–3716.

(31) Ren, S.; Chang, L.-Y.; Lim, S.-K.; Zhao, J.; Smith, M.; Zhao, N.; Bulović, V.; Bawendi, M.; Gradecak, S. Inorganic-Organic Hybrid Solar Cell: Bridging Quantum Dots to Conjugated Polymer Nanowires. *Nano Lett.* **2011**, *11*, 3998–4002.

(32) Peng, Z. a; Peng, X. Formation of High-Quality CdTe, CdSe, and CdS Nanocrystals Using CdO as Precursor. *J. Am. Chem. Soc.* **2001**, *123*, 183–184.

(33) Qu, L.; Peng, Z. A.; Peng, X. Alternative Routes toward High Quality CdSe Nanocrystals. *Nano Lett.* **2001**, *1*, 333–337.

(34) Li, J. J.; Wang, Y. A.; Guo, W.; Keay, J. C.; Mishima, T. D.; Johnson, M. B.; Peng, X. Large-Scale Synthesis of Nearly Monodisperse CdSe/CdS Core/shell Nanocrystals Using Air-Stable Reagents via Successive Ion Layer Adsorption and Reaction. *J. Am. Chem. Soc.* **2003**, *125*, 12567–12575.

(35) Hambrock, J.; Birkner, A.; Fischer, R. A. Synthesis of CdSe Nanoparticles Using Various Organometallic Cadmium Precursors. *J. Mater. Chem.* **2001**, *11*, 3197–3201.

(36) Yin, Y.; Alivisatos, A. P. Colloidal Nanocrystal Synthesis and the Organic-Inorganic Interface. *Nature* **2005**, *437*, 664–670.

(37) Liu, H.; Owen, J. S.; Alivisatos, A. P. Mechanistic Study of Precursor Evolution in Colloidal Group II-VI Semiconductor Nanocrystal Synthesis. *J. Am. Chem. Soc.* **2007**, *129*, 305–312.

(38) Peng, Z. A.; Peng, X. Nearly Monodisperse and Shape-Controlled CdSe Nanocrystals via Alternative Routes: Nucleation and Growth. *J. Am. Chem. Soc.* **2002**, *124*, 3343–3353.

(39) Manna, L.; Scher, E. C.; Alivisatos, A. P. Synthesis of Soluble and Processable Rod-, Arrow-, Teardrop-, and Tetrapod-Shaped CdSe Nanocrystals. *J. Am. Chem. Soc.* **2000**, *122*, 12700–12706.

(40) Peng, X.; Manna, L.; Yang, W.; Wickham, J.; Scher, E.; Kadavanich, a; Alivisatos, A. P. Shape Control of CdSe Nanocrystals. *Nature* **2000**, *404*, 59–61.

(41) Smith, A. M.; Nie, S. Semiconductor Nanocrystals: Structure, Properties, and Band Gap Engineering. *Acc. Chem. Res.* **2010**, *43*, 190–200.

(42) Li, Z.; Peng, X. Size/shape-Controlled Synthesis of Colloidal CdSe Quantum Disks: Ligand and Temperature Effects. *J. Am. Chem. Soc.* **2011**, *133*, 6578–6586.

(43) Li, Z.; Kurtulus, Ã z.; Fu, N.; Wang, Z.; Kornowski, A.; Pietsch, U.; Mews, A. Controlled Synthesis of CdSe Nanowires by Solution-Liquid- “Solid Method. *Adv. Funct. Mater.* **2009**, *19*, 3650–3661.

(44) Deng, Z.-X.; Li, L.; Li, Y. Novel Inorganic-Organic-Layered Structures: Crystallographic Understanding of Both Phase and Morphology Formations of One-Dimensional CdE (E = S, Se, Te) Nanorods in Ethylenediamine. *Inorg. Chem.* **2003**, *42*, 2331–2341.

(45) Liu, Y.; Qiu, H.-Y.; Xu, Y.; Wu, D.; Li, M.-J.; Jiang, J.-X.; Lai, G.-Q. Selective Synthesis of Wurtzite CdSe Nanorods and Zinc Blend CdSe Nanocrystals through a Convenient Solvothermal Route. *J. Nanoparticle Res.* **2006**, *9*, 745–752.

(46) Xi, L. F.; Lam, Y. M. Synthesis and Characterization of CdSe Nanorods Using a Novel Microemulsion Method at Moderate Temperature. *J. Colloid Interface Sci.* **2007**, *316*, 771–778.

(47) Huynh, W. U.; Dittmer, J. J.; Libby, W. C.; Whiting, G. L.; Alivisatos, A. P. Controlling the Morphology of Nanocrystal–Polymer Composites for Solar Cells. *Adv. Funct. Mater.* **2003**, *13*, 73–79.

(48) Shaviv, E.; Salant, A.; Banin, U. Size Dependence of Molar Absorption Coefficients of CdSe Semiconductor Quantum Rods. *Chemphyschem* **2009**, *10*, 1028–1031.

(49) Cunningham, P. D.; Boercker, J. E.; Placencia, D.; Tischler, J. G. Anisotropic Absorption in PbSe Nanorods. *ACS Nano* **2014**, *8*, 581–590.

(50) Zhu, H.; Lian, T. Enhanced Multiple Exciton Dissociation from CdSe Quantum Rods: The Effect of Nanocrystal Shape. *J. Am. Chem. Soc.* **2012**, *134*, 11289–11297.

(51) Wang, W.; Banerjee, S.; Jia, S.; Steigerwald, M. L.; Herman, I. P. Ligand Control of Growth, Morphology, and Capping Structure of Colloidal CdSe Nanorods. *Chem. Mater.* **2007**, *19*, 2573–2580.

(52) Green, M. The Nature of Quantum Dot Capping Ligands. *J. Mater. Chem.* **2010**, *20*, 5797.

(53) Stevenson, A. W.; Milanko, M.; Barnea, Z. Anharmonic Thermal Vibrations and the Position Parameter in Wurtzite Structures. I. Cadmium Sulphide. *Acta Crystallogr. Sect. B Struct. Sci.* **1984**, *40*, 521–530.

(54) Maiolo, J. R.; Atwater, H. A.; Lewis, N. S. Macroporous Silicon as a Model for Silicon Wire Array Solar Cells. *J. Phys. Chem. C* **2008**, *112*, 6194–6201.

(55) Zhao, L.; Pang, X.; Adhikary, R.; Petrich, J. W.; Jeffries-El, M.; Lin, Z. Organic-Inorganic Nanocomposites by Placing Conjugated Polymers in Intimate Contact with Quantum Rods. *Adv. Mater.* **2011**, *23*, 2844–2849.

(56) Gonzalez-Valls, I.; Lira-Cantu, M. Vertically-Aligned Nanostructures of ZnO for Excitonic Solar Cells: A Review. *Energy Environ. Sci.* **2009**, *2*, 19.

(57) Gupta, S.; Zhang, Q.; Emrick, T.; Balazs, A. C.; Russell, T. P. Entropy-Driven Segregation of Nanoparticles to Cracks in Multilayered Composite Polymer Structures. *Nat. Mater.* **2006**, *5*, 229–233.

(58) Ryan, K. M.; Mastroianni, A.; Stancil, K. a; Liu, H.; Alivisatos, A. P. Electric-Field-Assisted Assembly of Perpendicularly Oriented Nanorod Superlattices. *Nano Lett.* **2006**, *6*, 1479–1482.

(59) Gupta, S.; Zhang, Q.; Emrick, T.; Russell, T. P. "Self-Corralling" Nanorods under an Applied Electric Field. *Nano Lett.* **2006**, *6*, 2066–2069.

(60) Baker, J. L.; Widmer-Cooper, A.; Toney, M. F.; Geissler, P. L.; Alivisatos, A. P. Device-Scale Perpendicular Alignment of Colloidal Nanorods. *Nano Lett.* **2010**, *10*, 195–201.

(61) Ahmed, S.; Ryan, K. M. Self-Assembly of Vertically Aligned Nanorod Supercrystals Using Highly Oriented Pyrolytic Graphite. *Nano Lett.* **2007**, *7*, 2480–2485.

(62) Hung, A. M.; Konopliv, N. a; Cha, J. N. Solvent-Based Assembly of CdSe Nanorods in Solution. *Langmuir* **2011**, *27*, 12322–12328.

(63) Zhao, N.; Liu, K.; Greener, J.; Nie, Z.; Kumacheva, E. Close-Packed Superlattices of Side-by-Side Assembled Au-CdSe Nanorods. *Nano Lett.* **2009**, *9*, 3077–3081.

(64) Baranov, D.; Fiore, A.; van Huis, M.; Giannini, C.; Falqui, A.; Lafont, U.; Zandbergen, H.; Zanella, M.; Cingolani, R.; Manna, L. Assembly of Colloidal Semiconductor Nanorods in Solution by Depletion Attraction. *Nano Lett.* **2010**, *10*, 743–749.

(65) Li, L.-S.; Alivisatos, A. P. Origin and Scaling of the Permanent Dipole Moment in CdSe Nanorods. *Phys. Rev. Lett.* **2003**, *90*, 097402.

(66) Modestino, M. a.; Chan, E. R.; Hexemer, A.; Urban, J. J.; Segalman, R. a. Controlling Nanorod Self-Assembly in Polymer Thin Films. *Macromolecules* **2011**, *44*, 7364–7371.

(67) Xie, Y.; Guo, S.; Guo, C.; He, M.; Chen, D.; Ji, Y.; Chen, Z.; Wu, X.; Liu, Q.; Xie, S. Controllable Two-Stage Droplet Evaporation Method and Its Nanoparticle Self-Assembly Mechanism. *Langmuir* **2013**, *29*, 6232–6241.

(68) Singh, A.; Gunning, R. D.; Sanyal, A.; Ryan, K. M. Directing Semiconductor Nanorod Assembly into 1D or 2D Supercrystals by Altering the Surface Charge. *Chem. Commun. (Camb).* **2010**, *46*, 7193–7195.

(69) Shevchenko, E. V; Talapin, D. V; O'brien, S.; Murray, C. B. Polymorphism in AB(13) Nanoparticle Superlattices: An Example of Semiconductor-Metal Metamaterials. *J. Am. Chem. Soc.* **2005**, *127*, 8741–8747.

(70) Peng, B.; Li, G.; Li, D.; Dodson, S.; Zhang, Q.; Zhang, J.; Lee, Y. H. Vertically Aligned Gold Nanorod Monolayer on Arbitrary Substrates : Self-Assembly and Femtomolar. *ACS Nano* **2013**, *7*, 5993–6000.

(71) Correa-Duarte, M. A.; Pérez-Juste, J.; Sánchez-Iglesias, A.; Giersig, M.; Liz-Marzán, L. M. Aligning Au Nanorods by Using Carbon Nanotubes as Templates. *Angew. Chem. Int. Ed. Engl.* **2005**, *44*, 4375–4378.

(72) Wang, H.; Lin, W.; Fritz, K. P.; Scholes, G. D.; Winnik, M. A.; Manners, I. Cylindrical Block Co-Micelles with Spatially Selective Functionalization by Nanoparticles. *J. Am. Chem. Soc.* **2007**, *129*, 12924–12925.

(73) Dujardin, E.; Peet, C.; Stubbs, G.; Culver, J. N.; Mann, S. Organization of Metallic Nanoparticles Using Tobacco Mosaic Virus Templates. *Nano Lett.* **2003**, *3*, 413–417.

(74) Xu, J.; Hu, J.; Liu, X.; Qiu, X.; Wei, Z. Stepwise Self-Assembly of P3HT/CdSe Hybrid Nanowires with Enhanced Photoconductivity. *Macromol. Rapid Commun.* **2009**, *30*, 1419–1423.

(75) Pentzer, E. B.; Bokel, F. a; Hayward, R. C.; Emrick, T. Nanocomposite "Superhighways" by Solution Assembly of Semiconductor Nanostructures with Ligand-Functionalized Conjugated Polymers. *Adv. Mater.* **2012**, *24*, 2254–2258.

(76) Bokel, F. A.; Sudeep, P. K.; Pentzer, E.; Emrick, T.; Hayward, R. C. Assembly of Poly(3-hexylthiophene)/CdSe Hybrid Nanowires by Cocrystallization. *Macromolecules* **2011**, *44*, 1768–1770.

(77) Yui, K.; Aso, Y.; Otsubo, T.; Ogura, F. Novel Electron Acceptors Bearing a Heteroquinonoid System. I. Synthesis and Conductive Complexes of 5,5′-Bis(dicyanomethylene)-5,5′-Dihydro-Δ2,2′-Bithiophene and Related Compounds. *Bull. Chem. Soc. Jpn.* **1989**, *62*, 1539–1546.

(78) Yin, J.-F.; Chen, J.-G.; Lu, Z.-Z.; Ho, K.-C.; Lin, H.-C.; Lu, K.-L. Toward Optimization of Oligothiophene Antennas: New Ruthenium Sensitizers with Excellent Performance for Dye-Sensitized Solar Cells. *Chem. Mater.* **2010**, *22*, 4392–4399.

(79) Osaka, I.; McCullough, R. D. Advances in Molecular Design and Synthesis of Regioregular Polythiophenes. *Acc. Chem. Res.* **2008**, *41*, 1202–1214.

(80) Zhao, L.; Lin, Z. Crafting Semiconductor Organic-Inorganic Nanocomposites via Placing Conjugated Polymers in Intimate Contact with Nanocrystals for Hybrid Solar Cells. *Adv. Mater.* **2012**, *24*, 4353–4368.

(81) Liu, K.; Nie, Z.; Zhao, N.; Li, W.; Rubinstein, M.; Kumacheva, E. Step-Growth Polymerization of Inorganic Nanoparticles. *Science* **2010**, *329*, 197–200.

(82) Abbas, A.; Kattumenu, R.; Tian, L.; Singamaneni, S. Molecular Linker-Mediated Self-Assembly of Gold Nanoparticles: Understanding and Controlling the Dynamics. *Langmuir* **2013**, *29*, 56–64.

(83) Pramod, P.; Thomas, K. G. Plasmon Coupling in Dimers of Au Nanorods. *Adv. Mater.* **2008**, *20*, 4300–4305.

(84) Kumar, J.; Wei, X.; Barrow, S.; Funston, A. M.; Thomas, K. G.; Mulvaney, P. Surface Plasmon Coupling in End-to-End Linked Gold Nanorod Dimers and Trimers. *Phys. Chem. Chem. Phys.* **2013**, *15*, 4258–4264.

(85) Caswell, K. K.; Wilson, J. N.; Bunz, U. H. F.; Murphy, C. J. Preferential End-to-End Assembly of Gold Nanorods by Biotin-Streptavidin Connectors. *J. Am. Chem. Soc.* **2003**, *125*, 13914–13915.

(86) Salant, A.; Amitay-Sadovsky, E.; Banin, U. Directed Self-Assembly of Gold-Tipped CdSe Nanorods. *J. Am. Chem. Soc.* **2006**, *128*, 10006–10007.

(87) Mokari, T.; Rothenberg, E.; Popov, I.; Costi, R.; Banin, U. Selective Growth of Metal Tips Onto Semiconductor Quantum Rods and Tetrapods-Support Info. *Science (80-.).* **2004**, *304*, 1787–1790.

(88) Ni, W.; Mosquera, R. A.; Pérez-Juste, J.; Liz-Marzán, L. M. Evidence for Hydrogen-Bonding-Directed Assembly of Gold Nanorods in Aqueous Solution. *J. Phys. Chem. Lett.* **2010**, *1*, 1181–1185.

(89) Figuerola, A.; Franchini, I. R.; Fiore, A.; Mastria, R.; Falqui, A.; Bertoni, G.; Bals, S.; Tendeloo, G. Van; Kudera, S.; Cingolani, R.; et al. End-to-End Assembly of Shape-Controlled Nanocrystals via a Nanowelding Approach Mediated by Gold Domains. *Adv. Mater.* **2009**, *21*, 550–554.

(90) Nie, Z.; Fava, D.; Kumacheva, E.; Zou, S.; Walker, G. C.; Rubinstein, M. Self-Assembly of Metal-Polymer Analogues of Amphiphilic Triblock Copolymers. *Nat. Mater.* **2007**, *6*, 609–614.

(91) Ghezelbash, A.; Koo, B.; Korgel, B. a. Self-Assembled Stripe Patterns of CdS Nanorods. *Nano Lett.* **2006**, *6*, 1832–1836.

(92) Li, W.; Zhang, P.; Dai, M.; He, J.; Babu, T.; Xu, Y.; Deng, R.; Liang, R.; Lu, M.; Nie, Z.; et al. Ordering of Gold Nanorods in Confined Spaces by Directed Assembly. *Macromolecules* **2013**, *46*, 2241–2248.

(93) Kawamura, G.; Yang, Y.; Nogami, M. End-to-End Assembly of CTAB-Stabilized Gold Nanorods by Citrate Anions. *J. Phys. Chem. C* **2008**, *112*, 10632–10636.

(94) Zhai, L.; Pilston, R. L.; Zaiger, K. L.; Stokes, K. K.; Mccullough, R. D. A Simple Method to Generate Side-Chain Derivatives of Regioregular Polythiophene via the GRIM Metathesis and Post-Polymerization Functionalization. *Macromolecules* **2003**, *36*, 61–64.

(95) Geim, A. K.; Novoselov, K. S. The Rise of Graphene. *Nat. Mater.* **2007**, *6*, 183–191.

(96) Wang, X.; Zhi, L.; Müllen, K. Transparent, Conductive Graphene Electrodes for Dye-Sensitized Solar Cells. *Nano Lett.* **2008**, *8*, 323–327.

(97) Vickery, J. L.; Patil, A. J.; Mann, S. Fabrication of Graphene-Polymer Nanocomposites With Higher-Order Three-Dimensional Architectures. *Adv. Mater.* **2009**, *21*, 2180–2184.

(98) Li, X.; Wang, X.; Zhang, L.; Lee, S.; Dai, H. Chemically Derived, Ultrasmooth Graphene Nanoribbon Semiconductors. *Science* **2008**, *319*, 1229–1232.

(99) Seo, J. H.; Kim, D.-H.; Kwon, S.-H.; Song, M.; Choi, M.-S.; Ryu, S. Y.; Lee, H. W.; Park, Y. C.; Kwon, J.-D.; Nam, K.-S.; et al. High Efficiency Inorganic/organic Hybrid Tandem Solar Cells. *Adv. Mater.* **2012**, *24*, 4523–4527.

(100) Chung, I.; Lee, B.; He, J.; Chang, R. P. H.; Kanatzidis, M. G. All-Solid-State Dye-Sensitized Solar Cells with High Efficiency. *Nature* **2012**, *485*, 486–489.

(101) Sun, Y.; Welch, G. C.; Leong, W. L.; Takacs, C. J.; Bazan, G. C.; Heeger, A. J. Solution-Processed Small-Molecule Solar Cells with 6.7% Efficiency. *Nat. Mater.* **2012**, *11*, 44–48.

(102) Yin, Z.; Zhu, J.; He, Q.; Cao, X.; Tan, C.; Chen, H.; Yan, Q.; Zhang, H. Graphene-Based Materials for Solar Cell Applications. *Adv. Energy Mater.* **2014**, *4*, n/a–n/a.

(103) Xie, K.; Qin, X.; Wang, X.; Wang, Y.; Tao, H.; Wu, Q.; Yang, L.; Hu, Z. Carbon Nanocages as Supercapacitor Electrode Materials. *Adv. Mater.* **2011**, *24*, 347–352.

(104) Jiang, H.; Ma, J.; Li, C. Mesoporous Carbon Incorporated Metal Oxide Nanomaterials as Supercapacitor Electrodes. *Adv. Mater.* **2012**, *24*, 4197–4202.

(105) Service, R. F. Materials Science. New “Supercapacitor” Promises to Pack More Electrical Punch. *Science* **2006**, *313*, 902.

(106) Miller, J. R.; Simon, P. Materials Science. Electrochemical Capacitors for Energy Management. *Science* **2008**, *321*, 651–652.

(107) Liu, S.; Jia, H.; Han, L.; Wang, J.; Gao, P.; Xu, D.; Yang, J.; Che, S. Nanosheet-Constructed Porous TiO2-B for Advanced Lithium Ion Batteries. *Adv. Mater.* **2012**, *24*, 3201–3204.

(108) Ko, S.; Lee, J.-I.; Yang, H. S.; Park, S.; Jeong, U. Mesoporous CuO Particles Threaded with CNTs for High-Performance Lithium-Ion Battery Anodes. *Adv. Mater.* **2012**, *24*, 4451–4456.

(109) Bae, S.; Kim, H.; Lee, Y.; Xu, X.; Park, J.-S.; Zheng, Y.; Balakrishnan, J.; Lei, T.; Kim, H. R.; Song, Y. Il; et al. Roll-to-Roll Production of 30-Inch Graphene Films for Transparent Electrodes. *Nat. Nanotechnol.* **2010**, *5*, 574–578.

(110) Yin, Z.; Sun, S.; Salim, T.; Wu, S.; Huang, X.; He, Q.; Lam, Y. M.; Zhang, H. Organic Photovoltaic Devices Using Highly Flexible Reduced Graphene Oxide Films as Transparent Electrodes. *ACS Nano* **2010**, *4*, 5263–5268.

(111) Yin, Z.; Wu, S.; Zhou, X.; Huang, X.; Zhang, Q.; Boey, F.; Zhang, H. Electrochemical Deposition of ZnO Nanorods on Transparent Reduced Graphene Oxide Electrodes for Hybrid Solar Cells. *Small* **2010**, *6*, 307–312.

(112) Chen, J.-H.; Jang, C.; Xiao, S.; Ishigami, M.; Fuhrer, M. S. Intrinsic and Extrinsic Performance Limits of Graphene Devices on SiO2. *Nat. Nanotechnol.* **2008**, *3*, 206–209.

(113) Nair, R. R.; Blake, P.; Grigorenko, A. N.; Novoselov, K. S.; Booth, T. J.; Stauber, T.; Peres, N. M. R.; Geim, A. K. Fine Structure Constant Defines Visual Transparency of Graphene. *Science* **2008**, *320*, 1308.

(114) Wang, S.; Goh, B. M.; Manga, K. K.; Bao, Q.; Yang, P.; Loh, K. P. Graphene as Atomic Template and Structural Scaffold in the Synthesis of Graphene-Organic Hybrid Wire with Photovoltaic Properties. *ACS Nano* **2010**, *4*, 6180–6186.

(115) Guo, C. X.; Yang, H. Bin; Sheng, Z. M.; Lu, Z. S.; Song, Q. L.; Li, C. M. Layered Graphene/quantum Dots for Photovoltaic Devices. *Angew. Chem. Int. Ed. Engl.* **2010**, *49*, 3014–3017.

(116) Zhou, W.; Zhu, J.; Cheng, C.; Liu, J.; Yang, H.; Cong, C.; Guan, C.; Jia, X.; Fan, H. J.; Yan, Q.; et al. A General Strategy toward Graphene@metal Oxide Core–shell Nanostructures for High-Performance Lithium Storage. *Energy Environ. Sci.* **2011**, *4*, 4954.

(117) Li, S.-S.; Tu, K.-H.; Lin, C.-C.; Chen, C.-W.; Chhowalla, M. Solution-Processable Graphene Oxide as an Efficient Hole Transport Layer in Polymer Solar Cells. *ACS Nano* **2010**, *4*, 3169–3174.

(118) Liu, J.; Xue, Y.; Gao, Y.; Yu, D.; Durstock, M.; Dai, L. Hole and Electron Extraction Layers Based on Graphene Oxide Derivatives for High-Performance Bulk Heterojunction Solar Cells. *Adv. Mater.* **2012**, *24*, 2228–2233.

(119) Yu, D.; Yang, Y.; Durstock, M.; Baek, J.; Dai, L. Soluble P3HT-Grafted Graphene for Efficient Bilayer-Heterojunction Photovoltaic Devices. *ACS Nano* **2010**, *4*, 5633–5640.

(120) Tong, S. W.; Wang, Y.; Zheng, Y.; Ng, M.-F.; Loh, K. P. Graphene Intermediate Layer in Tandem Organic Photovoltaic Cells. *Adv. Funct. Mater.* **2011**, *21*, 4430–4435.

(121) Tung, V. C.; Kim, J.; Huang, J. Graphene Oxide:Single-Walled Carbon Nanotube-Based Interfacial Layer for All-Solution-Processed Multijunction Solar Cells in Both Regular and Inverted Geometries. *Adv. Energy Mater.* **2012**, *2*, 299–303.

(122) Miao, X.; Tongay, S.; Petterson, M. K.; Berke, K.; Rinzler, A. G.; Appleton, B. R.; Hebard, A. F. High Efficiency Graphene Solar Cells by Chemical Doping. *Nano Lett.* **2012**, *12*, 2745–2750.

(123) Zhang, L.; Jia, Y.; Wang, S.; Li, Z.; Ji, C.; Wei, J.; Zhu, H.; Wang, K.; Wu, D.; Shi, E.; et al. Carbon Nanotube and CdSe Nanobelt Schottky Junction Solar Cells. *Nano Lett.* **2010**, *10*, 3583–3589.

(124) Wang, H.; Yang, Y.; Liang, Y.; Cui, L.-F.; Casalongue, H. S.; Li, Y.; Hong, G.; Cui, Y.; Dai, H. LiMn(1-x)Fe(x)PO4 Nanorods Grown on Graphene Sheets for Ultrahigh-Rate-Performance Lithium Ion Batteries. *Angew. Chem. Int. Ed. Engl.* **2011**, *50*, 7364–7368.

(125) Lin, Y.; Li, X.; Xie, D.; Feng, T.; Chen, Y.; Song, R.; Tian, H.; Ren, T.; Zhong, M.; Wang, K.; et al. Graphene/semiconductor Heterojunction Solar Cells with Modulated Antireflection and Graphene Work Function. *Energy Environ. Sci.* **2013**, *6*, 108.

(126) Wang, Z.; Zhang, J.; Yin, Z.; Wu, S.; Mandler, D.; Zhang, H. Fabrication of Nanoelectrode Ensembles by Electrodepositon of Au Nanoparticles on Single-Layer Graphene Oxide Sheets. *Nanoscale* **2012**, *4*, 2728–2733.

(127) Valota, A. T.; Kinloch, I. A.; Novoselov, K. S.; Casiraghi, C.; Eckmann, A.; Hill, E. W.; Dryfe, R. A. W. Electrochemical Behavior of Monolayer and Bilayer Graphene. *ACS Nano* **2011**, *5*, 8809–8815.

(128) Wu, S.; Yin, Z.; He, Q.; Lu, G.; Zhou, X.; Zhang, H. Electrochemical Deposition of Cl-Doped N-Type Cu2O on Reduced Graphene Oxide Electrodes. *J. Mater. Chem.* **2011**, *21*, 3467.

(129) Gomez De Arco, L.; Zhang, Y.; Schlenker, C. W.; Ryu, K.; Thompson, M. E.; Zhou, C. Continuous, Highly Flexible, and Transparent Graphene Films by Chemical Vapor Deposition for Organic Photovoltaics. *ACS Nano* **2010**, *4*, 2865–2873.

(130) Bi, H.; Huang, F.; Liang, J.; Xie, X.; Jiang, M. Transparent Conductive Graphene Films Synthesized by Ambient Pressure Chemical Vapor Deposition Used as the Front Electrode of CdTe Solar Cells. *Adv. Mater.* **2011**, *23*, 3202–3206.

(131) Park, H.; Chang, S.; Jean, J.; Cheng, J. J.; Araujo, P. T.; Wang, M.; Bawendi, M. G.; Dresselhaus, M. S.; Bulović, V.; Kong, J.; et al. Graphene Cathode-Based ZnO Nanowire Hybrid Solar Cells. *Nano Lett.* **2013**, *13*, 233–239.

(132) Liu, Z.; Liu, Q.; Huang, Y.; Ma, Y.; Yin, S.; Zhang, X.; Sun, W.; Chen, Y. Organic Photovoltaic Devices Based on a Novel Acceptor Material: Graphene. *Adv. Mater.* **2008**, *20*, 3924–3930.

(133) Gupta, V.; Chaudhary, N.; Srivastava, R.; Sharma, G. D.; Bhardwaj, R.; Chand, S. Luminscent Graphene Quantum Dots for Organic Photovoltaic Devices. *J. Am. Chem. Soc.* **2011**, *133*, 9960–9963.

(134) Li, X.; Zhu, H.; Wang, K.; Cao, A.; Wei, J.; Li, C.; Jia, Y.; Li, Z.; Li, X.; Wu, D. Graphene-on-Silicon Schottky Junction Solar Cells. *Adv. Mater.* **2010**, *22*, 2743–2748.

(135) Ye, Y.; Gan, L.; Dai, L.; Dai, Y.; Guo, X.; Meng, H.; Yu, B.; Shi, Z.; Shang, K.; Qin, G. A Simple and Scalable Graphene Patterning Method and Its Application in CdSe Nanobelt/graphene Schottky Junction Solar Cells. *Nanoscale* **2011**, *3*, 1477–1481.

(136) Yang, N.; Zhai, J.; Wang, D.; Chen, Y.; Jiang, L. Two-Dimensional Graphene Bridges Enhanced Photoinduced Charge Transport in Dye-Sensitized Solar Cells. *ACS Nano* **2010**, *4*, 887–894.

(137) Yu, D.; Park, K.; Durstock, M.; Dai, L. Fullerene-Grafted Graphene for Efficient Bulk Heterojunction Polymer Photovoltaic Devices. *J. Phys. Chem. Lett.* **2011**, *2*, 1113–1118.

(138) Li, Q.; Guo, B.; Yu, J.; Ran, J.; Zhang, B.; Yan, H.; Gong, J. R. Highly Efficient Visible-Light-Driven Photocatalytic Hydrogen Production of CdS-Cluster-Decorated Graphene Nanosheets. *J. Am. Chem. Soc.* **2011**, *133*, 10878–10884.

(139) Jaegfeldt, H.; Kuwana, T.; Johansson, G. Electrochemical Stability of Catechols with a Pyrene Side Chain Strongly Adsorbed on Graphite Electrodes for Catalytic Oxidation of Dihydronicotinamide Adenine Dinucleotide. *J. Am. Chem. Soc.* **1983**, *105*, 1805–1814.

(140) Chen, R. J.; Zhang, Y.; Wang, D.; Dai, H. Noncovalent Sidewall Functionalization of Single-Walled Carbon Nanotubes for Protein Immobilization. *J. Am. Chem. Soc.* **2001**, *123*, 3838–3839.

(141) Lobez, J. M.; Afzali, A. Surface-Selective Directed Assembly of Carbon Nanotubes Using Side-Chain Functionalized Poly(thiophene)s. *Chem. Mater.* **2013**, *25*, 3662–3666.

(142) Hummers, W. S.; Offeman, R. E. Preparation of Graphitic Oxide. *J. Am. Chem. Soc.* **1958**, *80*, 1339–1339.